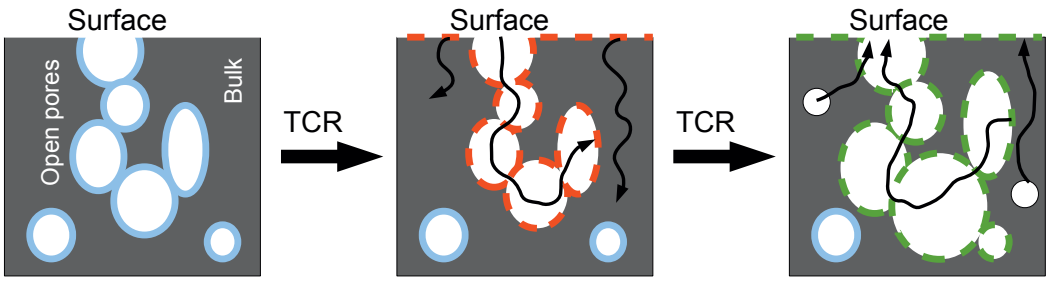

Fundamental processes of plasma and reactive gas surface treatment for the recovery of hydrogen isotopes from carbon co-deposits in fusion devices

Sören Möller

JÜLICH
FORSCHUNGSZENTRUM

Mitglied der Helmholtz-Gemeinschaft

Schriften des Forschungszentrums Jülich
Reihe Energie & Umwelt / Energy & Environment Band / Volume 222

Forschungszentrum Jülich GmbH
Institute of Energy and Climate Research
Plasma Physics IEK-4

Fundamental processes of plasma and reactive gas surface treatment for the recovery of hydrogen isotopes from carbon co-deposits in fusion devices

Sören Möller

Schriften des Forschungszentrums Jülich
Reihe Energie & Umwelt / Energy & Environment Band / Volume 222

ISSN 1866-1793 ISBN 978-3-89336-977-5

Bibliographic information published by the Deutsche Nationalbibliothek.
The Deutsche Nationalbibliothek lists this publication in the Deutsche Nationalbibliografie; detailed bibliographic data are available in the Internet at http://dnb.d-nb.de.

Publisher and Distributor: Forschungszentrum Jülich GmbH
Zentralbibliothek
52425 Jülich
Tel: +49 2461 61-5368
Fax: +49 2461 61-6103
Email: zb-publikation@fz-juelich.de
www.fz-juelich.de/zb

Cover Design: Grafische Medien, Forschungszentrum Jülich GmbH

Printer: Grafische Medien, Forschungszentrum Jülich GmbH

Schriften des Forschungszentrums Jülich
Reihe Energie & Umwelt / Energy & Environment, Band / Volume 222

D 61 (Diss. Düsseldorf, Univ., 2014)

ISSN 1866-1793
ISBN 978-3-89336-977-5

The complete volume is freely available on the Internet on the Jülicher Open Access Server (JUWEL) at www.fz-juelich.de/zb/juwel“

Abstract

The use of carbon-based plasma-facing wall components offers many advantages for plasma operation in magnetic confinement nuclear fusion devices. However, through reactions with the hydrogen based fusion plasma, carbon forms amorphous hydrogenated carbon co-deposits (a-C:H) in the vacuum vessels. If tritium is used to fuel the reactor, this co-deposition can quickly lead to an inacceptable high tritium inventory. Through co-deposition with carbon about 10% of the tritium injected into the reactor can be trapped. Even with other wall materials co-deposition can be significant. A method to recover the hydrogen isotopes from the co-deposits is necessary. The method has to be compatible with the requirements of the devices and nuclear fusion plasma operation.

In this work thermo-chemical removal by neutral gases (TCR) and removal by plasmas is investigated. Models are developed to describe the involved processes of both removal methods. TCR is described using a reaction-diffusion model. Within this model the reactive gas diffuses into the co-deposits and subsequently reacts in a thermally activated process. The co-deposits are pyrolysed, forming volatile gases, e.g. CO_2 and H_2O. These gases are pumped from the vacuum vessel and recycled. Applying the model to literature observations enables to connect data on exposure temperature, pressure, time and co-deposit properties. Two limits of TCR (reaction- or diffusion-limited) are identified. Plasma removal sputters co-deposits by their chemical and physical interaction with the impinging ions. The description uses a 0D plasma model from the literature which derives plasma parameters from the balance of input power to plasma power losses. The model is extended with descriptions of the plasma sheath and ion-surface interactions to derive the co-deposit removal rates. Plasma removal can be limited by this ion induced surface release rate or the rate of pumping of the released species.

To test the models dedicated experiments are conducted. Sets of a-C:D layers with different thickness and structure are exposed to TCR, using O_2 and NO_2, at temperatures of 470 to 630K and pressures of 2 and 20kPa to investigate the strong impact of exposure and layer properties, as predicted by the model. Plasmas produced by electron (ECR) and ion cyclotron frequencies (ICWC) are investigated with several base gases in a compact toroidal plasma device and the tokamak TEXTOR. The ion fluxes of these plasmas are investigated with Langmuir probes to allow the model comparison.

Pre/Post determination of the layers allows quantifying the removal rates of the tested methods. The areal density of deuterium and carbon is determined by nuclear reaction analysis and Rutherford-backscattering-spectrometry (NRA/RBS). Layer thicknesses are measured with ellipsometry. The experiments are conducted using well defined, high purity a-C:D layers deposited by plasma-chemical-vapour-deposition from CD_4 in a specifically adapted vacuum device to be able to separate the effects of layers properties and exposure parameters.

The experiments demonstrate that a 95% removal of a-C:D layers with NO_2–TCR at 630K is possible within 3min. The model´s prediction of a linear relation between the TCR rate and the co-deposits inventory is experimentally approved, validating its volume effect. The experiments with plasma removal reveal D_2 with a removal rate of $5.7 \pm 0.9 * 10^{15}$ D/(cm²s) as the fastest base gas in tokamaks. Comparisons with O_2 show that the higher sputtering yield of O is counteracted by an 11-fold lower ion surface flux density, introduced by fundamental properties of O_2. Pumping speed and partial exhaust gas pressures are identified as limiting factors for the removal rate, explaining differences to non-local observations from the literature. Furthermore, it is possible to remove O stored in surfaces in TEXTOR in, for fusion plasma operation, detrimental amounts by D_2-ICWC.

The models are in agreement with literature and new experimental data obtained in this work. Using the new knowledge, the methods can be adapted to future devices, e.g. ITER. TCR offers a fast removal with only logarithmic scaling with co-deposit inventory, while plasma removal results in good wall conditions for fusion operation. The proposed integral scenario combines both specific advantages to a fusion plasma compatible removal scenario. The determined removal rates and the technical specifications of ITER are used to calculate the removal time at 470K wall temperature for a tritium inventory of 700g to 10.7h in an application scenario.

Kurzfassung

Die Verwendung kohlenstoffbasierter plasmabegrenzender Wandmaterialien in Kernfusionsgeräten mit magnetischem Einschluss bietet viele Vorteile für den Plasmabetrieb. Durch Reaktionen mit dem wasserstoffbasierten Fusionsplasma lagern sich in den Vakuumgefäßen jedoch aus den Wandmaterialien kommende Kohlenstoffatome in kodeponierten amorphen Kohlenwasserstoffschichten (a-C:H) ab. Wird der Reaktor mit Tritium betrieben, kann dies schnell zu unakzeptabel großen Tritiuminventaren führen. Die Wasserstoff-Kodeponierung mit Kohlenstoff kann etwa 10% der Einlassmenge betragen und auch bei anderen Materialien signifikant sein. Verfahren zur Rückgewinnung der Wasserstoffisotope sind deshalb erforderlich. Diese Verfahren müssen mit den Anforderungen von Reaktorgefäßen und Plasmabetrieb kompatibel sein.

In dieser Arbeit wird die Abtragung sowohl mittels reaktiver Neutralgase (Thermo-Chemische Reinigung, TCR) als auch Plasmen untersucht. Modelle zur physikalischen Erklärung der in beiden Abtragungsverfahren ablaufenden Prozesse werden entwickelt. TCR wird mit einem Reaktions-Diffusionsprozess beschrieben. In diesem Modell diffundiert das reaktive Gas in die Kodeponierung um dort in einem thermisch aktivierten Prozess zu reagieren. Dabei bilden sich flüchtige Produkte, z.B. CO_2 und H_2O, die abgepumpt und recycelt werden. Durch Vergleiche des Modells mit der Literatur können Einzelbeobachtungen zu Expositionstemperatur, -druck, –zeit und Materialeigenschaften verknüpft werden. Zwei Grenzfälle von TCR (diffusions- oder reaktionsbegrenzt) werden definiert. Plasmaabtragung entfernt Kodeponierungen durch chemische und physikalische Wechselwirkung mit den auftreffenden Ionen. Mithilfe eines 0D Plasmamodells aus der Literatur werden die Plasmaparameter aus der Bilanz aus Eingangsleistung zu Plasmaverlusten berechnet. Um Abtragungsraten zu erhalten wird das Modell wird mit Beschreibungen der Plasmarandschicht und der Ionen-Wandwechselwirkung erweitert. Plasmaabtragungsraten sind entweder durch die ioneninduzierte Oberflächenfreisetzungsrate oder die Abpumprate des freigesetzten Materials limitiert.

Um die Modelle zu testen werden dedizierte Experimente durchgeführt. Sätze von a-C:D Schichten mit verschiedenen Dicken und Strukturen werden mit TCR in O_2 und NO_2 bei Wandtemperaturen von 470 bis 630K und Gasdrücken von 2 und 20kPa abgetragen, um den vom Modell vorhergesagten, starken Einfluss der Schichteigenschaften auf die Abtragungsraten zu untersuchen. Plasmen werden mithilfe von Elektronen- (ECR) und Ionenzyklotronresonanzfrequenzen (ICWC) in verschiedenen Gasen in einem kleinen, toroidalen Plasmagerät und dem Tokamak TEXTOR erzeugt. Die Ionenflüsse dieser Plasmen werden für den Modellvergleich mit Langmuirsonden vermessen.

Vorher/Nachher-Untersuchungen ermöglichen eine Quantifizierung der Abtragungsrate der getesteten Verfahren. Die Flächendichte von Deuterium- und Kohlenstoffatomen wird mit Kernreaktionsanalysen und Rutherford-Rückstreuspektrometrie (NRA/RBS) bestimmt. Schichtdicken werden mittels Ellipsometrie bestimmt. Die Experimente werden mit gut definierten, reinen a-C:D Schichten durchgeführt, um Effekte von Schichteigenschaften und Experimentiergrößen trennen zu können. Die Schichten werden in einer speziell angepassten Vakuumanlage per plasmaunterstützter, chemischer Gasphasenabscheidung in CD_4 erzeugt.

Die Experimente zeigen eine 95%ige Abtragung von a-C:D Schichten mit NO_2 bei 630K in 3min. Die Modellvorhersage eines linearen Zusammenhanges zwischen TCR-Rate und Kodepositionsinventar bestätigt sich. Die Experimente zur Plasmaabtragung stellen D_2 mit einer Abtragungsrate von $5{,}7\pm0{,}9*10^{15}$ D/(cm²s) als effektivstes Basis-Gas heraus. Vergleiche mit O_2 zeigen, dass dessen hohe Zerstäubungsausbeute durch eine 11-fach kleinere Ionen-Wandflussdichte überkompensiert wird, die durch dessen fundamentale Eigenschaften bedingt ist. Die Saugleistung der Vakuumpumpen und die Partialgasdrücke der Produkte werden als limitierende Faktoren für die Abtragungsrate identifiziert. Unterschiede zu nichtlokalen Untersuchungen aus der Literatur können so erklärt werden. In TEXTOR können in der Wand eingelagerte O-Atome mit D_2-ICWC entfernt werden, um deren schädlichen Einfluss auf Fusionsplasmen zu verhindern.

Die Modelle zeigen Übereinstimmung mit den experimentellen Daten aus der Literatur und dieser Arbeit. Das neue Wissen ermöglicht die Methoden für die Nutzung in zukünftigen Anlagen, z.B. ITER, zu adaptieren. TCR bietet eine schnelle Abtragung mit logarithmischer Skalierung mit dem Kodepositionsinventar, wohingegen die Plasmaabtragung fusionsplasmakompatible Wandbedingungen erzeugt. Das vorgeschlagene integrale Szenario kombiniert beide spezifischen Vorteile zu einem schnellen, fusionsplasmakompatiblen Abtragungsverfahren. Mit den gemessenen Raten und den technischen Spezifikationen von ITER wird eine Reinigungsdauer für ein T-Inventar von 700g von 10,7h bei 470K Wandtemperatur in einem Anwendungsszenario errechnet.

Table of Contents

1 Introduction

It is well known, that planet earth´s resources are limited. An ever growing population and industrial production will further boost the problem of resource shortage or high prices, respectively, in the future. One of the most important resources industrial societies need nowadays is electricity. A global growth of energy production and consumption of 40% was seen the last 20 years. Electric power is used to substitute other resources e.g. in mobility, household heating and material processing, thus saving those resources. Cheaper electric energy allows economically replacing and saving more resources by its usage. Low cost electricity is thus an important economic factor. Since most of today´s electric power production relies on limited resources, as coal or oil, electricity is also a limited resource. The pollution and the related change of the nature is a significant issue, which further increases the cost of electricity produced by conventional means.

Predictions show that the competition of exponential growth and limited natural resources can pose serious problems to our future society, affecting people's daily life possibly already in the middle of the 21st century (Randers 2012). With the over usage of our planet´s resources, humanity will not be able to supply a comfortable standard of living for all mankind causing severe recessions and social conflicts. The changeover to electric power which is independent of scarce resources and also cheap is a possible way to avoid this. The current approach for this is called renewable energy. Through the usage of wind, water and solar power significant amounts of resources are saved already today. These technologies are decentralized and dependent on local availability of their corresponding source, e.g. the local solar power density or wind speed. The difference between the daily and yearly power supply patterns of renewable power and the respective consumption patterns is an example of the unsolved problems of a full switch to renewable power. Providing additional options for future power production is thus mandatory to cope with the responsibility for future generations.

One of the options is the use of nuclear fusion of hydrogen isotopes. This form of nuclear energy has fundamental advantages compared to the nuclear power concepts employing fission with respect to the production of activated waste and operational accidents. Half-life times of the generated radioisotopes can be orders of magnitudes lower, with a proper choice of materials. The input fuel is not directly converted to long lived radioisotopes, but to helium (He). Only the activation of the reactor materials produces radioactive waste which has to be handled at the end of their lifetime. The necessary resources, namely the hydrogen isotope deuterium (D) and the metal lithium (Li), are widespread and available everywhere around the world. The available amounts of these isotopes on earth will be sufficient for several hundred thousand years of world power production, in contrast to currently used fuels.

For initiating the nuclear fusion process nuclei have to collide with sufficient kinetic energy to pass their mutual coulomb repulsion. The most promising approach to get sufficient

energy for a large number of particles is the confinement of a plasma in magnetic fields. The current technical developments focus on the so-called tokamak (Figure 1). This device produces a ring-shaped plasma in a toroidal chamber. A helical field is generated by the combination of toroidal field coils and a plasma current in toroidal direction. This magnetic configuration dramatically reduces the particle transport to the walls surrounding the plasma and thus leads to confinement of energy and particles.

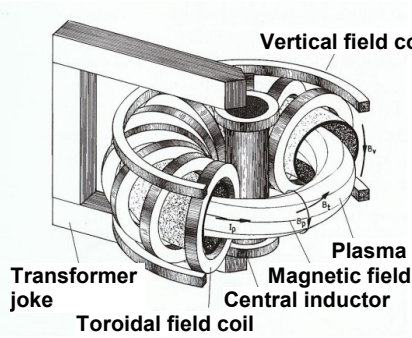

Figure 1: Scheme of the basic tokamak layout. The tokamak is currently the most advanced concept for magnetic confinement nuclear fusion. Figure from **(Neubauer et al. 2005)**

The main reaction foreseen for efficient energy production in future power plants is the fusion of deuterium (D) and tritium (T) in a plasma of about 10^8 K, confined by magnetic fields

$$\mathrm{D} + \mathrm{T} \rightarrow {}^4\mathrm{He} + \mathrm{n} + 17.6\mathrm{MeV} \quad (1)$$

This reaction produces an alpha particle which can provide heat to the fusion plasma and a neutron which can be used to produce new tritium by transmuting e.g. lithium. Potentially dangerous transmutations of reactor materials due to these neutrons can be effectively limited by proper material selection and production, thus leading to a potentially lower overall radioactivity than experienced in fission plants. Tritium cannot be found in nature, so tritium self-sufficiency is a major concern for fusion power plants. It has to be produced by the reactor itself, e.g. through the reaction

$${}^6\mathrm{Li} + \mathrm{n} \rightarrow {}^4\mathrm{He} + \mathrm{T} + 4.78\mathrm{MeV} \quad (2)$$

The fuel cycle thus uses D and ^{6}Li as educts, with ^{4}He, n and energy as products. To produce additional neutrons, which are necessary due to the inevitable losses of neutrons and tritium, for example the following neutron multiplication reactions can be employed

$${}^7\mathrm{Li} + \mathrm{n} \rightarrow {}^4\mathrm{He} + \mathrm{T} + \mathrm{n} - 2.47\mathrm{MeV} \quad (3)$$

$${}^9\mathrm{Be} + \mathrm{n} \rightarrow 2\,{}^4\mathrm{He} + 2\,\mathrm{n} - 1.57\mathrm{MeV} \quad (4)$$

Only with neutron multiplication a tritium breeding ratio (TBR=produced tritium per injected tritium) above 1 can be obtained, since the direct breeding from ^{6}Li only yields one T per fusion reaction. Even with neutron multiplication the TBR is expected to only reach a value of 1 to 1.2.

The power produced in the reactions (1) and (2) will be converted to heat which is converted to electrical power. The lower cost of the input fuels per generated energy unit is contrasted

by higher cost of the technological components in comparison to energy production by chemical reactions. The availability of a fusion power plant will, with the current status of knowledge, be determined by the lifetime of its inner components directly facing the plasma. The components suffer from high heat and particle loads originating from the plasma. The involved processes are summarized by the term plasma-wall interaction (PWI). A manifold of chemical and physical processes are involved, leading to a complex problem.

The plasma-wall interaction can lead to removal, so called sputtering, of material from the fusion vessel walls by interaction with the energetic plasma particles (Behrisch 2007). This released material will, depending on its properties and those of the surrounding plasma, be re-deposited in a different location of the vessel. Together with the originally sputtered particles, particles from the plasma, mainly hydrogen isotopes, can be co-deposited. The co-deposits can contain significant amounts, up to 50 atom % of hydrogen isotopes (Schwarz-Selinger, Keudell, and Jacob 1999; Temmerman et al. 2009) or even higher, depending on their elemental composition. This retention value strongly depends on the elemental composition of the co-deposits. The retention of tritium in co-deposits is a safety concern, and also poses a significant problem for the tritium self-sufficiency of a reactor. Tritium retention by co-deposition is thus a major concern for a fusion device.

Carbon as material for plasma-facing components has several advantages for fusion plasma operation. In contrast to other materials, the problem of hydrogen isotope retention is particularly severe if carbon is present in the wall materials (Roth et al. 2008), due to the strong chemical interaction between carbon and hydrogen. Carbon forms amorphous hydrogenated carbon (a-C:H) co-deposits, featuring the highest observed hydrogen isotope ratio and retention rates of up to 10% of the hydrogen isotopes injected into the fusion plasma. Several approaches to solve the retention problem by removing the co-deposits and recovering the hydrogen isotopes in-situ are under investigation. This work focuses on the removal of carbon co-deposits.

One of the approaches is thermo-chemical removal (TCR). This is a method based on the formation of volatile gases by thermally activated chemical reactions between a reactive gas and the heated co-deposits on the vessel surfaces. The volatile gases can be pumped out of the vessel and chemically reprocessed to recover the hydrogen isotopes. The majority of the investigations presented in the literature focused on carbon based co-deposits. Numerous experiments were conducted to evaluate the effect of the different experimental parameters (reactive gas pressure, surface temperature, etc.) on the removal rate of different co-deposit constituents. It was shown that the temperature dependence is well described by the Arrhenius function, describing thermally activated reactions (Davis and Haasz 2001; Davis and Haasz 2009). A linear connection between the initial co-deposit material content and its removal rate was observed and accounted to the homogenous (volumetric) nature of TCR (Davis and Haasz 2009). Porosity of a-C:H layers formed in tokamaks was analysed e.g. in (Martin et al. 2007; Richou et al. 2009; Kögel et al. 1988). The diffusion of gas through a-C:H necessary for a bulk effect was observed (Vasquez-Borucki,

Jacob, and Achete 2000). Typical values of the relative bulk porosity in the order of 10%, with pore size distributions centred below 1nm were observed in a-C:H layers (Jacobsohn et al. 2002). On the nanometer-scale the adsorption of reactive gas, introduced for co-deposit removal, inside the co-deposits during TCR was observed (Wang, Jacob, and Roth 1997). Different types and properties of carbon based co-deposits were identified depending on the conditions during deposition, e.g. (Schwarz-Selinger, Keudell, and Jacob 1999; Jacob and Möller 1993; Vasquez-Borucki, Jacob, and Achete 2000). Mass density (~1.3 to 2g/cm³), hydrogen content (20-50 atom %) and gas diffusion coefficients were seen to vary in limited ranges. A higher reactive gas pressure was seen to increase the removal rate, saturating at pressures above ≈100mbar for O_2 as the reactive gas (Ochoukov, Haasz, and Davis 2006). Time-resolved measurements were performed, showing a non-linear time evolution of the removal rate during the procedure (Davis and Haasz 1999). The feasibility of TCR for hydrogen recovery was shown and understanding was achieved in several aspects, but a comprehensive description of the physical processes and optimisation of the rates is missing.

A second approach for co-deposit removal and also wall conditioning for fusion plasma operation is the application of removal plasma discharges. The discharges can be distinguished whether a magnetic field can be applied during the discharge or not. In the latter class the glow discharge is the most common type. In this discharge a DC voltage is applied between a set of anodes and the vessel wall. Magnetic field compatible discharges are heated by high frequency generators, usually in the electron or ion cyclotron resonance frequency range. Since the magnetic fields of superconductors, which are most likely used in a reactor size device, cannot be easily switched off, the magnetic field compatible discharges are more likely to be applicable in future devices. Studies focusing on the ion cyclotron resonance frequency heated plasmas, the so called ion cyclotron wall conditioning (ICWC), yielded several results. Discharges were operated in a variety of magnetic field configurations and field strengths, revealing their influence on the plasma characteristics (Lyssoivan et al. 2009). The plasma-breakdown phase, the first ≤100ms, was characterized to understand the mechanisms of plasma production. The tokamak wall conditioning effect and material removal was shown on a global scale using mass spectrometric analysis of the pumped gases, e.g. (Douai et al. 2011; Sergienko et al. 2009). Isotope exchange of H and D was demonstrated and pumping speeds of the product gases were identified as a limiting factor (Wauters 2011). Technical aspects of gas feedback and antenna safety were investigated and solved. A computer model based on the balance of input power to plasma power losses of H_2 and He plasmas in a 0D approach was developed and yielded agreement with experimental observations (Wauters et al. 2011). This plasma-side understanding needed extension to a plasma-wall interaction model in order to understand how the plasmas finally remove material. The global investigations of removal did, so far, not reveal the local processes of surface removal and re-deposition and related limiting factors of the removal process. Only with this knowledge the optimisation of the discharges for nuclear fusion application will be possible.

The aim of this work is the investigation of the fundamental processes of co-deposit removal and hydrogen isotope recovery. The focus is put on carbon based co-deposits and the retention of deuterium in those. Thermo-chemical removal and plasma removal are chosen, as these are methods compatible with the special requirements of nuclear fusion devices. New models for both methods will be developed, based on the status of knowledge. The models will be tested with literature data. The new models will connect literature observations on the parameters influencing the removal rates, extending the present partial understanding to a complete picture. To benchmark the models new experiments, designed according to these models, will be conducted. Open questions revealed by the models will be investigated. Devices and sample analysis methods will be chosen and improved to provide the required experimental results. Dependencies revealed by the models will be compared with the new data and discussed. The parameters influencing the removal process and rate and with that the possibilities for removal optimisation in terms of speed and nuclear fusion requirements will be concluded. Based on the new data and understanding the aspects of technical limitations in application will be discussed and a nuclear fusion application scenario will be developed.

Section 2 presents the results of literature research on the investigated methods and the physical understanding necessary for the development of new models. In section 3 the experimental devices for sample preparation and exposure are introduced. Furthermore methods used to analyse the co-deposit properties and the removal success are described. In section 4 the new models for the description of the removal methods are derived and theoretical considerations and parameter studies are given. The experiments conducted for model validation are presented in section 5. The obtained results on removal rates are presented and compared to the models. The comparison yields the identification of the fundamental physics describing the removal methods. Considerations on the optimization and application of the tested methods lead to the conclusions in section 6. The section terminates with the outline of an integrated scenario for application in a fusion reactor, using the investigated methods. Based on this integrated scenario extrapolations to future fusion devices are calculated. A summary is given in the last section.

2 Physical basics and status of knowledge

2.1 Fuel retention in co-deposits by plasma-wall interaction

The hot and dense fusion plasma in the core of a tokamak or stellarator cannot be perfectly confined. This provides a high amount of energetic ions, neutral atoms and molecules to the plasma edge region, giving rise to a variety of physical and chemical processes with the surrounding materials. Compared to thermal energies, the high particle kinetic energy can induce additional processes. Areas with direct (line-of-sight) contact to the plasma are called plasma-wetted areas, while areas which are shadowed by other components from the plasma are called remote areas. The physical distinction is the composition and particle energy of the incident fluxes to these areas. The plasma wetted areas receive a broad range of particle kinetic energies, species and charge states. The remote areas on the other hand receive preferentially lower kinetic energy ion, neutral and radical fluxes, because particles can only reach them after surface or gas phase collisions. This leads to a relatively increased importance of chemical processes on remote areas.

The migration of material in tokamaks and stellarators is an unavoidable process. All surfaces are constantly bombarded with particles leading to implantation of these incident particles and also release of particles from the surfaces. The released particles migrate and can be deposited forming new material mixtures. These surfaces are also bombarded with particles, forming new solids and so on. In this process also hydrogen isotopes from the plasma can be incorporated, forming so-called co-deposits. Under these plasma deposition conditions material mixtures and amorphous material modifications occur. Amorphous materials do not have a long range order, but still feature short range orders based on the constituting elements bindings. Depending on several parameters, e.g. the growth rate, incident particle energy and species, surface temperature etc., the deposited solids can have different properties. Large amounts of hydrogen isotopes originating from the fusion plasma can be co-deposited, which poses additional safety and economy issues if tritium is used. Extrapolations show that, depending on the material choice for the plasma-facing components, the hydrogen isotope retention can reach levels of about 10% of the amount injected into the fusion plasma (Roth et al. 2008). This leads to severe issues for tritium self-sufficiency of a reactor and also conflicts with safety limits for the tritium inventory of the reactor. According to extrapolations for the future reactor ITER the inventory limit will be reached after about 10^5s of fusion plasma, see Figure 2. Co-deposition is for many materials by about one order of magnitude more effective in retaining hydrogen isotopes, compared to other effects as implantation and bulk diffusion. The hydrogen isotope retention issue is thus strongly related to co-deposition.

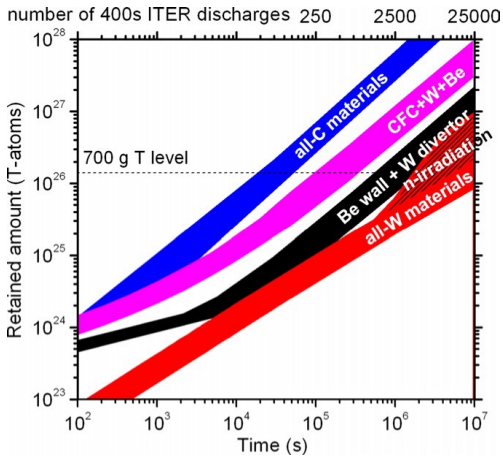

Figure 2: Tritium retention can become a critical issue after only a few hundred discharges in ITER, depending on the plasma-facing component materials. Figure from **(Roth et al. 2008)**.

2.2 Carbon co-deposits

Carbon is present in all fusion devices from different sources. Its chemistry with hydrogen makes it the most important element when considering hydrogen retention, since up to 50 atom% (H/C=1) of hydrogen was observed in carbon co-deposits. In a fusion device using carbon plasma-facing components, release from these materials is the main source of carbon in the device. The influx of CO_2 from atmospheric leakage, carbon admixtures in other materials, e.g. steels, or lubricants are additional, yet much smaller carbon sources. A large variety of ion, molecular and radical carbon compounds exists, e.g. CH_4, CH_3, $C_2H_2^+$. With surface sticking probabilities above 0 and below 100% these compounds can be transported to remote areas via surface collisions. Together with the carbon, hydrogen isotopes can be transported in these compounds, leading to observations of remote areas dominating the tritium retention in the JET tokamak (Coad et al. 2005). Elements not forming volatiles with hydrogen isotopes, e.g. tungsten, exhibit a fundamentally different behaviour of co-deposit formation. Non-volatile particles, e.g. metal atoms, released by the plasma contact usually have sticking coefficients close to 100%, inhibiting their transport to remote areas.

The chemistry of carbon and hydrogen isotopes is of high importance when considering the formation of carbon co-deposits in a fusion device. The variety of C-C and C-H bindings and stoichiometries gives rise to a wide space of possible co-deposit structures. In pure amorphous hydrogenated carbon (a-C:H) mixtures, carbon bonds (sp^3 diamond, sp^2 graphite), polymeric bonds with different hybridisation states (e.g. polyethylene $([CH_2]_n)$ sp^3, polybutadiene $([CH_2\text{-}CH]_n)$ sp^2+sp^3, polyacetylene $([CH]_n)$ sp^2) and voids can contribute to the effective material a-C:H and its structure and properties (Jacob and Möller 1993). This mixture will determine the ratio of hydrogen isotopes to carbon in the co-deposit (H/C), its hardness, density, optical properties, etc. and thus also the hydrogen retention of the layer

and the possibilities and rates of removal of these co-deposits. The freedom of these parameters is limited by physical constraints, leading to the distinction in two only roughly separated types: The soft, polymer like and the hard, diamond like a-C:H. Observations of material properties achieved und various deposition conditions (Figure 3) support this.

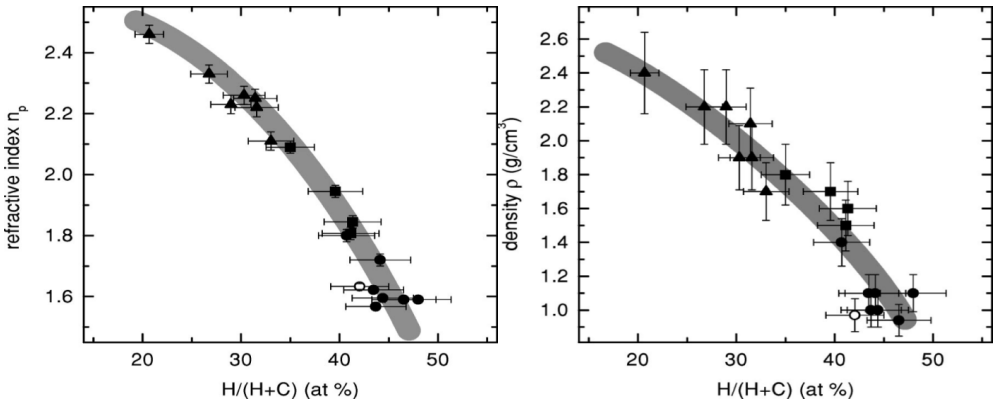

Figure 3: The accessible a-C:H properties are limited by physical constraints, all measured material properties are found to be in a corridor indicated by the grey band. The left-hand part of these corridors is related to hard a-C:H, while soft a-C:H is found on the right-hand part. Figures from **(Schwarz-Selinger, Keudell, and Jacob 1999)**.

The properties of a-C:H were seen to correlate with the deposition gas pressure, ion impact energy distribution, impact species, surface temperature during growth and growth speed (Robertson 2002). The growth physics is understood as a combination of several processes acting simultaneously, see Figure 4. Neutrals interact mostly with the surface by adsorption and subsequent chemical processes. The plasma ions, especially H^+ with its higher range compared to other ions, penetrate the surface into a depth of some nm. After thermalisation of the ions, molecules and bindings can form with the surrounding material. Hydrogen molecules formed inside the interaction layer leave it by diffusion. The layer grows by the combination of this sub-plantation of C and H ions and the surface reaction of radicals. Experimental evidence of a thin (1-2nm with 100eV impact energy) surface layer with a density and composition different to that of the bulk material supports this model (Robertson 2002).

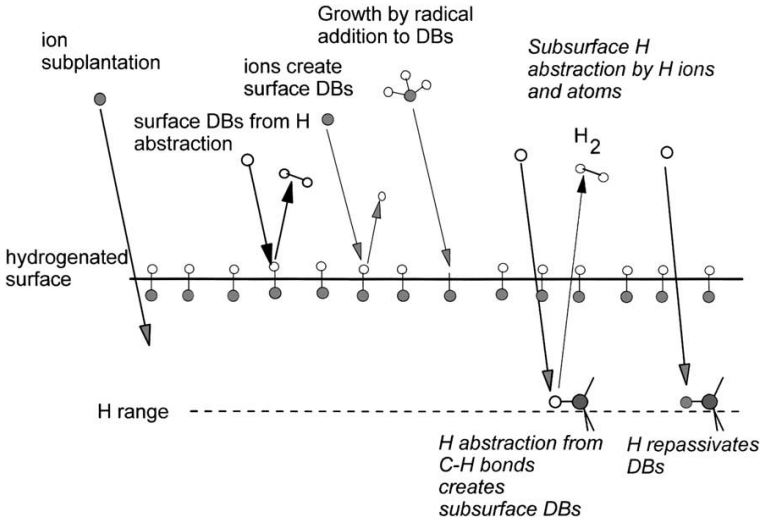

Figure 4: Component processes in the growth of a-C:H by plasma deposition. Carbon atoms in grey, hydrogen in white. DB: dangling bonds. Figure from **(Robertson 2002)**.

At deposition surface temperatures above about 200°C the diamond related sp^3 contribution strongly drops, because the growth of the metastable diamond, understood as a result of a high pressure region introduced by the sub-plantation process, becomes unfavourable. The H/C value drops monotonically with the ion impact energy, beginning at H/C≈1.2 at some eV to about H/C=0.4 at 1keV, for deposition at room temperature. The a-C:H density on the other hand has a maximum of about 2g/cm³ at around 300eV with lower values for higher and lower impact energies. A gas permeability of a-C:H only about 40-90% lower than that of polyethylene terephthalate was found (Vasquez-Borucki, Jacob, and Achete 2000). In this study soft layers showed a smaller permeability than hard layers. Whether this permeability can be attributed to the presence of nanopores or a high bulk diffusivity, and whether also an uptake of gas, as observed for many polymers, is possible, is so far unclear.

From the above observations it can be concluded that layers deposited in plasma-wetted and remote areas of a fusion device will exhibit different properties. Remote area co-deposits will face a higher radical fraction, lower ion impact energies and surface temperatures compared to plasma-wetted areas. This leads to soft a-C:H with H/C≈1 compared to the plasma-wetted co-deposits, which will probably be in the class of hard a-C:H with H/C≈0.4, according to the current understanding. For the topic of hydrogen isotope retention the co-deposits on remote areas will thus be more relevant, due to their higher hydrogen content. Observations on the tritium retention in JET support this assumption. In tokamaks carbon-based dust, produced by co-deposit fragmentation was additionally observed as a hydrogen retention mechanism in remote areas. An outgassing of hydrogen from a-C:H was not observed below 350°C (Robertson 2002) making hydrogen recovery from a-C:H by heating in vacuum an insufficient solution for technical application.

2.3 Thermo-chemical removal of carbon co-deposits

Thermo-chemical removal of carbon based co-deposits (a-C:H) was intensively studied, especially with O_2 as reactive gas. First investigations with alternative reactive gases, e.g. NO_2, were conducted (Alegre et al. 2013). The experimental investigation of the alternative reactive gases did, so far, not reach the same quality as for O_2. More data are required on the influence of gas pressure, surface temperature and co-deposit properties to conclude whether the physics of removal are similar to O_2.

The relation between removal rate and surface temperature was studied independently for the removal of the hydrogen/deuterium and the carbon component. Different removal rates were observed (Figure 5). The relation was found to follow the Arrhenius behaviour. The Arrhenius equation describes the reaction rates of thermally activated processes. The figures show two different Arrhenius behaviours in the tested temperature range for both constituents, indicating that different processes are dominating in the high and low temperature region. The slope in the high temperature region is smaller than the one in the low temperature region.

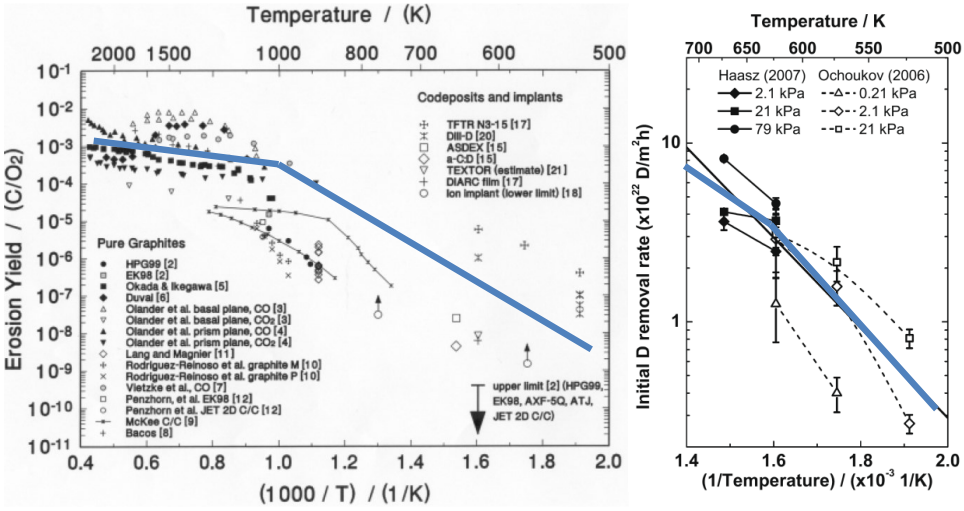

Figure 5: Arrhenius plot of the removal rate of carbon (left) and deuterium (right) by O_2. Carbon data were normalized to a value depending on the gas pressure during removal. Blue lines were added to indicate zones of different apparent activation energies, for explanation see section 4.1. Figures from **(Davis and Haasz 2001)** and **(Davis and Haasz 2009)**.

The effect of reactive gas pressure on the removal rate was investigated in (Ochoukov, Haasz, and Davis 2006). Co-deposits from two tokamaks were exposed to O_2 at three different temperatures. At low pressure the removal rate increased with pressure, but saturation was observed at higher pressures, see Figure 6. The behaviour was similar in all cases.

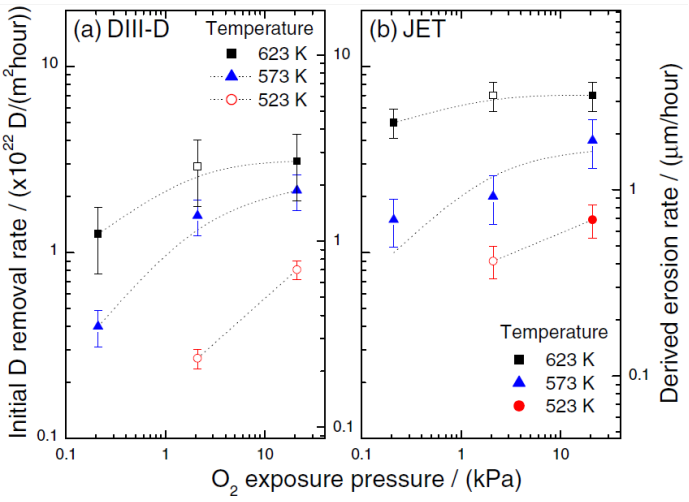

Figure 6: Pressure relation of the TCR removal rate with co-deposits from two different tokamaks at three different surface temperatures. Figure from **(Ochoukov, Haasz, and Davis 2006)**.

The relation of the removal rate to co-deposit inventory, which is with constant density proportional to its thickness, was studied. A linear relation was found and confirmed at several removal temperatures. Tokamak co-deposit inventories spanning two orders of magnitude were investigated (Figure 7). The relation was found to agree with the data in all points. It was concluded that TCR is a volume process, attacking the whole co-deposit at once.

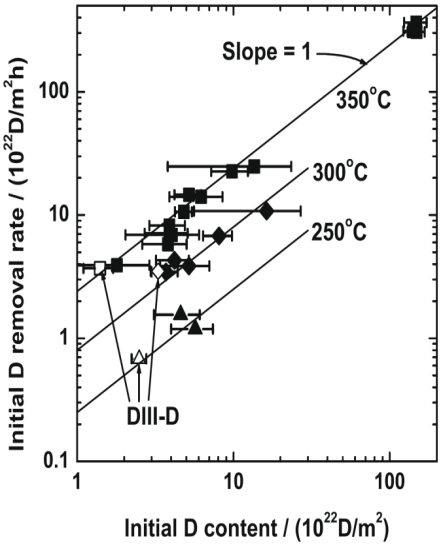

Figure 7: Removal rate of tokamak carbon co-deposits by O_2-TCR in relation to the initial deuterium inventory (proportional to co-deposit thickness). The lines indicate the behaviour of a volume process, where the removal rate is proportional to the inventory. Figure from **(Davis and Haasz 2009)**.

In several studies the time evolution of the removal rate was seen to exponentially decrease towards the complete removal of the co-deposits, e.g. (Haasz and Davis 1998; Alegre et al. 2013). A model on the time evolution of the removal rate was presented in (Wang, Jacob, and Roth 1997). The model was based on two processes. An oxidation layer forms in the top zone of the co-deposits, which expands with time. The removal rate increases by reactions throughout the volume of this oxidation layer. After a certain time, when the oxidation layer expands through the whole co-deposit, a maximum is reached. The final stage of removal is dominated by the co-deposit, and with that oxidation layer, thickness reduction and a corresponding removal rate decrease. The formation of such an oxygen loaded zone by TCR was found, as depicted in Figure 8.

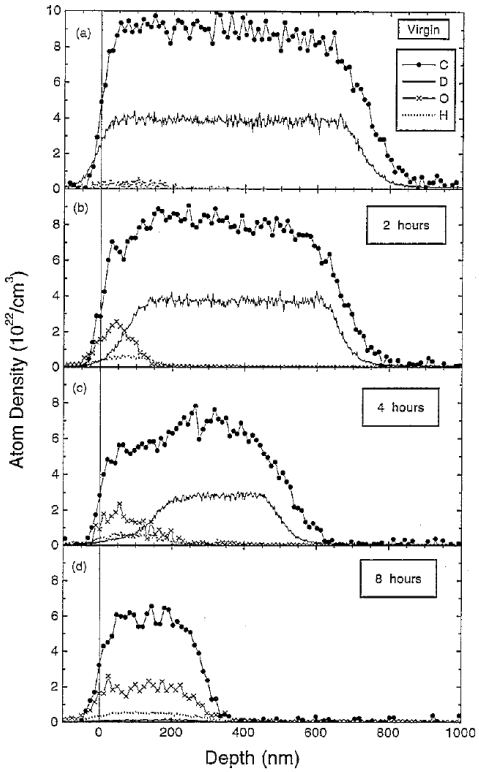

Figure 8: Air-TCR of an a-C:D layer. The layer composition was investigated in four time steps. The formation of an oxidation zone was found.This zone digs through the layer, reducing its thickness and content. Figure from **(Wang, Jacob, and Roth 1997)**.

2.4 Physical chemistry of removal by reaction-diffusion processes

The hydrogen recovery approach of thermo-chemical removal relies on the interaction of a reactive, neutral gas with heated co-deposits. Physical basics required for the investigations in this work are discussed in this section. The chemical reaction of a neutral gas with a solid involves several sub processes (Czeslik, Semann, and Winter 2007). In neutral gases the particle transport is given by diffusion and convection. As convection requires density gradients of the neutral gas it can be neglected in fusion device application. Diffusion is described by Fick`s law. The particle flux density *J* by diffusion is given by the gradient of the concentration *c* of the investigated species along spatial direction *x* and the diffusion coefficient *D*

$$J = -D * \frac{dc}{dx} \tag{5}$$

Assuming conservation of mass, the temporal change of the concentration by diffusion can

be calculated, yielding Fick`s second law. With the assumption of a constant diffusion coefficient the equation simplifies to

$$\frac{dc}{dt} = D * \frac{d^2c}{dx^2} \tag{6}$$

Chemical reaction rates of solids, liquids and gases are typically limited by the low kinetic energy of the involved particles. The reaction partners are usually bound in compounds. The bonds of these compounds have to be broken prior to the formation of new compounds. The energy necessary to overcome this activation potential E_A is provided by the thermal energy $k_B T_S$. Thermally activated reaction rates k are described by the Arrhenius equation

$$k = \sigma * \sqrt{\frac{\pi k_B T_S}{2m_P}} * e^{-\frac{E_A}{k_B T_S}} \tag{7}$$

This equation takes into account the exponential high energy tail of the Maxwell velocity distribution, a reaction cross-section σ and a collision frequency (particle mass m_P). Only high energy particles can overcome the reaction barrier E_A, yielding the exponential relation to the thermal energy.

Gas-solid reactions always involve the interaction of the gas with the solids surface. This interaction can be based on physical (e.g. Van-der-Waals) and chemical (e.g. covalent) interaction and strongly depends on both interaction partner species. The interaction potential binds gas particles to the surface, if it is attractive. Depending on the potential strength and the thermal energy surface bound species desorb after a certain time. This competition of adsorption and desorption leads to an equilibrium surface occupation by a gas, given by the balance of its surface residence time, the influx rate (defined by the gas pressure p_{Gas}) and the desorption rate. This equilibrium can be described by the Langmuir adsorption isotherm for an adsorption limited to a monolayer of surface adsorbed particles

$$L_L(p_{Gas}) = \frac{q_{Max} K_L p_{Gas}}{1 + K_L p_{Gas}} \tag{8}$$

The adsorption coefficients K_L and q_{Max} depend on the interaction potentials between the gas and the solid and the thermal energy. At higher adsorption densities, several layers of adsorbed particles will form. This case can be described by the Brunauer-Emmett-Teller (BET) isotherm (Roque-Malherbe 2007)

$$L_{BET}(p_{Gas}) = \frac{q_{Max} * K_{BET} * p_{Gas}}{(p_{Sat} - p_{Gas}) * (1 + \frac{(K_{BET} - 1)p_{Gas}}{p_{Sat}})} \tag{9}$$

In steady-state (constant gas concentration) the diffusive influx to the reaction zone is

balanced by the reactive loss to exhaust particles. The equilibrium gas concentration resulting in such a process is given by its reaction-diffusion equation

$$\frac{d^2c}{dx^2} = k * c \tag{10}$$

2.5 Physics of high frequency heated removal plasmas

Plasma is the 4th state of matter, bearing distinct properties. The thermal energy of the particles leads to a relevant amount of ionization of the base gas and thus to production of free ions and electrons, constituting the plasma. These components, in contrast to neutral particles, interact with electric and magnetic fields and generate those fields themselves. Especially in magnetic confinement nuclear fusion energy research it became obvious, that the dynamics of plasmas can be very complicated, depending on the plasma parameters, its geometry and the involved electromagnetic fields. The removal plasmas under investigation in this work are much simpler than magnetic confinement nuclear fusion plasmas. Neither plasma current is present in the removal plasmas nor any heating besides the high frequency coupling. This induces lower plasma particle and energy confinement compared to fusion plasmas. The description still requires a set of simplifications of the plasma dynamics to make them accessible for physical understanding.

A plasma can have a temperature, similar to the other states of matter, but since plasmas can receive heat input also by electromagnetic means and they consists of electron and ion species the temperature is more difficult to define. Each species can have its own temperature, which can differ from those of the other species, if collisional equilibration is slow compared to the lifetime of the individual plasma particles. Furthermore, heating can be limited, e.g. by high-frequency electromagnetic wave heating, to individual species. Very often (especially in the plasmas used in this work) these are the electrons, due to their at least 1836-fold lower mass than all ion species and with that higher susceptibility to varying electromagnetic fields.

Due to this small mass the electrons are, at similar thermal energies of the plasma species, also the fastest species in terms of velocity and thus contribute most to particle fluxes. In plasmas not confined by magnetic fields or along the magnetic field lines in confined plasmas, the electron flux will be larger than the ion flux. At a wall contact area the faster loss of electrons will charge up the plasma. To maintain the quasi-neutrality of the plasma, the ambipolar flux of ions and electrons to the walls has to be equalized. As negative charge depletes in the plasma, electrons get repelled by the electric field arranging between plasma and walls, while ions increase in speed and flux to the walls. A self-organized system evolves close to the wall, where a constant negative potential between plasma and wall is established in a way that positive ion and negative electron fluxes to the wall are equal, called the plasma sheath (Stangeby 2000). As the plasma-wall interactions are determined by the ion impact energy, this sheath and its ion acceleration effect is of great importance.

Inter-particle collisions, radiation and contact to surrounding walls provide effective sinks for plasma particles and the energy stored in the plasma. All laboratory plasmas are limited by walls, which act as a perfect drain for charged particles. Plasmas thus have to be continuously heated in order to exist in timescales longer than the plasma confinement time. Heating acts as a plasma source, due to the conversion of neutrals to plasma particles (ionisation). Together with the sinks this causes gradients of temperature and density in the plasma. The particle and heat transport coefficients are defined by stochastic movement, collisions and turbulences inside the plasma. By magnetic confinement of plasmas, the stochastic motion present in neutral gases and unconfined plasmas is restricted to a gyro-motion along the magnetic field lines. The gyration radius, also known as the Larmor radius r_L, is given by the particle mass m, its velocity in the plane perpendicular to the field line $v_\perp$, its charge state q and the magnetic field strength B.

$$\mathrm{r_L} = \frac{m v_\perp}{qB} \tag{11}$$

According to this gyro-motion the Bohm diffusion coefficient D_B for cross-field diffusion of electrons and ions can be formulated as (Stangeby 2000):

$$\mathrm{D_B} \propto \frac{k_B T}{e\, B} \tag{12}$$

with the Boltzmann constant k_B and the plasma species temperature T. In the approximation of purely diffusive transport, the plasma density will decay from the zone of heating (source) to the walls (sink), with a coefficient depending on the plasma temperature and magnetic field. The fundamental solution of the diffusion equation yields an exponential decay profile of density and temperature.

The impact of plasma particles to the wall of a nuclear fusion vessel has several unwanted aspects. Resulting processes are the migration of material, co-deposition of plasma species or implantation of impurities. To recover from those unwanted plasma-wall interaction effects, conditioning and removal plasmas can be applied. For conditioning plasmas, a higher degree of freedom with respect to the choice of plasma parameters is available than in a nuclear fusion plasma. By applying specific plasma temperatures, densities and ion species, the plasma-wall interaction can be altered to recover from the detrimental effects mentioned above. By exploiting chemical effects, specific elements, e.g. oxygen, carbon or hydrogen, can be removed from the vessel walls, while others, e.g. the plasma-facing components, stay relatively unaffected. Released volatile species, especially hydrogen isotopes, can be pumped out of the vessel and recovered.

At the current status of knowledge, the use of superconductors to provide magnetic fields in reactor size fusion devices is mandatory to achieve a net power gain from a tokamak or stellarator. Technical constraints in this technology do not allow for quick shut-down of the magnetic fields, which also constrains the application of conditioning and removal

techniques. Glow discharge plasmas are incompatible with magnetic fields perpendicular to their electric fields (Wauters 2011). Removal plasmas analysed in this work are, because of their compatibility with magnetic fields, electron cyclotron (ECR) and ion cyclotron frequency range plasmas (ICRF). ICRF heated plasmas intended for conditioning and removal are also called ion cyclotron wall conditioning (ICWC) plasmas. The presence of magnetic fields can be expected to lead to a higher similarity of the plasma-surface contact between nuclear fusion and ECR and ICWC discharges compared to glow discharges. This would result in an improved conditioning efficiency of ECR and ICWC plasmas, since glow discharges can leave relevant surfaces unaffected. Technical reasons allow higher input power in anode free plasmas and also the implementation in a magnetic confinement nuclear fusion device is easier, since ECR and/or ICRF generators and antennas are included in most designs for fusion plasma operation. These points significantly favour the application of resonance frequency range heated plasmas over glow discharges.

Several studies were conducted to improve the understanding of resonance frequency range heated plasmas intended for removal and conditioning, see especially (Wauters 2011). These plasmas can be used for wall conditioning of the plasma chamber, i.e. reducing the impurity influx originating from the plasma-wall contact during fusion plasmas. Conditioning and co-deposit removal both rely on the removal of specific constituents (impurities or hydrogen isotopes) from materials using the same physical mechanism. The reservoirs to deplete are usually much larger for co-deposit removal than for conditioning, though. Because of the similar physics both terms are used synonymic in this work. In the frame of (Wauters 2011) a computer model was developed to describe removal plasmas. The model simplifies the plasma to a zero dimensional object, where a given amount of power is coupled into a fixed volume with given magnetic field strength and neutral gas pressure. All possible elastic and inelastic processes of electrons, ions, atomic and molecular neutrals and the confinement of these are taken into account, defining the loss channels for plasma particles and power. Plasma temperature and density and the degree of ionisation of the gas develop according to the balance of input power and power losses. So far the code includes rate coefficients for hydrogen and helium species. Other species, especially carbon, can be treated as a dilute contribution (impurity) with a power loss factor. The values of electron collision power losses with H, He, C and O and the plasma temperature are shown in Figure 9. At electron temperatures in the range of 3eV, which are typical for removal plasmas due to the onset of significant collisional cross-sections, the power loss values differ by orders of magnitude between the four species.

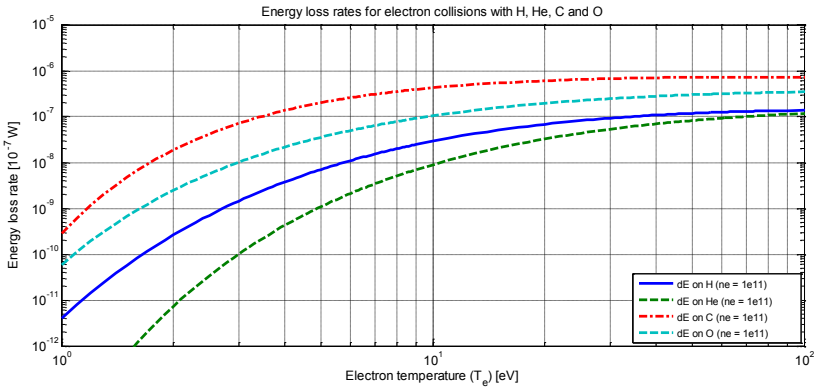

Figure 9: Total electron cooling rate for electron collisions with H, He, C and O as a function of electron temperature at a plasma density of $10^{11}/cm^3$ **(Wauters et al. 2011)**.

2.5.1 Ion-surface interaction by physical and chemical sputtering

The primary removal effect in removal plasmas is the process of material release by ion-surface interaction, called sputtering. Removal by sputtering requires impact energies of the incident particles of at least some eV, in contrast to thermo-chemical removal where only some ten meV are necessary. Sputtering becomes possible, if the energy transferred to surface bound particles is larger than the surface binding energy of the released particles. This kinetic energy can be provided by plasmas. Due to the limited range of ions in solids sputtering by removal plasmas only affects a shallow surface region (in this work up to 5nm). Reactions only take place in this ion interaction zone so the removal rate of co-deposits cannot depend on the co-deposit thickness, if they are thicker than the interaction zone.

One of the mechanisms of sputtering is called physical sputtering (Behrisch 2007). It is understood as a collision cascade between projectile and target particles, where the target particles are part of a solid before the collision and are released from the solid by the direct or follow-up collisions with the projectile. In nuclear fusion context, mainly the collision of a fast particle from the plasma with wall material is considered. The yield of this process, the amount of released particles per impact particle, has strong energy and incidence angle dependences. The yield increases by orders of magnitude from energies below eV up to a maximum, when the ion´s kinetic energy is sufficient to induce energetic collision cascades. At energies above this maximum an increasing share of the struck particles is too deep in the solid to leave it.

Chemical sputtering adds to physical sputtering for special combinations of incident particles and targets. The most common example is the bombardment of carbon with hydrogen isotope ions (Behrisch 2007), see Figure 10 for the combinations most important for this work. For the increased sputtering yield due to chemical sputtering a chemical interaction between the constituents and the formation of volatile products is necessary. These volatiles are formed in the ion interaction zone and leave the material by desorption. The chemical

reactions and product diffusion have temperature dependencies, leading to a temperature dependent chemical sputtering yield. The impact energy dependence of chemical sputtering has a broad plateau with a decrease of the chemical contribution to the yield at high energies (> some 100eV). This decrease is compensated by the onset of physical sputtering. At energies in the range of the chemical binding strength (<10eV) chemical sputtering can have a low energy threshold (Dadras and Krstic 2011). A primary angular dependence does not exist, since recoil movement is not important for chemical sputtering. It has been observed, that diffusion processes can be important for the actual release of volatiles (Behrisch 2007). At higher impact energies, when also the penetration depth is higher, a strong maximum with the solid´s temperature is observed. The yield can increase by about a factor of 10 between 500K and 800K for H on C erosion. This can be attributed to the diffusion of volatiles (most important products are C_xH_y) from the ion-penetration depth to the surface, which is significantly faster at higher temperatures. At even higher temperatures, the hydrogen density in the material decreases due to thermal desorption of hydrogen molecules and thus also the chemical reaction rate and yield decrease.

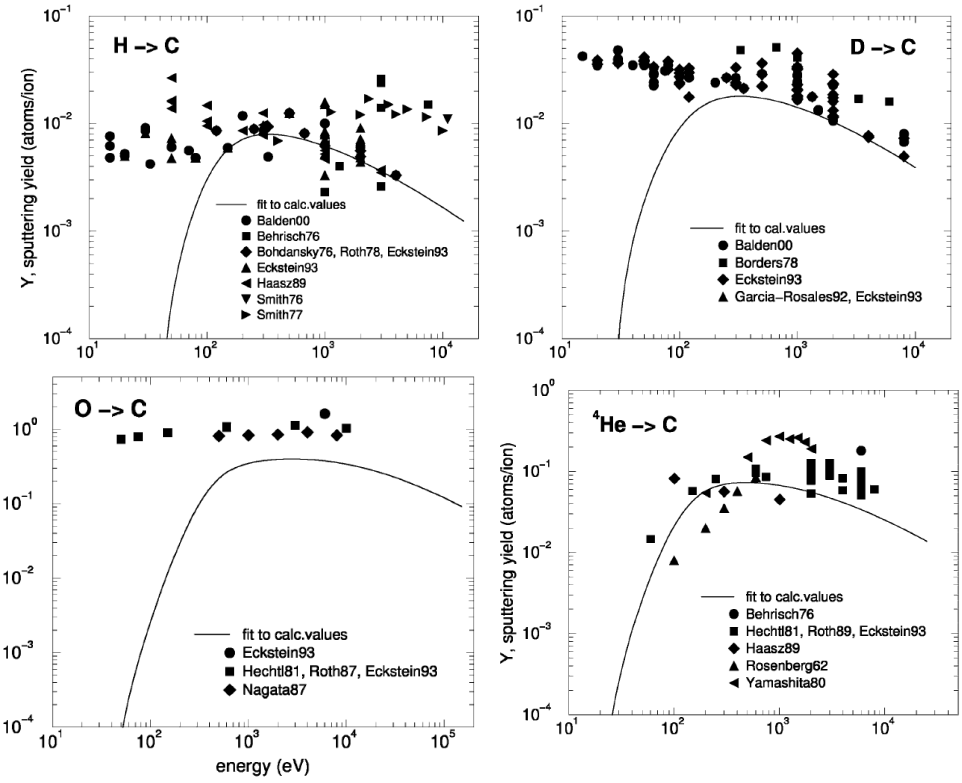

Figure 10: Carbon sputtering yields relevant for this work, figures from **(Behrisch 2007)**. The solid lines are modelling results for the physical sputtering contribution. The solid symbols represent experimental data (chemical + physical sputtering). While for the chemically active species H, D, O the yields deviate significantly at low energies, the chemically inert helium yields are well described by the model.

The simulation of physical sputtering and the calculation of its yields is possible with the binary collision approximation. In this approximation only two particle collisions are considered to be relevant for the actual sputtering process. By applying a Monte-Carlo method, incident particles are fired, with given initial speed and angle, to a surface consisting of the target particle mix. The primary particle collides with the targets and transfers energy according to momentum and energy conservation. The secondary particles can induce further collisions forming a cascade process. If a particle reaches the surface with a kinetic energy component perpendicular to the surface larger than the surface binding energy it is lost and counted as sputtered particle. The software SDTrim.SP (Mutzke et al. 2011) implements this physical concept and is used for the simulations presented in this work. The dynamic change of the target composition by implanted projectiles and preferential sputtering of species with higher yield is taken into account in all simulations. The approximation is very successful in describing experimental observations in the domain of physical sputtering, while for chemical sputtering literature values provided by experiments or molecular dynamics calculations have to be used.

2.5.2 Global gas balance studies

The removal of co-deposits and hydrogen isotopes by plasmas was studied by experimental means of global mass spectrometric gas analysis and optical spectroscopy in several fusion devices. Hydrogen isotope removal was mainly studied with the intention of isotope exchange, e.g. D to H, of the hydrogen isotopes retained in the fusion vessel walls. The isotope exchange includes only the small inventories present in the ion interaction zone of the surfaces. Since plasma removal only affects this zone, the physics of isotope exchange and removal is the same. The continuous removal of H from the wall surfaces and its substitution by D by D_2-ICWC was observed in the JET tokamak, see Figure 11.

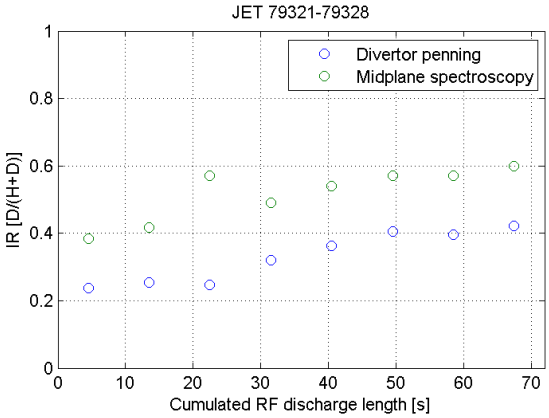

Figure 11: Isotopic exchange from H to D in the JET tokamak using D_2-ICWC removal plasmas. The intensity ratio (IR) of D to H line radiation increased in the course of a series of discharges at two observation positions (green and blue). Figure from **(Wauters 2011)**.

Several base gases, e.g. NH_3, O_2, H_2, for the removal plasmas were tested (Sergienko et al. 2009). It was observed that the partial pressures of removal product species rise during the

discharge up to a saturation value (Wauters 2011). After ending the discharge a further increase of the partial pressure was observed, combined with a decay related to pumping, see Figure 12. The pressure increase after the plasma discharge was attributed to an outgassing of the species implanted into the surfaces by the plasma. The devices pumping speed and the partial pressures of exhaust products, were identified as limiting factors for the global removal rates (Wauters 2011; Douai et al. 2011).

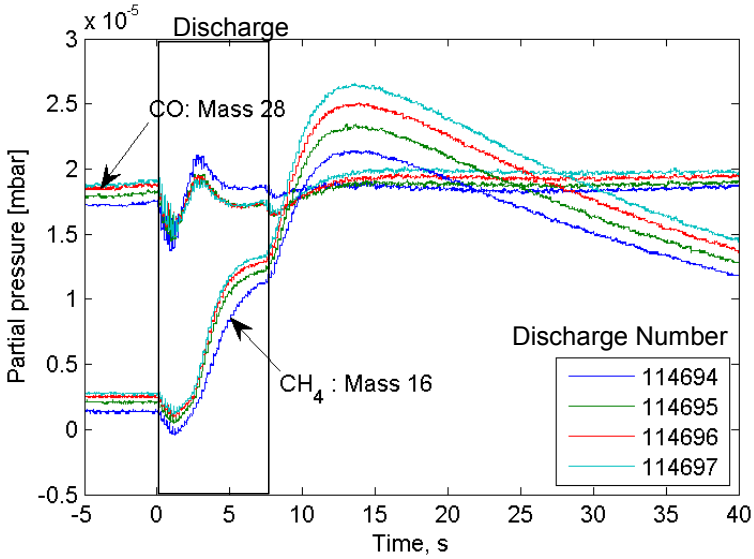

Figure 12: Evolution of partial pressures of methane and carbon monoxide during four consecutive H_2-ICWC discharges in TEXTOR. The methane pressure increased during the discharges (grey zone) reaching a saturation value defined by the balance of surface release vs. pumping + re-deposition. After the discharges the gas balance is defined by different processes. The methane levels increase with discharge number. Figure from **(Wauters 2011)**.

2.5.3 Effects of geometry

In magnetized plasmas electrical potentials E develop inside structured surfaces due to the magnetic field and the plasma sheath. This leads to $E \times B$ forces guiding particles inside the gaps of the structured surfaces (Dejarnac et al. 2008). This preferential movement affects the distribution of flux densities and incidence angles of the ions in the structured surfaces, which is important when considering deposition and sputtering yields in the gaps. In (Schulz et al. 2011) the removal in gaps was investigated experimentally, also in differential view of magnetized high-frequency heated and glow-discharge plasmas. A removal effect in rectangular trenches to a depth in the order of the ion larmor radius was found in the high-frequency heated plasmas, while for glow discharges only the surfaces parallel to the vessel wall were affected. This aspect of plasma removal will not be treated in this work, but has to be mentioned for a complete picture of its physical and technical aspects.

The tokamak geometry and magnetic field configuration of removal plasmas give rise to charged particle drifts in the vertical and horizontal directions, altering the spatial distribution of the plasma particles. The particle drift velocity due to a gradient ∇B_T of the toroidal magnetic field B_T in a tokamak is given by (Wesson 2004):

$$v_{\nabla B} = -\rho_L * \frac{\nabla B_T}{B_T} * v_\perp = -\frac{m}{q} * \frac{\nabla B_T}{{B_T}^2} * v_\perp^2 = -\frac{\nabla B_T}{{B_T}^2} * \frac{8 k_B T}{\pi\, q} \tag{13}$$

The perpendicular velocity $v_\perp$ was assumed to be Maxwell-distributed. The associated current density is obtained by multiplying velocity and charged particle density *n*

$$I_{\nabla B} = -e * n * \frac{\nabla B_T}{{B_T}^2} * \frac{8 k_B T}{\pi\, q} = -n * \frac{\nabla B_T}{{B_T}^2} * \frac{8 k_B T}{\pi\, z} \tag{14}$$

This current is independent of the particle mass and opposite in direction for electrons (z=-1) and ions (z≥1) and will lead to a charge separation in conditioning plasmas, since in contrast to fusion plasmas no poloidal field component is present. Besides the gradient drift, a curvature drift I_{curv} is present with a drift velocity described by the same equation as the gradient drift but with the parallel instead of the perpendicular velocity. Assuming a direction independent velocity distribution the total vertical current density is (Wesson 2004)

$$I_V = 2 * I_{curv} + I_{\nabla B} = -24 n * \frac{\nabla B_T}{{B_T}^2} * \frac{k_B T}{\pi\, z} \tag{15}$$

This charge separating current generates a vertical electrical field *E* in the vessel, producing an $E \times B$ force acting outwards

$$v_{ExB} = \frac{E \times B}{B^2} \tag{16}$$

The combination of these drifts gives rise to small density gradients to produce fluxes balancing the drift fluxes. The highest electron density is expected in the top low-field side and the highest ion density in the bottom low-field side, depending on the magnetic field polarisation, respectively (see Figure 13).

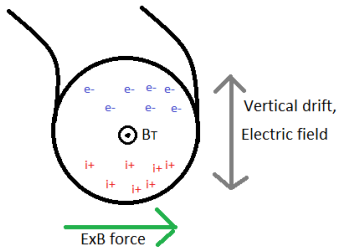

Figure 13: Tokamak geometry is producing density gradients and charge separation in removal plasmas. Ions and electrons are separated and pushed outwards.

3 Experimental arrangements

3.1 Multi-purpose vacuum chamber PADOS

For the experimental verification of the models developed in this work, reproducible co-deposits and sample exposure to TCR in a well-defined vacuum vessel are necessary. The cylindrical vacuum chamber PADOS (Figure 14) is adapted to provide two distinct operational scenarios for a-C:H deposition and TCR. In order to reduce the influence of varying co-deposit properties on the experimental results, a method for producing large numbers of identical co-deposit layers on substrates is developed. For TCR pure gases (>99.5%) and constant conditions are used to obtain clear experimental results.

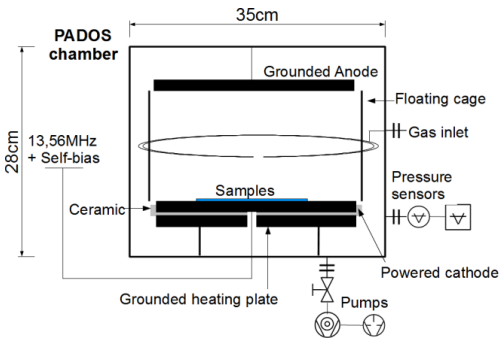

Figure 14: Schematic sketch of the PADOS chamber and the attached devices used for deposition and TCR experiments. Two configurations can be employed by changing the lower plates. Figure from **(Möller et al. 2014)**

Plasma-Enhanced Chemical Vapor Deposition (PECVD) is chosen as it is a laboratory method for producing a-C:H layers with structural properties similar to co-deposits growing in tokamaks. Constant co-deposit properties can be achieved by applying constant gas pressure, bias voltage (and with that ion impact energy) and surface temperature (Robertson 2002). These parameters are chosen as close as possible to tokamak conditions, yet the conditions still differ significantly in some points, especially the deposition rate. The configuration shown in Figure 14 employs a capacitively coupled, parallel plate plasma discharge. The lower electrode is powered by a 600W, 13.56MHz radio-frequency generator, operated to provide a constant self-bias voltage to the powered electrode. Impedance matching of the power coupling is done by a computer controlled matching network, achieving >95% coupling. The frequency of the applied capacitive discharge is high enough to leave the ions unheated and couple the power only to the plasma electrons. The ambipolar plasma flux induces a negative voltage, the self-bias, which biases the powered electrode. The ions are attracted by this voltage, providing their kinetic impact energy on the samples. The self-bias voltage is measured across a coupling capacitor in the input line. The powered electrode is covered from underneath by an isolating ceramic and the grounded heating plate to prevent plasma production at its backside. Via this plate the samples can also be heated to provide a defined surface temperature during deposition, measured by a type-K thermocouple. The upper electrode and the vacuum vessel are grounded. A floating cage restricts the lateral extent of the plasma. Gas is injected via up to three mass flow controllers. A 28 l/s turbo-molecular pump balances the constant gas influx during

deposition, resulting in a fixed neutral gas pressure. During the discharges the absolute pressure is monitored by a baratron pressure transmitter with a range of 0.2 to 10^{-4}mbar.

The second configuration, used for thermo-chemical removal experiments, is obtained by removing the powered cathode and the ceramic isolator. The polished stainless steel heating plate was free of deposition, which only occurred on the cathode and ceramics plates. This prevents exposure of unintentionally introduced carbon layers possibly affecting the intended exposure. The plate can be heated by a resistive wire up to 1000K. The plate temperature is monitored with a type-K thermocouple. The samples are placed directly on the heating plate. Prior to inserting reactive gas into the chamber, the chamber is evacuated to its base pressure of 10^{-6}mbar. During pump-down the samples are heated to the targeted exposure temperature, in order to desorb surface attached impurities. When base pressure and exposure temperature are reached, the pumping valve is closed and the gas inserted. The pressure is monitored by two baratron absolute pressure gauges in the range of 1000 to 0.1mbar. A leak rate of $7*10^{-5}$mbar/s is observed, which blends the reactive gas with air. The resulting partial pressure of air is negligible compared to that of the reactive gas.

3.2 Toroidal magnetic plasma devices TOMAS and TEXTOR

TOMAS is a laboratory scale (major radius R=0.78m, plasma radius r=0.262m) plasma device to generate magnetized, toroidal plasmas. The vacuum vessel and plasma facing wall is made of stainless steel with a torus volume of 1.06m³. 16 actively cooled copper coils produce a toroidal magnetic field of up to 0.12T at 2kA coil current. Conditions similar to high frequency heated plasmas in tokamaks can be generated to test removal and conditioning plasmas. The plasmas run continuously, allowing reaching a certain exposure time faster than in TEXTOR. The versatile device is equipped with a load lock for sample exchange to allow fast pump-down. Samples were inserted via a rod into the plasma on the central plasma axis. Feed-throughs for temperature measurement, sample heating and

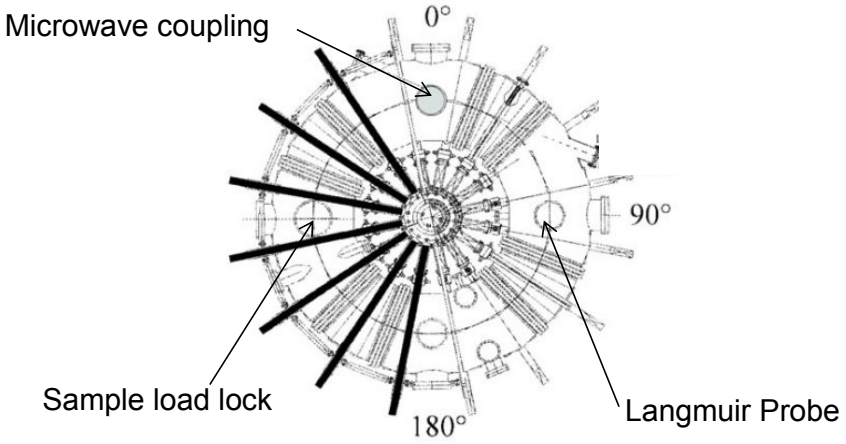

Figure 15: Schematic drawing of the toroidal magnetic plasma chamber TOMAS and the position of samples, Langmuir probe and microwave coupling. Thick black lines give exemplary coil positions.

diagnostics were attached to the rod. The rod can be on vessel or floating potential. Figure 15 shows a device schematic diagram.

The vacuum system employs a 3-stage pumping system with a turbo-molecular pump of 2.2m³/s nominal N_2 pumping speed. A base pressure of 10^{-7}mbar was reached. A 3-channel gas inlet system controlled by individual electronic mass flow controllers was connected to the device. The neutral gas pressure was measured by a penning cold-cathode gauge for pressures <10^{-3}mbar and a 3-stage baratron system with a total range of 2000 to 10^{-5}mbar. For plasma generation and heating a 2kW microwave generator of 2.45GHz was attached to the vacuum chamber by an air waveguide and a cooled coupling window. In contrast to a tokamak no additional magnetic fields or plasma currents can be applied. A Langmuir probe and a mass spectrometer were attached to the device for plasma and gas diagnostic.

TEXTOR (Neubauer et al. 2005) is a limiter tokamak of large plasma radius R=1.75m, minor plasma radius r=0.475m and a plasma volume of 7.8m³. The chamber and plasma volume have a circular poloidal cross-section. All plasma facing components are made of carbon fiber ceramics, the liner (r=0.55m) is made of stainless steel. The device is equipped with 16 toroidal field copper coils capable of generating up to 3T toroidal magnetic field. Additional coils for the generation of vertical and radial fields are available. Three limiter groups are positioned around the plasma volume. The toroidal belt limiter called ALT is positioned at r=0.48m. The ALT consists of 8 blades each equipped with a turbo-molecular pump. The pumps yield a total pumping speed, calculated from partial pressure fall-off times of mass spectrometry, of 2.07m³/s (D_2), 0.96m³/s (NH_3) and 0.86m³/s (N_2). The total plasma wetted area of the ALT is 3.4m². The high field side is covered by the DED limiter on an area of 11m² at r=0.477m. The main limiter at r=0.475m is the poloidal limiter with structures on the top and bottom of the vessel and a total area of 2m². Samples can be inserted via two load locks, so-called limiter locks. The limiter locks are equipped with various feed-throughs as in TOMAS. Additionally the radial position *r* of the sample holders can be electronically adjusted. Limiter lock 1 is located at the bottom of the vessel and limiter lock 3 on the top. Schematics diagrams of the TEXTOR vessel, showing the positions of the relevant systems, are given in Figure 16.

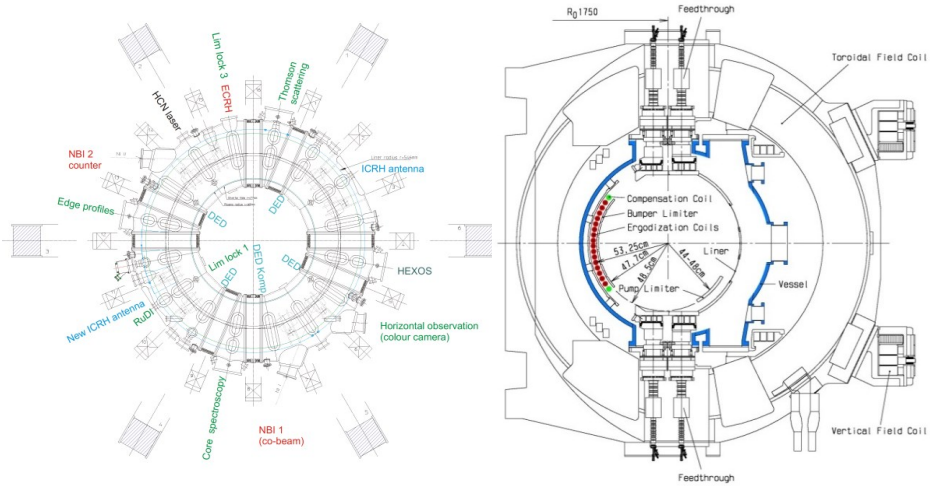

Figure 16: TEXTOR vessel and position of experimental arrangements (Lim lock 1 and 3), plasma-facing structures and ICRH antennas used for ICWC plasma generation. Top view on the left image and a poloidal cut (Figure from **(Giesen et al. 1997)**) on the right image.

3.2.1 Langmuir probe diagnostics

For the determination of the plasma temperature, density and ion flux of the removal discharges in TOMAS and TEXTOR Langmuir probes are applied. A Langmuir probe collects information about plasmas it is brought in contact with, by collecting a voltage-dependent current. The collected current is determined by the volume density and velocity distribution of electrons and ions in the plasma and the resulting fluxes. For the determination of the plasma parameters from the current-voltage characteristics probe theories from (Piel 2010) and (Stangeby 2000) were used. The current-voltage characteristics of a Langmuir probe can be divided into three regions, the ion saturation region, the transition region and the electron saturation region, as shown in Figure 17.

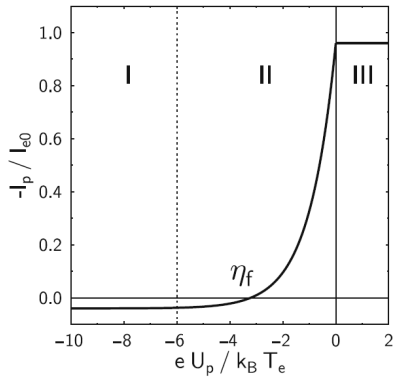

Figure 17: Normalized current-voltage characteristics of a flat surface Langmuir probe, figure from **(Piel 2010)**. With ion saturation (I), transition (II) and electron saturation (III) regions.

In the ion saturation region the negative voltage applied to the probe is high enough to repel roughly all incoming electrons, while attracting as many ions as the plasma can deliver. In the ideal case the corresponding areal current density I_{sat} is

$$\mathrm{I_{sat}} = 0.61 * n_{i0}\sqrt{k_B * T_e/m_i} \tag{17}$$

With the typical plasma temperatures T_e≈3eV achieved in the plasmas applied in this work, see section 4.2.1, a voltage >20V is sufficient to reach this region. The ion saturation current I_{Isat} can be retrieved from the intersection of a linear fit to the ion saturation region with the voltage axis ($U=0$)

$$\mathrm{I(U)} = a * U + I_{Isat} \tag{18}$$

This takes a voltage dependent expansion of the current collection of the probe volume into account. In the transition region electrons reach the probe depending on their Maxwell-distributed kinetic energy. The electron temperature T_e can be determined by fitting a Maxwell tail to the transition region

$$\mathrm{I(U)} = I_{Esat} * \exp\left(\frac{e(U - U_{Plasma})}{k_B T_e}\right) \tag{19}$$

Finally, in the electron saturation region, as many electrons as the plasma can deliver are collected, while all ions are repelled. The current is by the ratio of ion to electron mass higher due to the higher electron mobility

$$\mathrm{I_{Esat}} = I_{sat} * 0.65\sqrt{m_i/m_e} \tag{20}$$

The ion density can be retrieved by feeding I_{sat} from equation (18) into equation (17) and using the electron temperature as determined by equation (19) or by the modelling (section 4.2). In low temperature plasmas single ionized ions will dominate the ion population due to their lower ionisation energy. The ion and electron density in the core plasma, far away from sinks, will be equal due to the quasi-neutrality of plasmas.

Two specific setups of surface Langmuir probes were used. The rotatable Multi-Langmuir probe (Rack et al. 2013) features in total 18 circular probe heads of 4.55mm diameter to collect the ion saturation current (biased to fixed -176±2V). The probe heads were arranged in two rows of 9 probes, each row spanning a distance of 54mm. Both rows were positioned on the opposite sides of a rotatable holder in TEXTOR. By rotating the probe head and moving it in radial direction, angular and radial ion saturation current profiles were obtained. The probe currents were converted to a voltage with a gain of 5V/1A by the means of an isolation amplifier. The voltage was digitized by a multi-channel setup of 1MHz analog-digital converters (ADC). Linear gain and offset were determined for all probe heads by a

combination of zero-current and fixed current (with a 20.9kΩ resistor) calibration done after the measurements.

The second Langmuir probe setup was positioned on the so called staircase holder (see following section for more details). A grounded tower supports the flat probe head positioned close to the exposed samples (see Figure 19). The probe head consists of an outer guard ring and an inner circle used for the measurement. Both areas were kept at the same potential, but the current was only measured from the inner circle. The guard ring reduces the effect of voltage dependent collection volume expansion for the inner circle by catching the current of the expanding volume, leaving only the fixed volume above the inner circle for current collection. The electronic control and data evaluation system was developed and described in (Maximov 2011). Several modifications were made to adapt the system to the experimental requirements and to reduce the signal noise. Four shunt resistors in the range of 10Ω to 1000Ω were electronically selectable for generating a voltage drop at the ADC input in the range of -10V to 10V, depending on the plasma conditions. The signals were transferred by an isolation amplifier. Voltage and current signals of the probe were simultaneously sampled, yielding the full current-voltage characteristic.

3.2.2 Sample arrangement

For exposing samples to conditioning plasmas, a special holder was designed (Figure 19). The stainless steel holder supports up to 76 circular silicon samples of 11mm diameter and can also be refitted to other sample shapes. The samples were attached by a thin stainless steel foil. The foil covered part of the samples to provide an unexposed reference area on each sample. The radial distance of the top surface to the plasma core was adjusted by support structure movement (limiter lock) in the range of radial coordinate r=43..54cm on TEXTOR. The staircase design allowed for simultaneously exposing samples at 3 additional radial positions, +1.5cm, +3cm and +4.5cm in radial direction. In each position surfaces parallel and perpendicular to the toroidal direction were available. The holder was equipped with a resistive heating system, for adjusting the surface temperature during the removal experiments. For temperature monitoring a type-K thermo-element was connected to the arrangement, close to the top surface.

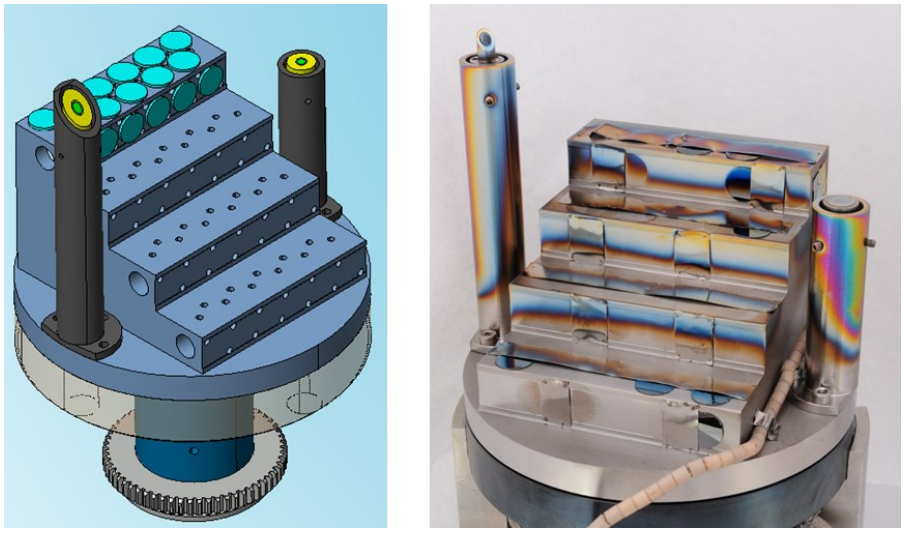

Figure 19: Staircase holder CAD drawing and post exposure photo. Some details were changed compared to the drawing. The fringes on the photo originate from interference on thin carbon films deposited during exposure in TEXTOR. The radial position where the fringes disappear corresponds to the main limiter position. Carbon originates from the TEXTOR limiters and is transported to the holder. Parallel transport enhances the impurity pick-up at the radial positions where the holder itself is the main limiter.

A surface Langmuir probe at the radial position of the uppermost surface was attached for measuring the plasma parameters close to the samples. A second Langmuir probe 36mm above the uppermost surface was intended for determining the core plasma properties outside the plasma sheath. This probe was not used for technical reasons.

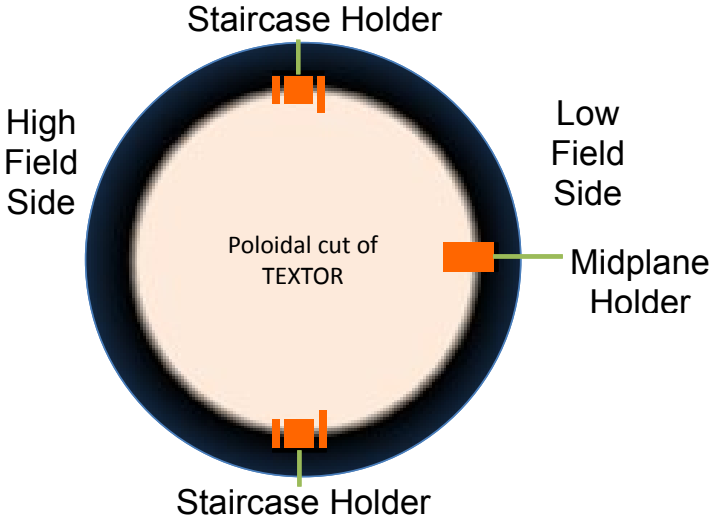

Figure 18: Schematic of the position of the sample holders in TEXTOR. Limiter lock 1 is at the bottom, limiter lock 3 at the top of the vessel. The plasma (central zone) intersects the holders.

3.3 Thin film characterization methods

The analysis of a-C:D and other deposits in the experimental part of this work is done with a set of methods described in the following section. The layers are deposited with thicknesses accessible by these methods of thin film analysis. The choice of analysis methods is based on the quantification necessary for testing the models presented in section 4.

3.3.1 Nuclear reaction analysis and Rutherford backscattering spectrometry

Nuclear reaction analysis (NRA) and Rutherford backscattering spectrometry (RBS) are methods for direct, non-destructive determination of areal densities of all elements and isotopes in a thin film, the target (Wang 2009). The target is bombarded with projectiles of a specific kinetic energy, in this work ^{3}He with mainly 2.4MeV kinetic energy. The projectile can undergo elastic scattering (Rutherford scattering) or inelastic scattering (e.g. nuclear reactions) with the target constituents. The energy of the products of a 2-body collision (projectile and target) is determined by the reaction product masses, the involved energy and the conservation of impulse and energy. In principle a clear identification of the target particle is possible from the products energy spectrum. In nuclear reactions the total energy can differ from the projectile energy by a value of *Q*, coming from the mass defect of projectile, target and products of the specific reaction. The amount of reactions of each type per incident particle is determined by their specific probability, the cross-section. The reaction cross-sections for Rutherford backscattering can be calculated a-priori from coulomb scattering. The cross-sections of nuclear reactions can, because of the complex strong nuclear interactions, only be experimentally determined. Necessary cross-section data was taken from (IAEA Nuclear Data Services n.d.).

To determine the amount of target particles stored in a co-deposit its volume has to be completely probed by the projectiles. The investigated layer has to be thin for the projectile. The projectiles lose energy when passing through matter by collisions with the electrons and nuclei, limiting their range. In the range of kinetic energies of some MeV, the stopping of particles from H to ^{4}He is dominated by electronic stopping. The Bethe-Bloch formula, along with a set of higher order corrections, is currently the best description of the losses associated with electronic stopping, with deviations from experimental values usually in the range of some percent. The software SRIM2013 (Ziegler, Biersack, and Littmark 2013) implements this and was used for stopping calculations in this work. For the stopping in compounds the Bragg rule (linear mixing) was applied. Whether a layer can be considered as thin is determined by the projectile energy, the layers stopping properties and the specific reaction (i.e. element) under investigation. The experimental and co-deposit parameters were chosen according to these limitations.

The amount of deuterium and carbon was measured using the following nuclear reactions

$$^{3}\mathrm{He} + ^{12}\mathrm{C} \rightarrow \mathrm{p} + ^{14}\mathrm{N} + 4.779\mathrm{MeV} \qquad (21)$$

$$^{3}\mathrm{He} + \mathrm{D} \rightarrow \mathrm{p} + {}^{4}\mathrm{He} + 18.352\mathrm{MeV} \quad (22)$$

Reaction (21) features two additional excited states of the nitrogen nucleus, as a result of the reaction, but only the reaction to the ground state was considered. In both reactions the proton gains most of the reaction energy. This proton leaves the co-deposit and can be detected by an energy resolving detector to identify the reaction. The target composition and elemental areal density ρ can be calculated for each specific reaction from

$$\rho = \frac{I}{\frac{D}{e}\Omega * \frac{d\sigma(E,\phi)}{d\Omega}} \quad (23)$$

with the number of detected educts *I* (the protons), the collected projectile dose *D/e* ($^{3}He^{+}$ ions), the area of the detector in units of solid angle Ω and the differential reaction cross-section $d\sigma/d\Omega$ in the detector direction.

Due to the amount of involved non-linear processes and experimental aspects, the calculation requires a computer program. In this work the software SIMNRA 6.06 is used (Mayer 1997). The program includes the effects of particle stopping in matter, energy dependent cross-sections, device geometry and technical layout to simulate energy spectra. The spectra are compared and fitted to the experimental data using a χ^2-minimization by varying the target composition, incident dose and detector calibration. The incident dose is fitted using the RBS spectrum, while NRA is used to fit the target composition. The obtained fit represents the measurement result. The corresponding error $\Delta\rho$ of the areal density measurement ρ of each constituent is given by the individual errors of the measurement quantities and the Gaussian error propagation rules.

$$\Delta\rho = \rho\sqrt{\left(\frac{\Delta I}{I}\right)^2 + \left(\frac{\Delta D}{D}\right)^2 + \left(\frac{\Delta\Omega}{\Omega}\right)^2 + \left(\frac{\Delta\sigma}{\sigma}\right)^2} \quad (24)$$

ΔI is given by the standard deviation of the Poisson distribution:

$$\Delta I = \sqrt{I} \quad (25)$$

Errors of cross-sections were given to about 8%, *D* and Ω had an error of 5% in the given setup. The error in I can be adjusted by changing *D* or the exposure time, respectively. Usually 100 to 200 events were detected for a given reaction, resulting in an absolute error of about 15%.

The device setup used for sample exposure is shown in Figure 20. A U-shaped part with minus 300V bias is used to reflect the secondary electrons released by the projectile impact. The setup is mounted in a vacuum chamber attached to the ion accelerator. The chamber pressure is kept $<10^{-6}$mbar in order to get negligible stopping (<0.01keV) in the remaining gas.

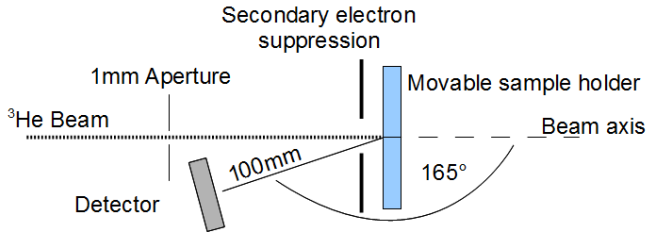

Figure 20: Schematic of the NRA/RBS setup. The projectile beam is coming from the left.

The reaction products are captured in backscattering geometry at a scattering angle of 165°. Only the light products are detected. For particle detection and energy sensing a circular, silicon surface barrier detector of 8mm diameter with a depletion zone of 1.5mm thickness is used. The detector converts the particle energy to a proportional voltage pulse. The pulse is amplified and converted to a digital signal which is logged by the PC. Simultaneously the integral projectile dose is summed by a counter. The used electronic system is shown in Figure 21. The detector system has an energy resolution of 20keV FWHM.

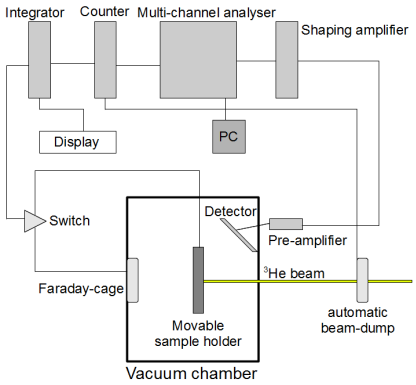

Figure 21: Scheme of electronics used for data acquisition of NRA/RBS.

3.3.2 Ellipsometry

Ellipsometry is an optical method for the determination of the optical properties and thickness of optically thin films. A setup as shown in Figure 22 is used to probe the thin co-deposits with linearly polarized light in a certain wavelength range (here 270-1000nm). By interaction of the photons with the solid the light properties are changed upon reflection and transmission, depending on the solid´s optical properties and the light wavelength.

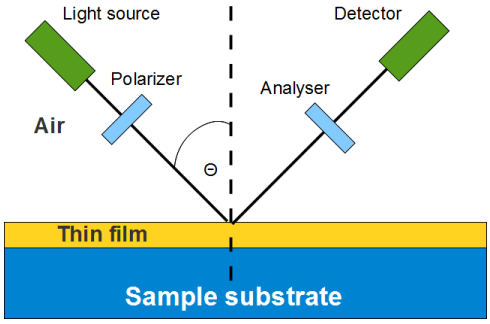

Figure 22: Schematic of the setup of an ellipsometric measurement.

After the interaction the light is elliptically polarized, giving the analysis method its name. The change of the incoming light with respect to polarization and amplitude is recorded by the analyser and detector as wavelength dependent sets of Ψ, Δ. Ψ, Δ are defined by the complex ratio of the parallel r_p and perpendicular r_s polarization components with respect to the incidence plane

$$\frac{r_p}{r_s} = tan(\Psi(E))\, e^{-i\Delta(E)} \tag{26}$$

The device is used to determine the optical properties refractive index *n*, absorptive index *k* and the thickness of a-C:H films. A Forouhi-Bloomer model

$$n(E) = n(\infty) + \frac{\left(\frac{AB\left(E_g^2 + C\right)}{\sqrt{4C - B^2} * \left(1 - E_g C\right)} - \frac{2AB^2 E}{\sqrt{4C - B^2} * \left(2 + E_g B - E_g^2 + C\right)}\right)}{E^2 - BE + C} \tag{27}$$

$$k(E) = \frac{A\left(E - E_g\right)^2}{E^2 - BE + C} \tag{28}$$

is used for the a-C:H layer description. Here *A, B, C,* E_g and *n(∞)* are fitting parameters and *E* is the photon energy or wavelength, respectively. This model allows to determine the wavelength dependent optical properties by fitting the parameters to the measured Ψ, Δ spectra. Since the optical properties of the substrates used in this work are known and the samples are surrounded by air, the optical system is completely described by a 3 layer model (air-layer-substrate), allowing to determine the co-deposit properties.

For all measurements θ=27° (see Figure 22) is used. This angle is close to the Brewster angle of most samples, where the ratio of equation (26) is maximized. The Ψ, Δ spectra are recorded in a wavelength range of 270 to 1000nm and the fitting is done in the same range with the program Spectra Ray 2. The program uses χ^2 minimization to match model and measurement, giving also a qualitative measure for the result quality. The errors of the Ψ, Δ measurement are specified to be about 1°. The resulting statistical errors of the

measurements are negligible. A systematic error due to imperfect optical models can be expected, but is not quantified. An example of a measurement result is depicted in Figure 23. For a-C:H layers the observed optical properties were mostly independent of the wavelength and in agreement with literature observations (Schwarz-Selinger, Keudell, and Jacob 1999). In combination with the elemental composition determined by NRA/RBS it is possible to calculate co-deposit mass densities.

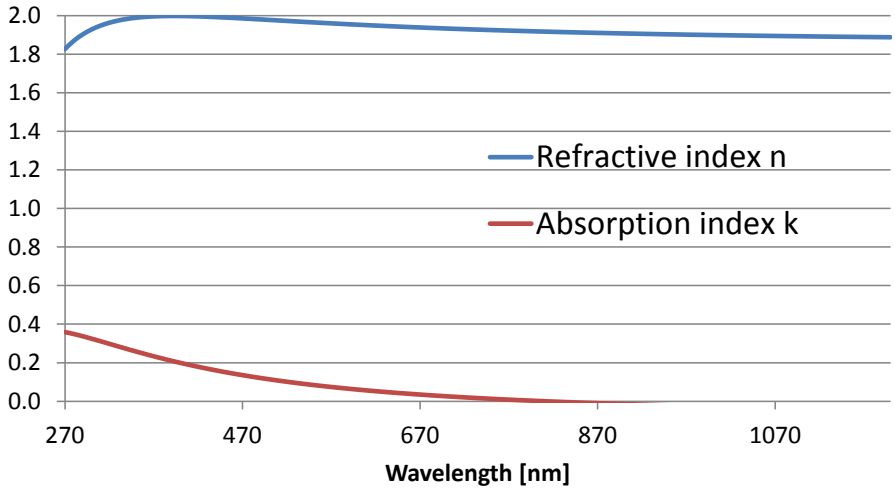

Figure 23: Typical spectrum of the refractive index n and absorption index k of an a-C:D layer. Both values can be considered as constant >400nm.

4 Modelling results

Based on the existing data and partial understanding by models for single aspects of the removal methods under investigation in this work, new models are developed and discussed in this section. Parameters studies demonstrate which quantities are, according to the models, important for the removal rates. Experimental validation of the new models with experiments based on this understanding, are presented in section 5.

4.1 Description of thermo-chemical removal by reaction-diffusion processes

For carbon based co-deposits, which are of special interest as depicted in section 2.2, several advantages of thermo-chemical removal (TCR) and short removal times were already demonstrated with laboratory and tokamak a-C:H co-deposits, e.g. (Davis and Haasz 2009). Observations concerning the relation of TCR rates to the gas pressure, surface temperature, initial material content, and thickness and removal rate time evolution have to be connected and underlying physics of the process have to be revealed by a physical model.

The method of TCR is simple and cheap in application, since only a reactive gas is injected into the vacuum vessel and the treated materials have to be heated to a certain temperature, depending on the involved gas and co-deposits. The actual removal is induced by chemical reactions between the hydrogenated co-deposits (A+DT) and the reactive gas (B), forming stable volatiles (AB) which can be exhausted by pumping and reprocessed for hydrogen isotope (DT) recovery, as in its simplest case depicted in (29). The neutral gas is, in contrast to e.g. plasma or photon based methods, not restricted by any kind of electromagnetic field or shallow structures of complicated geometries, giving in principle a homogenous removal from all surfaces in the vessel.

$$(\mathrm{A}+\mathrm{DT})+\mathrm{B} \xrightarrow{\mathrm{TCR}} \mathrm{AB}+\mathrm{DT} \xrightarrow{\mathrm{separation}} \mathrm{DT} \tag{29}$$

For the calculation of removal rates and understanding of chemical reactions a physical model is derived. The diffusion of reactive gas through the co-deposits into their volume is, within this model, of central importance for most of the observations and the speed of the process itself. Significant diffusion velocities can originate either from an open porosity inside the material or from a bulk material having high gas permeability. Both physical concepts result in the same behaviour and can thus be treated equally in a mathematical sense. The porosity of a-C:H layers formed in tokamaks was observed, e.g. in (Martin et al. 2007; Richou et al. 2009). Porosity was also found in laboratory carbon deposits (Kögel et al. 1988; Jacobsohn et al. 2002). Typical values of the relative volume porosity C_{Por} in the order of 10%, with pore size distributions centred below 1nm were observed in a-C:H layers. The permeability of a-C:H for gas was described in (Vasquez-Borucki, Jacob, and Achete 2000).

All inner and outer surfaces of the co-deposits provide adsorption sites for the injected reactive gas. This reservoir is filled by the reactive gas influx to the co-deposit. The amount of reactive gas particles in this reservoir defines the density of reaction partners available for removal. From the surface adsorption sites the reactive gas can penetrate into the material. Subsequently to the diffusive influx, chemical reactions take place in the volume. The product volatiles, the exhaust gas, leave the material by diffusion and can be removed from the vessel by pumping. The microscopic processes are assumed to be much faster than the macroscopic co-deposit removal and the removal process can thus be considered to be in quasi-steady state. The steps of the process are depicted in Figure 24.

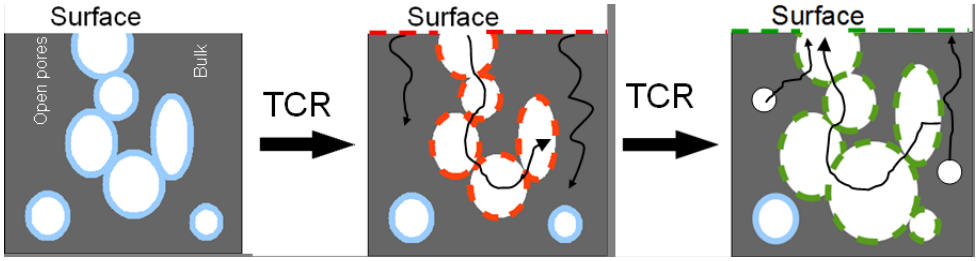

Figure 24: Three steps of TCR. Left: An arbitrary mixture of bulk and pores constitute the co-deposit. Centre: The reactive gas is adsorbed on all accessible surfaces (red dashed lines) and diffuses into the bulk material with a range into the volume depending on the material properties. Right: The reactive gas loading interacts chemically with the material (green dashed lines) and forms volatiles. The volatiles leave the material by the same diffusion mechanisms, material is removed. The reactions can occur in the whole volume, depending on the access of reactive gas to the volume. The macroscopic density decreases.

In steady-state the diffusive influx of reactive gas particles has to be balanced by the reactive loss to exhaust particles. The diffusion can be seen as a source term for particles at a certain depth in the co-deposit *x*, balanced by a sink given by the reaction of reactive gas particles n_R with material constituents n_C to exhaust particles (basics in 2.3):

$$D * \frac{d^2 n_R(x)}{dx^2} = \sum_i k_i * n_R(x) * n_C \tag{30}$$

Here *D* is the gas diffusion coefficient, k_i the reaction coefficient of one of the possible chemical reactions *i* with the layer constituents, $n_R(x)$ the density of the reactive gas at the depth *x* of the layer and n_C the material constituents density (co-deposit density). The sum over *i* is taking all possible reaction paths of the constituent with the reactive gas into account, e.g. the formation of CO, CO_2 by reactions between O_2 as the reactive gas and C in a-C:H as the removed material. In the following, the sum over *k* will be omitted without restriction of generality.

For solving the differential equation, two boundary conditions have to be set:

$$n_R(0) = L(p_{Gas}) \tag{31}$$

$$n_R(\infty) = 0, \tag{32}$$

with a function L, describing the adsorption of reactive gas on surfaces at the gas pressure p_{Gas}. This function takes also into account the gas capacity, given by the chemical interaction and the available surface area (open pores and outer surface).

Equation (31) states that at the surface of the material ($x \to 0$), where the particle transport by diffusion is infinitely fast, the layer contains the amount of the reactive gas which can be adsorbed on its surfaces at the given outer gas pressure. The second condition, equation (32), is the result of having the only gas source at the surface, while having losses by reactions throughout the material. Therefore all reactive gas particles are consumed by reactions at infinite depth. The remaining gas capacity may fill up with exhaust particles, which can only be lost at the surface. With this information, the differential equation (30) can be solved, yielding

$$n_R(x) = L * e^{-x\sqrt{n_c * k/D}}. \tag{33}$$

With this density distribution of reactive gas particles in the material, the total number N_R of these particles per unit surface area can be calculated for a co-deposit of thickness z:

$$N_R(z) = \int_0^z n_R(x)dx = \sqrt{\frac{D}{k * n_c}}\left(1 - e^{-z\sqrt{n_c \frac{k}{D}}}\right) * L \tag{34}$$

This can be inserted into a second order chemical reaction equation, describing the reaction between two particles (Czeslik, Semann, and Winter 2007), to get the total number of reactions R_L per unit surface and time:

$$\begin{aligned} R_L(T_S, p_{Gas}, z) &= k * N_R(z) * n_C \\ &= k * \sqrt{\frac{D}{n_c k}} * \left(1 - e^{-z\sqrt{n_c \frac{k}{D}}}\right) * L * n_C . \end{aligned} \tag{35}$$

To describe the reactive gas adsorption L the Langmuir (equation (36)) and the BET (Brunauer, Emmett, Teller) (equation (37)) approaches (Roque-Malherbe 2007) can be employed.

$$L_L(p_{Gas}) = \frac{q_{Max} K_L p_{Gas}}{1 + K_L p_{Gas}}, \tag{36}$$

$$L_{BET}(p_{Gas}) = \frac{q_{Max} * K_{BET} * p_{Gas}}{(p_{Sat} - p_{Gas}) * \left(1 + \frac{(K_{BET} - 1) p_{Gas}}{p_{Sat}}\right)}, \tag{37}$$

where K_L and K_{BET} are the adsorption coefficients in the Langmuir and BET theory, respectively, q_{Max} is the maximum loading of reactive gas particles per volume and p_{Sat} is the pressure at which a saturation occurs. The Langmuir model is based on single layer adsorption on surfaces and thus simpler than the BET model, which also describes multi-

layer adsorption of gas particles occurring at higher pressures. The functions are depicted in Figure 25 with a set of parameters variations. Significant differences between both adsorption models arise only at higher pressures. The adsorption coefficients, which are physically based on the interaction potentials of reactive gas and solid and surface properties determine the amount of adsorbed gas and thus influence the resulting removal rate at a given pressure.

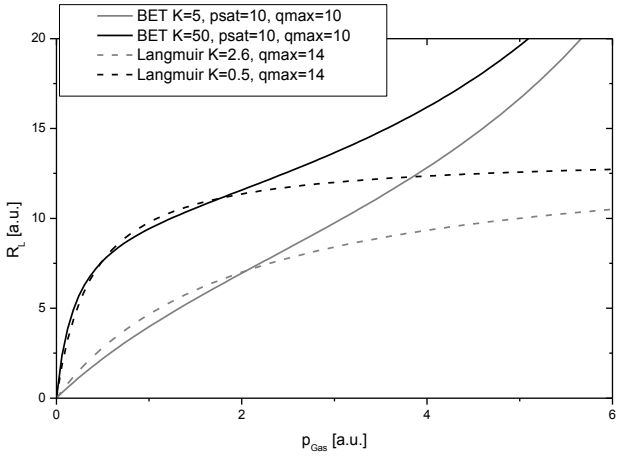

Figure 25: Comparison of Langmuir and BET theory and the resulting pressure dependence of the removal rate. Both models show a similar behaviour in the low pressure range, while significant differences can be observed for higher pressures due to multilayer adsorption present only in the BET model. The value of the adsorption coefficient K influences the amount of adsorbed gas in the material. Note that parameters with similar meaning, e.g. *K*, do not necessarily have comparable numerical values in both models.

The chemical reaction rate between the material and the reactive gas, coefficient *k*, can be described by the Arrhenius equation (Czeslik, Semann, and Winter 2007), in agreement to observations (section 2.3):

$$k = A * e^{-\frac{E_A}{k_B T_S}}, \tag{38}$$

where *A* is a collision frequency factor, k_B the Boltzmann constant, E_A the activation energy of the chemical process and T_S the material temperature. This equation describes thermally activated reactions and is thus a physically adequate description. The factor *A* can further be described by a thermal particle velocity (mass m_R), connected with a collision frequency, and a collision cross-section *P:*

$$A = P * \sqrt{\frac{\pi k_B T_S}{2 m_R}}. \tag{39}$$

Inserting *k* from (38), *A* from (39) and L_{BET} from (37) into (35), we obtain the following equation for the removal rate of the co-deposit R_L

$$R_L(T_S, p_{Gas}, z) = \sqrt{P * \sqrt{\frac{\pi k_B T_S}{2m_R}} * e^{-\frac{E_A}{k_B T_S}} * n_c * D * \left(1 - e^{-z\sqrt{\frac{n_c * P * \sqrt{\frac{\pi k_B T_S}{2m_{Molecule}}} * e^{-\frac{E_A}{k_B T_S}}}{D}}}\right)} * \left(\frac{q_{Max} * K_{BET} * p_{Gas}}{(p_{Sat} - p_{Gas}) * \left(1 + \frac{(K_{BET}-1)p_{Gas}}{p_{Sat}}\right)}\right) * n_C. \quad (40)$$

For a complete description of the total removal rate R_{Total}, a surface removal term $R_{Surface}$ and an inverse reaction term R_I have to be included in the calculation:

$$R_{Total} = R_L(T_S, p_{Gas}, z) + R_{Surface}(T_S, p_{Gas}) - R_I \quad (41)$$

Under usual conditions their contributions are below the detection limits and thus negligible, since the outer surface area is much smaller than the inner one for a typical co-deposit. Inverse reactions of the exhaust particles are suppressed due to their endothermic nature.

In most application cases, e.g. the removal of a-C:H by O_2 at 350°C, the process is reaction-limited, i.e. the diffusion D of gas particles in the material occurs much faster than their reactions k with its constituents as indicated by exposure temperature and co-deposit inventory scaling (section 2.3). Increasing the material thickness z has a similar effect as a lower diffusion coefficient on the reactive gas density in depth, since the diffusion has to pass a longer distance. Thick layers will thus reach diffusion limitation with higher diffusion coefficients D than thin layers. Figure 26 illustrates the effect of $z\sqrt{n_c k/D}$ (see equation (35)) on the reactive gas concentration $n_R(x)$, showing a nearly constant $n_R(x)$ for the reaction-limited case $z\sqrt{n_c k/D}$=10^{-4}. The reactive gas concentration gradient, which drives the diffusive transport, can thus be very small. The concentration can be assumed constant in depth. The higher $z\sqrt{n_c k/D}$ gets, the steeper the concentration gradient will be.

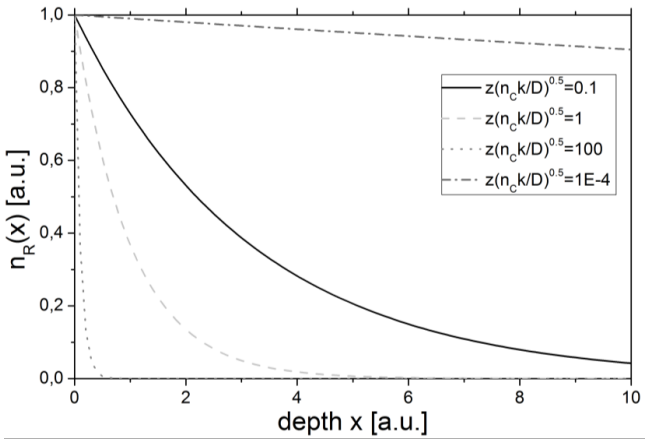

Figure 26: Parameter study showing the effect of $z\sqrt{n_c k/D}$ on the reactive gas concentration in depth.

The depletion of reactive gas in depth will lead to a sub-linear scaling with material inventory and thickness *z*, respectively. This results in a lower removal rate and a limitation of the reactions to a zone close to the surface. The process with high $z\sqrt{n_c k/D}$ is called diffusion-limited. The result of this depletion of reactive gas in depth is shown in Figure 27. The removal rate first increases with increasing surface temperature (increasing *k*), according to the Arrhenius function. The slope is reduced below the Arrhenius behaviour at the point where the process changes from reaction to diffusion limitation and the reactive gas starts to get depleted in deeper parts of the layer.

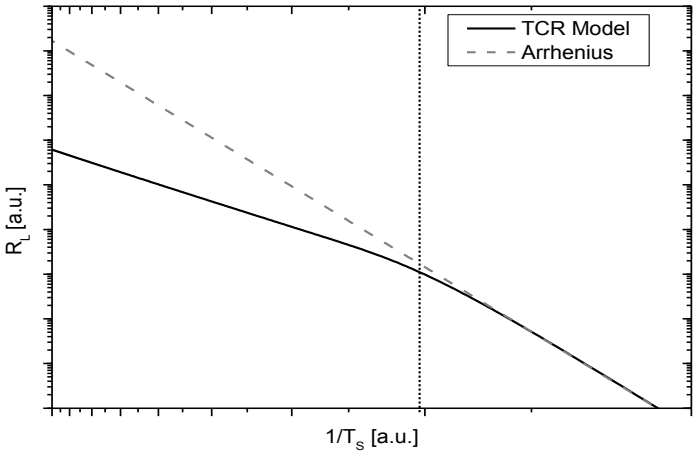

Figure 27: Arrhenius plot, showing the transition from reaction (low T_S, *right part*) to diffusion (high T_S, *left part*) limitation with temperature (dotted line) and the resulting decrease of the removal rate R_L below the Arrhenius behaviour (dashed line). Compare to Figure 5.

In the reaction-limited case the exponential depth dependence of n_R is well described by its first-order approximation,

$$e^{-z\sqrt{n_c\frac{k}{D}}} \approx 1 - z\sqrt{n_c\frac{k}{D}}\,. \tag{42}$$

Under the relatively low pressures of TCR in fusion devices (around 10 kPa), the Langmuir model for single layer adsorption is usually sufficient. Taking this into account a simplified relation for the removal rate can be derived from (35):

$$R_S(T_S, p_{Gas}, z) = P * \sqrt{\frac{\pi k_B T_S}{2m_R}} * e^{-\frac{E_A}{k_B T_S}} * z * \frac{q_{Max} K_L p_{Gas}}{1 + K_L p_{Gas}} * n_C. \tag{43}$$

This approximation of the general formula (40) is intended to provide access to the relevant dependencies, while reducing the number of free parameters when fitting to the experimental data. The disadvantage is the non-applicability to diffusion-limited cases.

Formulas describing the parameters K_L (44), D (45) and P with certain assumptions can be found in (Roque-Malherbe 2007), (Czeslik, Semann, and Winter 2007):

$$\mathrm{D} = r_{Pore} * \sqrt{\frac{\pi k_B T_S}{2 m_R}} \tag{44}$$

$$K_L = K_{L0} * e^{\frac{E_{AS}}{k_B T_S}} \tag{45}$$

With the help of models for those parameters and data for E_A and C_{Por}, a-priori calculations of the removal rate would be possible. However, with the amount of necessary assumptions for analytical formulas, adsorption binding energy E_{AS} and the need for additional, error prone measurements (porosity), a high uncertainty of such calculations can be expected. Therefore the removal rate equations will be used for comparison with experimental data and fitting of these parameters.

Separating the simplified formula (43) into the relations to z, p_{Gas} and T_S, a set of fitting formulae can be obtained to compare the model with experiments:

$$R(z) = C(T_S, p_{Gas}) * z \tag{46}$$

$$R(p_{Gas}) = C(T_S,\, z) * \frac{K_L p_{gas}}{1 + K_L p_{gas}} \tag{47}$$

$$R(T_S) = C(z,\, p_{Gas}) * \sqrt{T_S} * e^{-\frac{E_A}{k_B T_S}} \tag{48}$$

These partial formulae tackle only one parameter, while the rest are condensed to a proportionality factor C which can be obtained by fitting. The influence of co-deposit and reactive gas interaction properties (E_A, D, m_R, P) is also included in the constant.

4.1.1 Comparison to literature

The experiment presented in (Davis and Haasz 2009) shows the initial deuterium removal rate in relation to the initial deuterium content (Figure 7). The initial content can be directly connected to the layer thickness. As already stated in (Davis and Haasz 2009), the measured removal rate exhibits a linear relationship with respect to the initial content. This was seen to be valid for initial contents spanning over two orders of magnitude. Equation (46) connects this observation to the reactive gas content in the layer. Taking typical values of the layer density of ≈1.5g/cm³ and D/C of ≈0.4, a maximum layer thickness of ≈25µm was investigated in these experiments. Since the linearity holds even for this thickness, it can be concluded that a diffusion limitation does not occur for a thickness up to at least ≈25µm of typical tokamak carbon co-deposits. The linear relation between co-deposit inventory and

TCR rate is of central importance for the method, as it defines a fundamental difference in removal behaviour of TCR to methods only affecting the co-deposit surface.

Equation (47) was applied to data from (Ochoukov, Haasz, and Davis 2006) on the relation between the removal rate and the gas pressure. Figure 28 shows that the fit describes the data for both temperatures (300°C and 350°C) well, indicating that the Langmuir model is an adequate description of the gas adsorption in those layers. High pressure effects, as described by the BET theory, seem to be negligible in the tested pressure range (0.21-21 kPa).

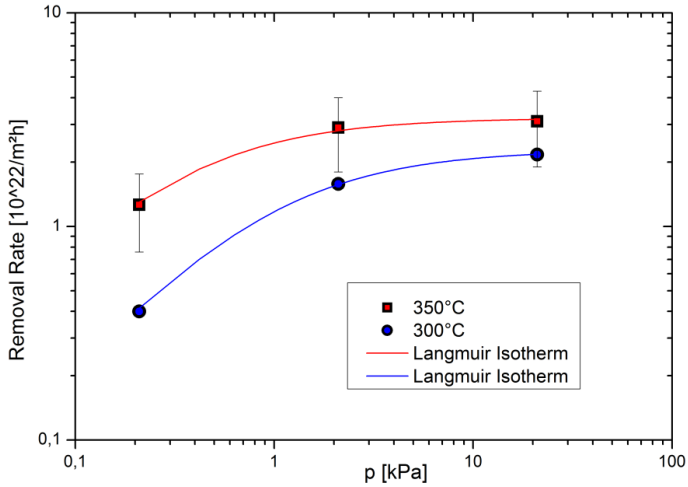

Figure 28: Fit of the pressure dependence with data from **(Ochoukov, Haasz, and Davis 2006)** with a Langmuir adsorption model. A good agreement is found to the modeled behavior.

The dependency of the removal rate on the surface temperature was investigated in detail. An overview of results for the carbon removal is presented in Figure 5. The data exhibit an Arrhenius-like behaviour, which is also used in the model (equation (48)). The scatter can be explained by the use of different layer textures (Davis and Haasz 2001) and by the normalization to the incident O_2 flux, not taking into account the non-linear pressure effect (equation (47)). A change of behaviour occurs at temperatures above 1000K, resulting in removal rates lower than predicted by the Arrhenius relation. In line with these observations in (Balden et al. 2005) the Arrhenius behaviour for graphite erosion by oxygen was also seen up to 1000K. The same saturation effect is observed for the deuterium removal rate by O_2-TCR in (Davis and Haasz 2009), starting at about 700K. This saturation can be explained by a transition from the reaction to diffusion limited case of the removal process as shown in Figure 27. At higher temperatures the reaction rates *k* increase according to the Arrhenius relation (equation (48)), while the diffusion increases at slower rates, e.g. equation (44). This leads to a depletion of the reactive gas in deeper parts of the layer, Figure 26, as described in the complete model, equation (40).

The time evolution of the removal process also can be addressed, although it is not explicitly included in the formulae above. It was seen e.g. in (Davis and Haasz 1999; Haasz and Davis 1998) that the instantaneous TCR removal rate shows a non-linear behaviour, with a maximum in an intermediate stage and smaller rates in the beginning and end of the removal process, see Figure 29. This is an indicator for the presence of two competing processes. Within the scope of the model the processes can be identified from equation (43) as an increase in gas capacity q_{Max} and a decrease of the areal reaction partner density $z \cdot n_C$ with the course of time. The time behaviour of these two parameters, especially q_{Max}, can at this point only be estimated. For $z \cdot n_C$ an exponential decay is assumed, since the reaction rate for removing material is proportional to $z \cdot n_C$, leading to a differential-equation with an exponential solution. Since the material is removed mainly by volume reactions it is reasonable to assume that q_{Max} starts at a certain initial value q_{Max0}, given by the initial structure. With continuing removal it gradually approaches a maximum, since more surface area is generated by the volume removal. This porosity increase first accelerates the removal, but in the final stage of removal, the porosity growth will decelerate with decreasing reaction partner density. The time evolution can thus be described by functions asymptotically reaching the maximum $q_{Max\text{-}inf}$ for q_{Max} and zero for $z \cdot n_C$:

$$q_{Max}(t) = q_{Max0} + \left(q_{max-inf} - q_{Max0}\right) * erf(t/\tau_a(R_L)) \tag{49}$$

$$[z * n_C](t) = z_0 * n_{C0} * e^{-t/\tau_b(R_L)}, \tag{50}$$

where the initial values are indicated with a zero index. The characteristic times τ_a and τ_b will show a connection to the removal rate R_L, i.e. they will also be related to T_S and p_{Gas}. This model of the time evolution extends the literature model presented in section 2.3.

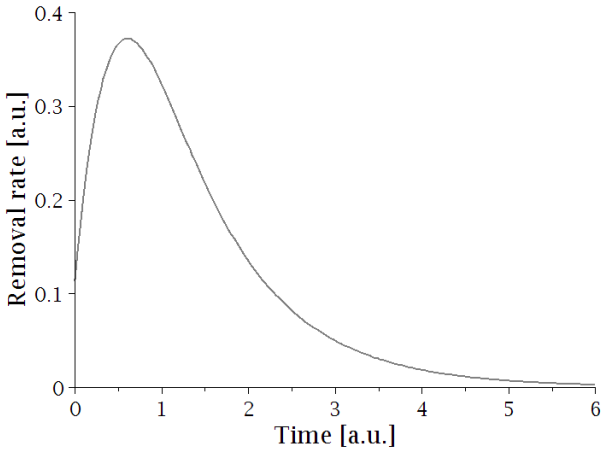

Figure 29: Sketch of the time evolution of the TCR rate according to the two competing processes model. Gas capacity increases, while zn_C decreases, resulting in non-linear behaviour.

The data in (Haasz and Davis 1998) are given as the total deuterium content. The removal rate equation was integrated over the time prior to the fitting in order to obtain the total

amount of removed material. The assumptions of a linear increase of q_{Max} and a linear decrease of the layer content z give a rough agreement (Figure 30). A better agreement is reached with assumptions from equations (49), (50).

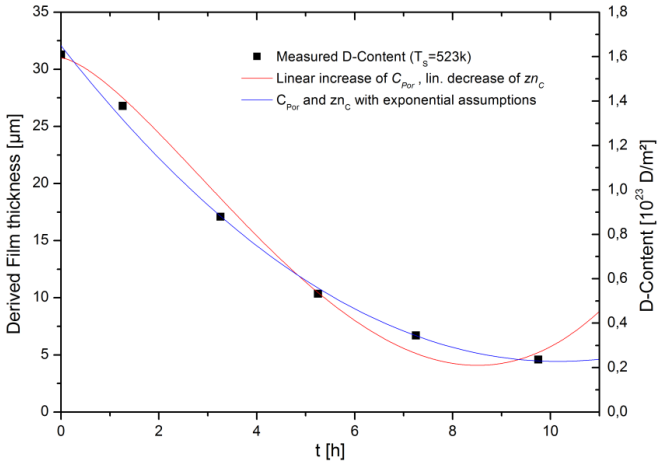

Figure 30: Time evolution of the D-content during O_2-TCR fitted with two models for time-dependent q_{Max} and $z*n_C$, data from **(Haasz and Davis 1998)**. The film thickness was derived by layer density assumptions, neglecting density reduction.

4.1.2 Effects of reactive gas dilution by reaction products

According to equation (40) the removal rate depends on the pressure of the reactive gas. In the removal reaction the reactive gas is consumed and exhaust gas is produced. At spatially constant pressure, arranged due to mass flow, this dilutes the reactive gas and thus can reduce the removal rate. In general, the speed of thermo-chemical removal will be reduced, if the exhaust gas pressure on the co-deposit surface is >0. To calculate the extent of this effect, the total volume of the device vessel V_{Device} and the applied removal gas pressure p_{Gas} have to be taken into account. If the size of co-deposit inventory and the chemistry of the removal are known, the amount of exhaust particles N_{exh} can be calculated and compared to the initial amount of reactive gas N_{R0}. The value γ_{Final} will give the percentage of gas dilution of the reactive gas and thus the percentage by which the removal rates will be reduced at the end of the process in first order approximation. In the case of a-C:H removal carbon and hydrogen isotope containing exhaust gas species have to be considered. Additional unreactive remnants of the reactive gas, e.g. N_2 when using NO_2, were neglected.

$$\gamma_{\mathrm{Final}} = \frac{N_{R0}}{N_{R0} + N_{Exh}} = \frac{V_{Device} * \frac{p_{Gas}}{k_B T}}{V_{Device} * \frac{p_{Gas}}{k_B T} + (aN_C + bN_{DT})} \tag{51}$$

Where the constant a is the number of carbon containing molecules per removed C atom and b the corresponding value for H,D,T atoms. As an example the removal of a-C:H by O_2 would lead to

$$C + O_2 \rightarrow CO_2 \xrightarrow{\text{yields}} a = 1 \quad (52)$$

$$4H + O_2 \rightarrow 2H_2O \xrightarrow{\text{yields}} b = 0.5 \quad (53)$$

if the main exhaust products of this removal are CO_2 and H_2O. The amount of carbon N_C and hydrogen isotope N_{DT} atoms retained in the co-deposits is defined by the co-deposit properties and also the amount of inventory accumulated before applying removal. To keep γ_{Final} small, e.g. <10%, gas exchange by pumping and injection can be applied during the removal, or a higher p_{Gas} can be applied.

4.1.3 Geometry effects

The main transport mechanism for neutral gases is diffusion, defined by a free movement between collisions of the particles with each other and the surrounding walls. A main parameter for the transport coefficient is the mean free path of the particles in the gas connecting two subsequent collisional processes by a straight line movement

$$\lambda = \frac{k_B T}{\sqrt{2}\pi\, p_{gas}\, d^2} \quad (54)$$

This value is inversely proportional to the gas pressure p_{gas} and the square of the minimal distance between two particles d. If the mean free path gets equal to or larger than the geometrical dimensions of a surrounding structure, the transport will change from the gaseous diffusion to the so called Knudsen flow and finally at even smaller structures to the surface diffusion regime. The diffusion mass transport gets smaller, the smaller the structure is, sketched in Figure 31. In nuclear fusion application the smallest device geometrical sizes are in the order of mm in so-called gaps and thus large compared to the mean free path at TCR gas pressures. The spatial equilibration of gas pressures within the vessel will thus not be hindered by reduced diffusion speeds. A change in removal rates is thus not expected and was also not observed in small gaps (≥0.5mm) and other like structures (Möller 2010). For diffusion of reactive gas into the volume of co-deposits the diffusion coefficient strongly depends on the path size, e.g. the pore diameter.

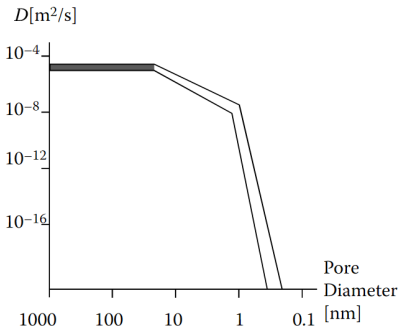

Figure 31: Relation between diffusivity and structure size of the transport path. At structure sizes <100nm a significant reduction of the diffusion coefficient, related to the transition from molecular to Knudsen diffusion, can be expected. Figure from **(Roque-Malherbe 2007)**.

4.2 Description of plasma impact removal

Plasma impact removal (PIR) utilizes plasma scenarios different from magnetic confinement fusion plasmas. The plasmas are heated by a high frequency in the range of the electron or hydrogen ion cyclotron frequency. The plasmas are confined only by the toroidal magnetic field and can thus offer more flexibility than fusion plasmas.

4.2.1 Modelling studies of plasma discharges in magnetic fields

In this section the model presented in section 2.5 is used to investigate the influence of the experimental parameters gas pressure p_{gas}, toroidal magnetic field B_T, coupled input power P_{RF} and the elemental composition on the plasma parameters. These parameters provide the accessible space of the plasma parameters. The plasma parameters in turn define the plasma-wall interaction and by that the possibilities and rates of removal. Knowledge of the accessible parameter space is thus important for discharge tailoring. The following simulations are carried out for a TEXTOR device (section 3.2) with a pressure of $4*10^{-4}$mbar H_2, a magnetic field of 0.23T, an input power of 85kW and an impurity concentration of 0, if not stated differently. The parameters are chosen to be close to application parameters in the later experiments in TEXTOR, but are in principle arbitrary. The simulation runtime is chosen long enough to reach equilibrium values for all parameters, especially the gas pressure. In this limit the plasma breakdown and gas consumption become irrelevant. About 99% of the plasma ions are found to be H^+ and about 1% H_2^+ in all simulation runs, other species are only present in negligible fractions. The wall fluxes under the given conditions are thus, as a modelling result, dominated by H^+ ions. Ion temperatures are found to be in the order of 0.5eV.

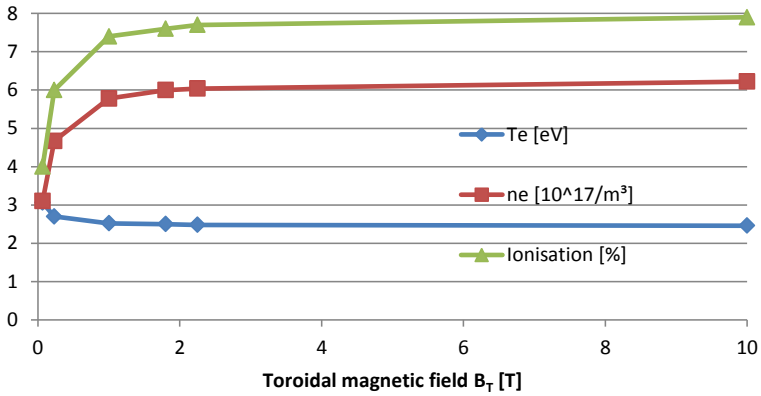

Figure 32: Modelled effect of the toroidal magnetic field in a TEXTOR ICWC discharge on the plasma parameters.

Varying the toroidal magnetic field is seen to have a significant impact on the plasma parameters for values below 1T (Figure 32). At higher values the plasma parameters saturate (in the TEXTOR device size), the difference between 1T and 10T becomes negligible (<10%). The most important effects within the model are the improved ion and electron confinement and the associated improved transfer of power from the heated electrons to the ions. Above about 1T the power losses by transport are reduced and the radiation losses dominate the plasma equilibrium. In a high frequency heated plasma the power coupling efficiency can depend on B_T, with lower coupling efficiencies observed at higher field strength (Lyssoivan et al. 2009). The effect of increased density can thus be counteracted by a reduced input power to the plasma, leaving only little impact of B_T. The modelling results do not take this into account.

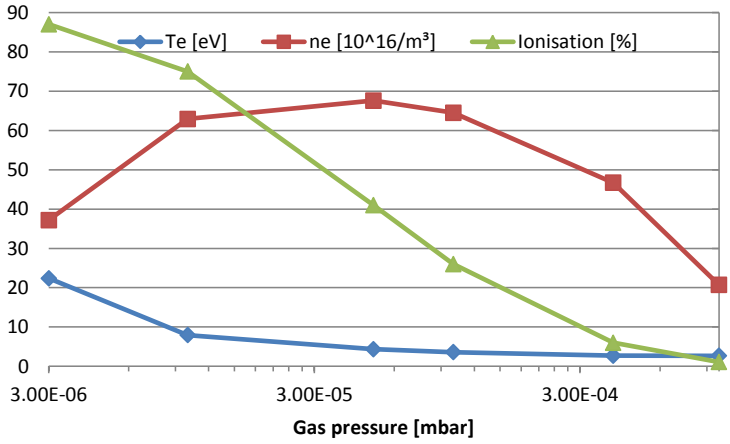

Figure 33: Modelled effect of the neutral gas pressure in a TEXTOR H_2-ICWC discharge on the plasma parameters.

The neutral gas pressure provides both a reservoir for new ions, but also a sink for power by collisions with unconfined neutrals which have confinement times several orders of

magnitude shorter than the ion confinement times, as calculated by the model. These competing processes lead to a maximum in density present in the modelling results at around $5*10^{-5}$mbar (Figure 33). At lower pressures the gas is nearly fully ionized. Additional power input beyond the full ionization threshold leads to an increase in plasma temperature to balance the power losses, since new ions cannot be generated from the neutral gas anymore. The gas pressure is thus a parameter to vary between plasma temperature and density, if it can be controlled by a fast feedback system. A large part of the available particles can be implanted/pumped into the vessel walls in the start-up phase of the removal plasma, leading to a significant pressure drop with an according deviation of the plasma parameters from the target values. At lower pressures impurities ejected into the plasma by the removal process can contribute a larger fraction to the particle population leading to a relative increase in their plasma cooling and flux contribution. A technical lower limit for the gas pressure can be given by the device´s base pressure and leak rate.

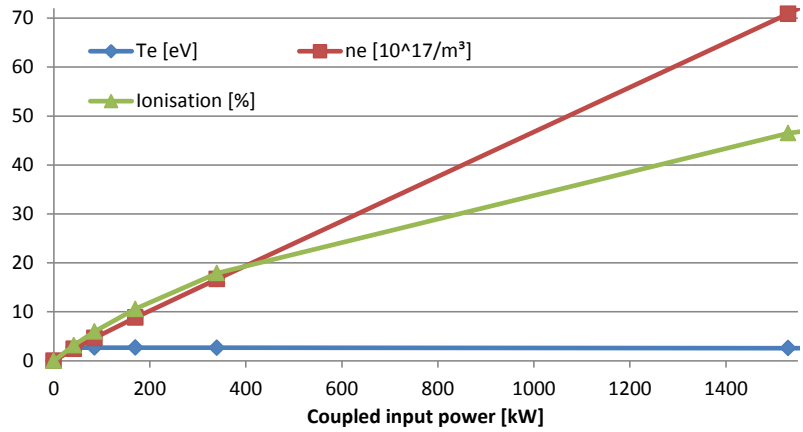

Figure 34: Modelled effect of the input power in a TEXTOR ICWC discharge on the plasma parameters. The highest values are technically not feasible, yet illustrate the validity of assuming a linear relation between input power and plasma density over a wide range of values.

The coupled input power has a very straightforward effect in a broad range of values. Since all losses are scaled by the amount of involved particles the losses scale linear with the plasma density and thus also with the input power (Figure 34). A linear connection between plasma density and input power with constant plasma temperature is violated by <10% in the whole range accessible by the TEXTOR systems. The input power can be treated as a scaling factor for plasma removal, as higher values will linearly increase the plasma removal rate, removal can be understood as atoms/energy of input power.

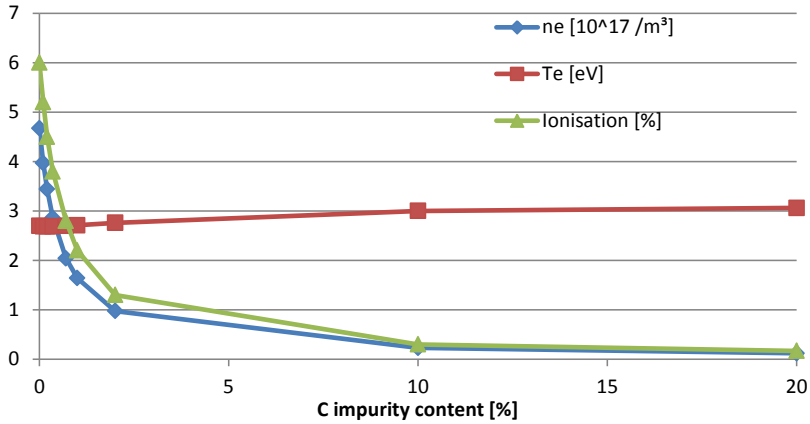

Figure 35: Parameter study of the plasma density n_e vs. C plasma impurity content. For impurity content >20% no plasma breakdown is possible within the model, due to high power losses. The 0D-model takes a global average of the impurity density, not taking into account spatial variations due to different transport properties of different plasma species.

Conditioning aims at removing material from the wall. This material, here called impurity, will be present in the plasma and accumulate over time with a saturation concentration depending on the sinks and sources for the impurity. Carbon is used as an exemplary impurity, but the effect of increased plasma cooling will be similar for most impurity species (e.g. oxygen or tungsten in an H plasma), only with different magnitude. The plasma density is seen to reduce with increasing impurity concentration. This in turn reduces the ion wall flux and conditioning rate, see equation (17).

Besides carbon which is always present by the removal effect of a-C:H also oxygen, as a base gas, is investigated by modelling. To scale the plasma model from H_2 to O_2 plasmas without knowing the detailed plasma collisional cross-sections several similarity considerations are employed. This results in an approximate solution for the O_2 plasma parameters. The transition from a predominantly neutral gas to a fully ionized plasma was investigated with the model in (Wauters 2011). For H and He plasmas the transition takes place in the range of T_e=2-3eV, defined by the onset of relevant cross-sections for ionizing reactions and also the strong increase of electron collision cooling in this temperature range. The similar molecular dissociation and ionization energies and ionisation rate coefficient (Stangeby 2000) of H_2 and O_2 induce similarities with respect to the plasma temperature (Wauters 2011). All power losses are assumed to be proportional to the plasma density. The ratio of the plasma densities of H_2 and O_2 plasmas are then determined by the ratio of losses, since the electron temperatures are similar, as depicted above. The loss ratio by electron collisions for O and H plasmas was given in (Marchand et al. 1995) with a value of about 8 at 2.7eV (see Figure 9). The transport losses on the other hand are inversely connected to the particle mass, via the particle fluxes. The losses are thus smaller for oxygen compared to hydrogen. This combination of changed losses leads to a reduced plasma density and a small reduction of the plasma temperature in the modelling result. The different reaction cross-sections and reaction path (for example the presence of negative O ions) are not treated by this

approximate implementation of O plasmas. Using the standard conditions of H_2-ICWC defined in the beginning of this section and implementing the temperature dependent electron cooling coefficient and mass of oxygen into the model, the parameters of the extrapolated O_2 plasma model are obtained (Table 1).

Plasma species	T_e [eV]	n_e [10^{16}/m³]	Ionisation [%]	E_i [eV]	I_{sat} [A/m²]
H_2	2.76	46.6	6	7.4	739
O_2	1.9	16.1	2	7.6	53

Table 1: Comparison of the parameters of H_2 and O_2 plasmas modelled for TEXTOR. O_2 plasma parameters are derived by an electron power loss scaling approximation from H_2 plasmas.

The comparison of O_2 to H_2 plasmas shows a reduction of the plasma density by a factor of 2.9 and a reduced plasma temperature by 0.9eV. In case the power losses are dominated by particle transport and not by electron collision losses as in TEXTOR, the ratios of the plasma parameters can also change to the opposite. In addition to the lower temperature and density of O_2 plasmas the wall fluxes additionally reduce with the square-root of the ion mass ratio (equation (17)).

4.2.2 Plasma sheath implications

In low temperature plasmas (T_e<≈20eV), the plasma sheath determines the energy of all ions hitting the walls by the sheath potential drop. The potential evolves due to the neutrality of ambipolar flux of ions and electrons. These plasma conditions typically occur in low confinement time plasmas, e.g. at the edge of a tokamak plasma or in removal plasmas. An analytical model of the plasma sheath in a plasma with T_i<T_e was presented in (Emmert et al. 1980) and also confirmed by a-priori particle kinetic simulations (Berberich 2012). A simpler analytical equation, the fluid description (Stangeby 2000), was confirmed to be in good agreement with these results, even in collision-less (low density) plasmas. The initially Maxwell distributed ion velocities are transformed by the acceleration in the plasma sheath to a narrow energy distribution (Figure 36). The particle fluxes finally impinging on the wall are, especially for plasmas with T_e/T_i>>1, practically mono-energetic due to the sheath acceleration. The kinetic energy provided by the sheath potential V_s is given in the fluid description (Stangeby 2000) by

$$V_s = \frac{1}{2} * ln\left(2 * \pi * \frac{m_e}{m_i}\left(1 + \frac{T_i}{T_e}\right)\right) * \frac{k_B T_e}{e} \tag{55}$$

For H plasmas the fluid description results in a sheath potential of 2.7 times the electron temperature in eV. In comparison to 2.56 derived by the analytical theory and values of 2.3 to 2.6 derived by particle simulations only a minor difference is found. The distribution function f of the impinging ion energy E_i can thus be approximated by the Delta function

$$f(E_i) \approx \delta(E_i - V_s) = \delta\left(E_i - \frac{1}{2} * ln\left(2 * \pi * \frac{m_e}{m_i}\left(1 + \frac{T_i}{T_e}\right)\right) * \frac{k_B T_e}{e}\right) \tag{56}$$

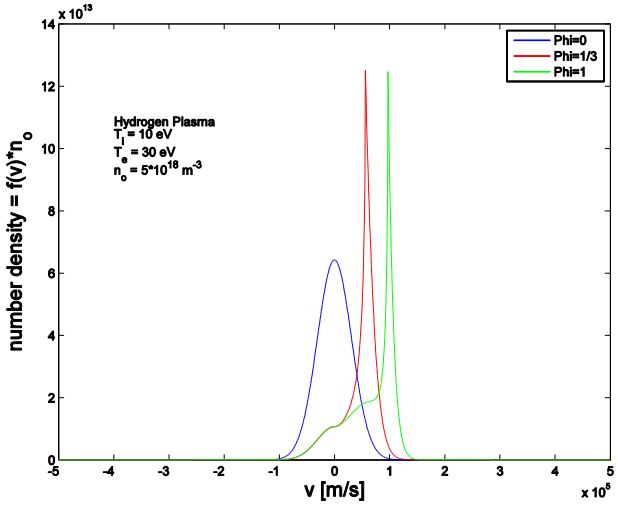

Figure 36: Illustration of the sheath effect on the ion impact velocity distribution. The ion velocity distribution at the sheath edge (Phi=0) is Maxwellian. In the sheath (Phi=1/3) and at the wall (Phi=1) it gets compressed. Only particles with v>0 will contribute to the wall flux and faster particles yield higher flux, so the ion impact energy distribution is even more compressed. Reconstructed from **(Emmert et al. 1980)**.

According to this equation, the ion impact energy is mainly determined by the electron temperature of the plasma, since the sheath potential has to fulfil the ambipolar flux neutrality. The ion mass has a small impact, with higher ion masses requiring higher acceleration potentials to maintain the ambipolar flux neutrality. If several ion species are present in the plasma, the lower mass ions will have a higher weight for the ion impact energy calculation, since their contribution to the positively charged flux is larger.

The ion flux density, in form of the ion saturation current, reaching the wall can be calculated as given in equation (17). As plasmas are quasi-neutral the central ion density n_{i0} is equal to the electron density n_e divided by the ion charge z. The particle flux scales linear with the plasma density, but only square-root with its temperature. For maximizing the flux, the plasma density is thus the determining factor. It has to be noted, that heavier ions show a reduced flux at the same plasma parameters, due to their reduced speed.

In magnetized plasmas the equation is only valid if wall and magnetic field are perpendicular to each other (Stangeby 2000). As soon as this is violated $E \times B$ drifts will change the particle movement in the plasma sheath and a magnetic pre-sheath will develop. The ion flux density can change according to the angle θ between surface and magnetic field lines

$$\mathrm{I_{sat\theta}} = I_{sat} * \sin(\theta) \tag{57}$$

The electrostatic field of the plasma sheath will, even in the case of an inclined magnetic field, force the ions to impact wall surfaces with normal incidence. This is relevant for the calculation of sputtering. In the special case of the magnetic field and surface being perfectly parallel equation (59) has to be extended by the so-called funnelling effect. The transport

parallel to the magnetic field does not give a contribution to the surface flow anymore. Particles can still reach the surface by their gyro-motion along the magnetic field, if the Larmor-radius (equation (11)) intercepts the surface area. For small surfaces compared to the magnetic flux surface area, e.g. local limiters or probes, this effect collects, by the effective particle transport parallel to the magnetic field, currents like a funnel. This current density can be much larger than the current density normally outflowing from the magnetic flux surface. The effect will be treated as an additional constant which in complex ways depends on the plasma, magnetic configuration and probe size

$$\mathrm{I}_{\mathrm{total}} = I_{sat\theta}(\theta) + I_{funnel} \tag{58}$$

4.2.3 Removal process

Having obtained the plasma parameters, the important effects of the plasma sheath and the impact on the material release by sputtering, it is possible to calculate the surface removal rate by plasmas. The areal removal rate density R_P of a plasma method is determined by the product of sputtering yield Y at ion impact energy E_i and the incident ion flux density, represented by the ion saturation current density I_{sat}:

$$R_P = Y(E_i) * I_{sat}/e \tag{59}$$

The incident flux is determined by the plasma parameters and can be calculated from the plasma parameters, equation (17), yielding

$$R_P = Y(E_i) * \frac{0.61 * n_{i0}}{e} * \sqrt{k_B * T_e/m_i} \tag{60}$$

The plasma density is, according to this equation, of the same importance as the sputtering yield. The flux density has only a square-root relation to the plasma temperature. The ion impact energy is proportional to the plasma temperature T_e, according to equation (55). The sputtering yield has a complex relation to the impact energy which cannot be treated analytically, see for example Figure 10. Plasma density and temperature are determined by the balance of input power and power losses of the plasma (section 4.2.1). For a maximum surface release rate a gas with maximum sputtering yield at accessible ion energies (<100eV) and minimum plasma cooling effect and thus maximum ion density and wall flux is required.

The co-deposit material removed by PIR is ejected into the plasma. In the plasma it can be ionized and contribute to plasma cooling as seen in the last section, but also contribute to the wall flux. The returning material flux Γ_m can be re-deposited by sticking to the surfaces with a probability S, reducing the effective removal rate.

$$R_{eff} = R_p - S * \Gamma_m \tag{61}$$

The more material is accumulated, the smaller the effective removal rate will be. The actual

removal of co-deposits from the vessel is done by the device vacuum pumps in the form of volatile gases. If no volatile gas is formed, e.g. by impact of a noble gas on a pure carbon surface, the material will, after several re-erosion steps, stick somewhere in the machine on a surface not accessible by the plasma and cannot be removed from there (wall pumping). These areas will be remote areas. To remove a major part of the material beforehand, its extraction from the device by pumping has to be more effective than its re-deposition. The equilibrium partial pressure of each product gas is determined by the balance of pumping and influx by surface removal. The effective removal rate R_{eff} can thus be limited either by the pumping speed constant P [volume/time] of the device or, in case of fast pumping, the surface removal rate. The product gas particle pumping rate is given by the pumping constant P and the gas particle density, defined by the partial pressure p_{gas}, gas temperature T_{Gas} and the Boltzmann constant k_B. With this and the surface area A_{wall} affected by plasma removal, an effective removal rate of pumping can be stated

$$R_{eff} * A_{wall} = \frac{P * p_{Gas}}{k_B T_{Gas}} \tag{62}$$

This equation is valid for each released species. To calculated the removal of a specific element the equation has to be summed over all product species i with partial pressure $p_{i,Gas}$ and scaled with their respective content c_i (e.g. c_i=2 for carbon in C_2H_2).

$$R_{eff} * A_{wall} = \sum_i c_i * \frac{P_i * p_{i,Gas}}{k_B T_{Gas}} \tag{63}$$

Only neutral gas can be pumped, ions are confined by the magnetic field. To prevent strong material accumulation during PIR the plasma can be pulsed applying a duty cycle. In the off phase no ions are generated and all removed particles can be pumped.

In fusion devices co-deposits can consist of several different elements as so called mixed materials. These species, e.g. carbon, tungsten, beryllium and hydrogen isotopes, contribute in different quantities to the co-deposits total content. Due to different chemical and physical sputtering yields, some of the constituents will be preferentially removed in comparison to others. In the regime of slow pumping, a further preferential removal effect can be induced by the involved volatile pumping channels specific to each element (equation (67)). As an example the removal of a mixed carbon and tungsten layer by deuterium plasmas was investigated in (Wang et al. 2012). It was observed, that with increasing percentage of W in C the removal of carbon was strongly reducing, indicating the effect of preferential sputtering. The preferential sputtering yielded a depletion of C in the ion interaction zone, leaving a structure of nearly pure W. Deuterium has a sputtering threshold on tungsten of about 200eV, so no sputtering can be expected under the investigated conditions. This resulted in a very strong decrease of the total sputtering yield. At initial W concentration of >10%, the removal completely stopped after a certain fluence necessary to deplete the interaction zone. The W surface layer shielded the a-C:W underneath. This

rather extreme case shows, that for the removal of mixed layers discharges have to be tailored, e.g. by adjusting the gas pressure, to compensate for the different elemental effects and the involved thresholds and release behaviour.

The modelling results provide insight to the optimization of removal plasma discharges. The input power has a linear relation to the plasma density. The maximum technically feasible input power is thus the best choice for fast surface release of material. The neutral gas pressure offers the most flexible point of optimisation. By the gas pressure, density and wall flux can be maximized or a certain ion impact energy can be achieved by using lower pressures yielding higher plasma temperatures. A feedback controlled pressure inlet can be necessary in practical application to counter wall pumping effects. Impurities were seen to have a detrimental effect on the removal efficiency by reducing the plasma density drastically. A significant accumulation in the plasma can be avoided by sufficient pumping speed and/or a plasma duty cycle <100%. Using a lower removal rate to increase the pumped fraction offers an option, since the steady-state impurity concentration is defined by the balance of release (by plasma removal), re-deposition and pumping.

4.3 Required experimental investigations

The models presented in this section require experimental verification. Several aspects of the models were compared to literature data, but the models revealed aspects not investigated so far. New experiments, designed according to these open questions, are required.

The TCR model emphasizes the importance of reactions in the co-deposit bulk for the removal rate by the discovery of the diffusion and reaction limited regimes. In the literature tokamak co-deposits were investigated with respect to this question, but tokamaks feature complex deposition conditions and material mixtures. The exposure of well-defined laboratory samples of several thicknesses is necessary to close the gap. A second aspect is the importance of chemical interaction for TCR. Most literature data were obtained with O_2 as reactive gas. The effect of chemistry and the validity of the assumed models for temperature, pressure, time and co-deposit structure effects have to be investigated with an alternative reactive gas.

The model of plasma removal needs verification by local sample removal rates. The global analysis found in the literature was identified to be pumping speed limited and thus cannot deliver the surface release rates provided by the model. Sample exposure to removal plasmas is necessary in different base gases to investigate the impact of the cooling properties specific to each gas species. Plasma ion flux analysis has to be carried out in parallel to co-deposit removal in order to separate the influence of flux and sputtering yield, since the removal rate is given by their product.

5 Experimental results and comparison with models

5.1 Sample preparation

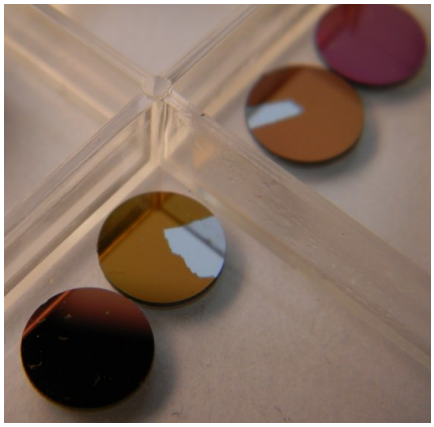

Figure 37: Photography of 4 samples typically used for the experiments. The silicon discs are coated with a-C:D layers. The two discs in the centre were partly covered during deposition for analysis purpose.

For all experiments samples are prepared in the vacuum chamber PADOS, see section 3.1, by PECVD on polished (roughness R_a<5nm), high purity (>99.999%) silicon discs of 11mm diameter and 0.3mm thickness. The substrates are only cleaned using 2-propanol prior to deposition. Surface analysis of the substrates evidences no oxygen or other impurities on the substrates, so further cleaning is not necessary for good layer adhesion. The deposition plasmas are fed with 99% purity CD_4 to deposit a-C:D layers on the substrates. Fixed self-bias voltages of 100V or 300V with neutral pressures of 1-6Pa CD_4 are applied. Due to the device properties of PADOS, an input power of 30-45W is resulting at 100V bias and 170W at 300V bias. The surface temperature is monitored during deposition by a type-K thermocouple, with a typical value of about 200°C. Deposition rates of about 200nm/h are achieved. The deposition conditions, especially the input power, slightly vary for the different experiments and during the course of each deposition. The growth of co-deposits on vessel surfaces and the impact on electrical conductivity is responsible for these changes. Exemplary samples used for the following experiments are shown in Figure 37.

The deposited a-C:D layers are analysed by the methods depicted in section 3.3 for material content (D, C, and impurities), optical properties and thickness. The layer density is calculated using the material content determined by NRA/RBS and the ellipsometric thickness. The layers are pre-characterized, exposed and then post-characterized. All layers exhibit a high purity, determined by NRA/RBS. No inclusion of metals, oxygen or other impurities is found in the co-deposits, with detection thresholds of 10^{15} at/cm². The purity (C+D+H) is thus >99.9 atom%. H content cannot be determined with the given methods. The H content is assumed to be small, due to the deposition gas purity. H bears nearly the same chemistry as D, so the influence of H on structural layer properties is negligible. No layer delamination is observed on any sample.

5.2 Thermo-chemical removal

Several studies of different parameters are conducted. Some of the results obtained in the framework of this thesis are already published. Section 5.2.1 and 5.2.2 are using figures and tables and literally cite excerpts from the publication (Möller et al. 2014). Section 5.2.3 is based on the publication (Wauters et al. 2013) also related to this work.

5.2.1 TCR rate proportionality to layer thickness (O_2)

By keeping the deposition parameters (pressure 8Pa, bias voltage -100V, gas flow 20sccm CD_4, surface temperature 200°C) constant and varying the deposition time (60 to 300min), five different a-C:D layer thicknesses (130-700nm) on polished, high-purity, single crystalline silicon substrates were produced. A refractive index of n(589nm)=1.65, D/C=0.9 and a density of 1.35±0.1g/cm³ was measured.

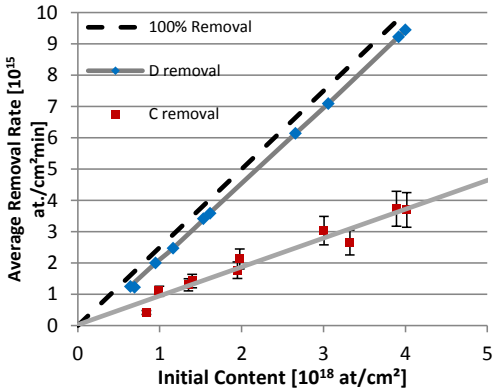

Figure 38: Removal rate of D and C vs. initial areal content of the corresponding element. The dashed line indicates complete removal, the grey lines are linear fits to the data points.

After pre-characterization, the samples were simultaneously exposed in PADOS to TCR at 350±5°C and 1±0.01kPa O_2 for 400min. For each thickness two samples were exposed. The removal rate is calculated by taking the difference between pre- and post-exposure inventory, divided by the exposure time. O retention in the remaining layers was measured by RBS to values of 5 to 55*10^{16} O/cm² with higher values detected in thicker layers. A proportionality of the O content with the remaining layer thickness cannot be clearly stated, due to the low precision of the method. It cannot be identified, whether the O originates from the TCR process or air and water going into the layer from the atmosphere, but earlier studies observed O-uptake during TCR (Wang et al. 2012). The remaining layers were measured with ellipsometry, showing a reduced density of 1.1±0.2g/cm³, increased n=2 and absorption index k=0.18 as well as a thickness reduction of 30%.

Figure 38 shows the fit of equation (46) to the experimental data. The plot shows the removal rates of D and C together with a dashed line, corresponding to the complete removal of the initial content during the experiment, illustrating the maximum attainable, time averaged removal rate in this experiment. The measured removal of D is close to this maximum and is therefore, as the instantaneous removal rate decreases strongly in the final stage (Haasz and Davis 1998), only a lower limit for the removal rate. Possible deviations from the straight line may be hidden by the nearly complete removal. The C removal is at an intermediate stage (~40% removed) and thus not distorted by the effects of nearly complete removal.

All C data points are in good agreement with the linear fit, thus confirming the assumption of a linear relation between the initial content and the TCR rate. The TCR rate of C with O_2 is seen to be significantly smaller than that of D. The negligible value of $R_{surface}$ of the C fit points out the importance of the inner surfaces for TCR. Deviations from the linear relation can arise from differences in the properties of the exposed layers. This scatter around the

linear assumption is within the NRA measurement errors, supporting the outcome of the pre-characterization of similar layer properties.

5.2.2 Thermo-chemical removal by NO_2

For the NO_2 experiments layers were deposited in PADOS on Si substrates with 100V bias and 6Pa gas pressure. The layers have a refractive index n=1.7, k=0.01 and D/C=1.1. The deposited layer thickness of type (i) was 550nm and contains $3.5*10^{18}$ D/cm² and $3*10^{18}$ C/cm². Type (ii) had a thickness of 140nm, containing $8.9*10^{17}$ D/cm² and $7.8*10^{17}$ C/cm². Lower porosity layers (type (iii)) were deposited with 300V and 6Pa. The deposited layer thickness of 330nm contains $1.9*10^{18}$ D/cm² and $2.1*10^{18}$ C/cm² with D/C=0.9 and n=2.0. The samples were exposed to a set of conditions, listed in table 2.

T_S [°C]	p_{Gas} [kPa]	Time [min]	D Rate [10^{15} at/cm²s]			C Rate [10^{15} at/cm²s]		
			(i)	**(ii)**	**(iii)**	**(i)**	**(ii)**	**(iii)**
[a]350	20	3	17.0	4.3	2.0	8.8	3.2	-5.7
[a]350	20	15	3.5		0.5	1.6		0.3
350	20	10	5.8	1.5	0.7	5.1	1.3	0.3
350	2	3	18.3	5.0	-1.0	12.4	4.3	-3.7
275	2	20	2.6	0.7	0.2	1.6	0.2	0.1
200	2	20	0.3	0.3	-0.2	0.5	0.0	-0.1
275	2	3	15.7	3.4	0.4	9.1	2.6	1.3
275	2	15	3.4			1.3		
350	20	3	19.2	5.0	4.9	15.1	4.3	3.3

[a]**Exposure to O_2, all other to NO_2**

Table 2: TCR experiments with O_2 and NO_2 on a-C:D of (i) 15% porosity, 550nm thickness, (ii) 15% porosity, 140nm thickness and (iii) <3% porosity, 330nm thickness. Error of p_{Gas}: 6.7%; T_S: 4%; D and C rate: 20% of material content. Negative values are, within their specific errors, compatible with zero.

The sample exposure to NO_2-TCR was done in an experimental device similar to PADOS (Alegre et al. 2013).

The effect of gas pressure on the removal rate was weak in the tested range. To fit the pressure relation a Langmuir adsorption isotherm (equation (47)) is used with the data of 350°C with 2 and 20kPa NO_2 and 3min exposure. This function was chosen to describe the reactive gas loading of pore surfaces (Richou et al. 2009). At 10^{-4}Pa and 350°C no removal was observed, giving a third data point. The low amount of data points only constrains the function assumed to describe the behaviour (Figure 39).The adsorption coefficients K_L derived for D (K_L=9.1, A_2=19.3) differ from those for C (K_L=2, A_2=15.5).

Three experiments were conducted for the temperature relation at 2kPa with 3min (350°C, 275°C) and 20min (200°C) exposure time. An additional data point is provided by the observed zero removal at room temperature. Fitting the TCR rates with an Arrhenius function, equation (48) results in a good agreement for D and C (Figure 39). An activation energy of 0.76 ± 0.02 eV with a pre-factor A_3=2.5 ± 0.6 $*10^{22}$ at/cm²s for the D reaction and E_A=0.79 ± 0.07 eV and A_3=3.1± 4.0 $*10^{22}$ at/cm²s for the C reaction with NO_2 is determined.

Note that the point for 200°C is in an early removal stage (90% left), while the other points where mostly removed (5-10% left). The errors in E_A and A_3 do not include systematic errors.

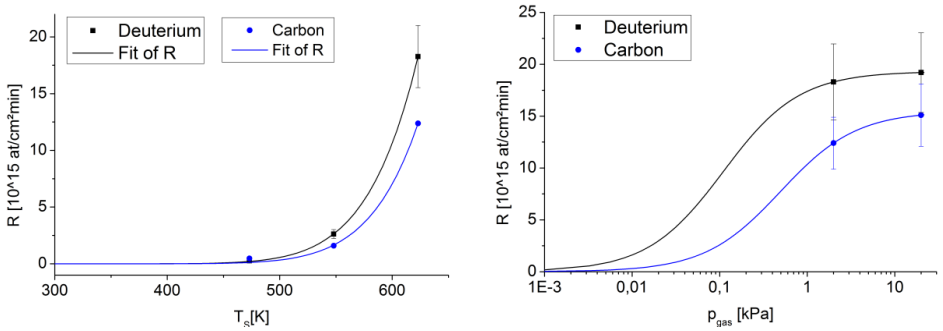

Figure 39: TCR rates of NO_2 on a-C:D layers (D/C=1) of type (i). Left: Temperature relation with fitted Arrhenius functions. Right: TCR rates related to gas pressure with Langmuir isotherms.

In addition to pure a-C:D layers mixed W-C-H layers were exposed. The layers were produced in a sequential W magnetron sputter and acetylene RF discharge in a device describe in (Acsente et al. 2011). The initial composition of the two W-C-H layer types was $3*10^{18}$ C/cm², $1.9*10^{18}$ W/cm² (W/C=0.6) and $7*10^{18}$ C/cm², $9*10^{17}$ W/cm² (W/C=0.12), respectively. Both included about 10^{18} O/cm² already in pre-characterization. The layers were exposed to TCR simultaneously with the a-C:D layers. The exposures lead to delamination of the layers in several cases. No change of W and C content was detectable with the NRA/RBS measurements in both layer types. The H content was not measured. A significant increase of the O content was detected with values of O/W=2-3 in all exposed layers, pointing to a possible formation of stoichiometric tungsten oxides.

The relation of the TCR rate on the surface temperature has been investigated. An activation energy of 1.7 eV was measured in (Balden et al. 2005) for the reaction of O_2 with graphite and 0.5eV for D in a-C:D (Davis and Haasz 2009). The activation energies for NO_2 with D and C in a-C:D are found to be ≈0.78eV. The use of NO_2 was seen to show significant decrease of the time necessary for the removal procedure in comparison to O_2. The lower limit of the wall temperature necessary for TCR was found to be around 200°C.

5.2.3 Impact on magnetic fusion plasma operation

The presence of oxygen, originating from oxygen compounds used in TCR, in plasma facing materials with its strong plasma cooling capability (see section 4.2.1) can have significant impact on fusion plasma operation. The effective plasma cooling of oxygen can pose an insuperable barrier for reaching higher plasma temperatures necessary for nuclear fusion with a given input power. To investigate this and a possible recovery from this state by plasma impact removal, a study with dedicated implantation of oxygen into the TEXTOR vessel walls and PFCs by $^{18}O_2$-ICWC is conducted in the frame of this work (Wauters et al. 2013). The oxygen presence after the procedure prevented subsequent fusion plasma start-up, as indicated by increased oxygen line radiation. Surface analysis of the marker isotope

after $^{18}O_2$-ICWC and particle balance shows retention of 1.9 ± 0.9 10^{20} O/m² on plasma facing surfaces (14.4m²). 10^{17} oxygen atoms are released in two unsuccessful ohmic plasma start-ups after the wall loading. The resulting volume density, with the TEXTOR plasma volume of 8m³, of 6.3*10^{15} O/m³ is in good agreement with the limit of oxygen allowable during a tokamak discharge of 10^{-3} to 10^{-2} (Ashby and Hughes 1981) and the typical fusion plasma densities of TEXTOR in the range of 10^{18}/m³ to 10^{20}/m³, supporting the assumption of a radiative collapse. After application of TCR oxygen can also be present in the vessel by surface adsorption and oxide formation. The amount of O stored by these mechanisms is probably different since ions penetrate the materials by different means than neutral gas molecules. Data presented in section 615.2.1 show a significant oxygen retention in remaining a-C:H after TCR. The presence of oxygen in co-deposits and also oxides formed on other surface is thus probable.

Over 10^4 fusion plasma discharge attempts would be required to deplete the observed oxygen reservoir. As an option for faster recovery of fusion plasma compatible wall conditions, plasma impact removal by D_2-ICWC (see section 4.2) is tested after the wall loading. The study shows that oxygen is largely removed from the plasma-facing surfaces by 1h47min of 10% duty cycle D_2-ICWC, as determined by surface analysis in the post-characterization of exposed surfaces. The retention in remote areas seems to be significantly less affected, but the uncertainties of the extrapolation are relatively large. Fusion plasma discharge initiation is possible after the D_2-ICWC treatment, emitting less oxygen line radiation. This proves the feasibility of wall conditioning by plasma impact removal with hydrogen isotopes after oxygen loading. The oxygen retained in remote areas seems to be relatively unimportant for the fusion plasma operation, but is also inaccessible by D_2-ICWC.

5.2.4 Conclusions for thermo-chemical removal

The effectivity of thermo-chemical removal of carbon based co-deposits with O_2 and NO_2 is demonstrated. The developed reaction-diffusion model is found to be in agreement with literature data on O_2 and also with the new NO_2 data.

The observations with O_2-TCR (Figure 38) show a linear relation between the removal rate and the co-deposit thickness proving the bulk effect of TCR. The model relates this effect to the presence of reactive gas in the volume and fast gas diffusion in comparison to the reaction speed. This diffusion-limited regime provides reactive gas to the whole layer volume at a faster rate than it is lost by reaction. The presence of oxygen in remaining layers after TCR further validates this existence of reactive gas in the material. The transition to the diffusion-limited regime was observed in the literature, but the necessary temperatures are not tested in this work.

The exposure of a-C:D deposited at 300eV ion impact energy results in an at least 5-fold slower removal by NO_2-TCR compared to 100eV deposits. Higher ion impact energy was seen to increase the gas permeability (related to coefficient *D*) through a-C:H (Vasquez-Borucki, Jacob, and Achete 2000). A reduction of gas capacity q_{Max}, e.g. by less inner surface area

(pores), and a change of the adsorption and reaction properties K_L, E_A e.g. by predominance of a different carbon binding are possible explanations for the reduced removal rate within the current understanding of a-C:H structure. The transition to the diffusion-limited regime is also depending on reaction and diffusion parameters (Figure 26) and thus also on the co-deposit properties. The difference in removal rates was at least a factor five, pointing out the high importance of co-deposit structure and growth conditions for TCR processes.

The removal rate of NO_2-TCR is seen to scale with the surface temperature according to the Arrhenius equation. The literature observations for O_2 are thus in agreement to the NO_2 data. The significant difference in the rates of O_2 and NO_2 can be related to the strong importance of co-deposit to reactive gas chemistry (P, E_A, K_L, q_{Max}) as predicted by the model. The removal by NO_2 exhibits only slightly different rates for deuterium and carbon in contrast to literature observations with O_2. The higher effectivity of NO_2 can be related to the weaker binding of O in NO_2 in comparison to O_2. The weaker bond of one of the O in NO_2 allows easier extraction of one O from the molecule to form the exhaust products H_2O and CO. The different behaviour with respect to deuterium and carbon removal indicates the importance of individual elemental product channels, where carbon offers different molecular channels than hydrogen isotopes.

The relevance of adsorption processes was seen in the literature, with a fit presented in Figure 28. The new data for NO_2 are in agreement with the physical adsorption model, but the low amount of data points does not allow a defined statement. In the understanding of adsorption, the effect of the gas pressure on the removal rate becomes very small, if the adsorption density reaches a full surface-monolayer. The data indicate that a full monolayer is approximately reached at the tested exposure and chemical interaction conditions applied in the NO_2-TCR experiments.

The exponential decay of removal rates with progressing removal is observed also for NO_2 with different exposure times under fixed conditions. The model connects the effect to the loss of reaction partner density n_C during removal, similar to the effect of co-deposit thickness. Observations in the literature show the same effects, occasionally connected with an increase of removal rates in the beginning of the process. The competition of an increase in co-deposit reactive gas capacity to the reaction partner density decrease is a possible explanation.

The effect of chemical reaction of oxygen with plasma-facing and remote surfaces in a nuclear fusion device is investigated by ^{18}O plasma implantation. Chemical reactions can occur with all surfaces, as the neutral gas has access to all areas and the vessel surfaces in TEXTOR are above 150°C. The retention effect of TCR reactive gas is seen to be relevant for nuclear fusion application, as it shows a detrimental effect on fusion plasma cooling. Treatment with hydrogen based plasmas to invoke chemical reactions with the retained oxygen successfully releases the oxygen to re-establishing fusion plasma operation.

In this work laboratory samples are investigated, showing the same behaviour as observed on tokamak co-deposits in the literature. The fundamental structure of the co-deposits relevant for TCR is thus apparently similar. The investigation of TCR on co-deposits from laboratory devices under similar conditions of surface temperature, neutral gas pressure and ion impact energy is seen to provide adequate substitutes for removal investigations of nuclear fusion co-deposits.

5.3 Plasma impact removal

5.3.1 ECR plasmas in laboratory device

To test the model predictions two devices of different size and properties have to be employed. TOMAS is chosen, as it is a reliable and easy to handle laboratory device. It thus provides a suitable basis for assessing the physics of plasma removal with a larger set of different gases and conditions than in a nuclear fusion device. The combination of toroidal magnetic field and microwave heating lead to similar removal plasmas as in tokamak devices. For all experiments in TOMAS the set of parameters shown in Table 3 are applied. These parameters are kept constant to obtain a change of plasma parameters and removal effectivity only by the impact of the inserted gas species.

Input Power	Gas pressure	Sample Temperature	On axis field	Coil current	Base pressure
1.5kW	0.1Pa	250°C	0.066 T	1150 A	<0.0001Pa

Table 3: Removal discharge parameters applied in all TOMAS experiments.

The values were found in an earlier work to provide the maximum possible plasma density in TOMAS (Matveeva 2008). The exposure time is adapted to reach a measurable co-deposit thickness contrast, without reaching a total removal. The removal is observed via an optical camera as change in the interference colour of the a-C:D layers on the substrates. In all except two cases the samples are grounded with the vessel wall. The sample temperatures are kept at 250°C during the exposures.

The plasma is analysed via a Langmuir probe installed at the same radial position as the samples. The ion saturation current and the plasma temperature are extracted from the probe characteristics. Large uncertainties are present in the values, since significant noise is observed in all probe measurements. The results and the derived values are depicted in Table 4. The ion impact energy E_i is derived from the plasma temperature T_e and equation (56). The plasma density n_e is calculated using the ion saturation current I_{sat} and equation (17). The plasma parameters are seen to differ from the TEXTOR values shown in the next section. In TEXTOR typically higher confinement and thus higher density with lower temperature are observed.

	H_2	D_2	NH_3	He	Ar	N_2	O_2	ArD_2
I_{sat} [A/m²]	46	27	41	136	45	72	13	91
U_{float}[-V]	17	15	10	16	50	20	2	11
T_e [eV]	10	9	9	16	20	10	2,6	12
n_e [10^{16}/m³]	2.7	2.9	7.8	10	20	17	5	16
E_i [eV]	27.9	28.2	37.8	56.0	90.0	41.1	10.6	37.7

Table 4: The plasma parameters were determined by a Pin-Langmuir probe using the full characteristics, positioned at the same radial coordinate as the samples, but on the opposite side of the torus.

The samples are prepared in PADOS. Polished Silicon wafers are coated in one run with a-C:D layers of 510±15nm thickness at 300V bias and 6Pa. The layers initially consist of $2.3\pm0.3*10^{18}$ D/cm² and $4.3\pm0.5*10^{18}$ C/cm² resulting in D/C=0.56±0.05. They are exposed with a part of the sample shadowed from the plasma. The pre-exposure value is taken after the experiment from the shadowed area and thus also includes thermal desorption effects. The thermal desorption effect is seen to be negligible by comparison with fresh samples. The results are shown in Figure 40 and Figure 41 for all investigated conditions.

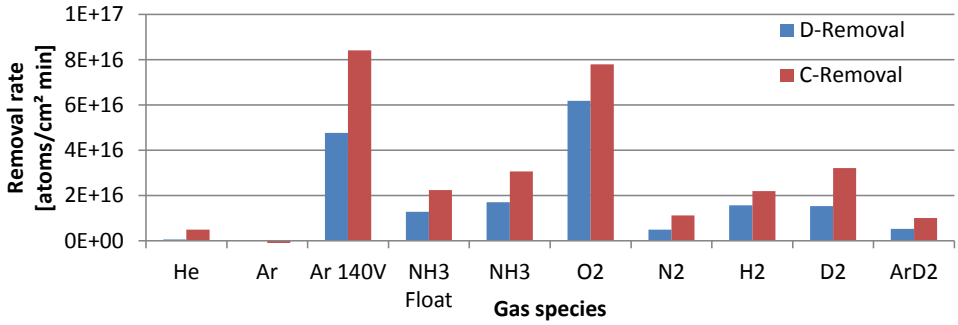

Figure 40: Removal rate of a-C:D layers with different gas species and ion energies in TOMAS, measured by NRA/RBS.

The highest removal rate is obtained with Ar with -140V bias on the substrate holder. Oxygen yields a similar rate of $1.3\pm0.3*10^{15}$ C/cm²s. All other gases` rates are more than a factor of 2 smaller. D_2 and NH_3 take the third place with about $5.2\pm1*10^{14}$ C/cm²s. For NH_3 floating and grounded (E_i=38eV) sample conditions are compared. The yield is slightly lower in the floating case (factor 1.4), probably due to the lower ion acceleration potential (Floating potential: 10V → E_i=28eV). Mixing Ar and D_2 in equal amounts leads to a rate even lower than the average rate of the pure species. Enhanced sputtering yields due to the combination of a noble gas and hydrogen impact, as summarized in (Behrisch 2007), is not found here. The noble gases and nitrogen, as a nearly inert species, do not show significant removal without biasing.

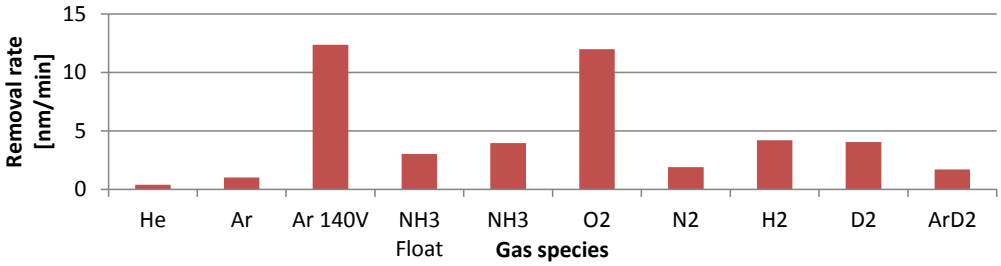

Figure 41: Thickness reduction rates obtained by the different plasma gases, measured by ellipsometry.

Only minor changes of the D/C ratio are observed in the comparison of pre- and post-exposure measurements. The reduction of thickness is also corresponding with the reduction of carbon content, compare Figure 40 and Figure 41. These two facts indicate that plasma impact removes material only from the surface, keeping the deeper parts of the material unaffected.

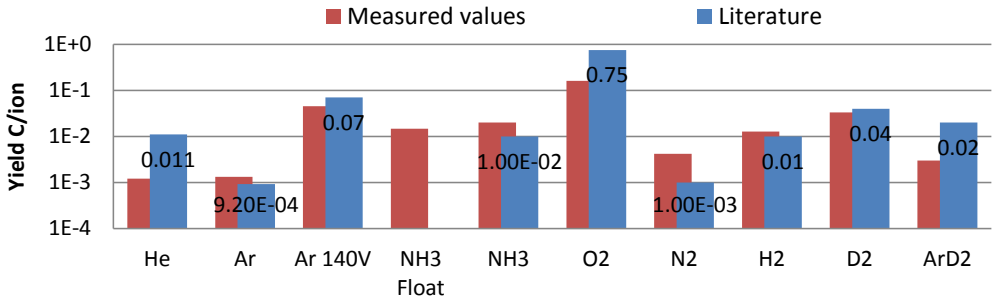

Figure 42: Comparison of the experimental ion C sputter yields with dynamic sputtering calculations including chemical sputtering data from the literature (H, D, O on C) on an a-C:D layer with D/C=0.56 as used in the experiments. Incidence energies E_i are given in Table 4. Particles are expected to arrive as atomic ions, because the ionization potentials are higher than the bond-breaking potentials for H_2, D_2, N_2, O_2, NH_3.

The removal rate normalized to the incident ion flux (I_{sat}) is the particle sputtering yield. This value is compared to values calculated for physical sputtering by SDTRIM.SP with the ion impact energy given in Table 4 and the surface temperature of 250°C. The model is used in dynamic surface mode, taking into account the change of surface composition during the exposure. A flux of $3*10^{20}$ions/m²s, a fluence of 10^{20}ions/cm² and 10^5 projectiles are used to reach stable solutions. Literature data for the yields of the chemically active species H, D, O and N are taken from (Behrisch 2007). The yield for NH_3 is calculated by only using the H chemistry and neglecting the N chemistry. With this, the synergistic effect of the C-N-H chemistry can be understood as the difference between the yields of H_2 and NH_3. The dynamic SDTRIM.SP calculations reveal a full depletion of deuterium from the ion surface interaction region by preferential sputtering. In conclusion the carbon yield is limiting the process and the yield for removing deuterium is equal to the carbon yield times the D/C ratio of the layer. Only in the case of D_2 plasmas a slightly lower D yield can be expected due to implantation by the plasma. Within the uncertainties the yields of H_2 and NH_3 can be

considered equal, indicating that only H is responsible for the removal and synergistic effects are small at the provided ion impact energies.

5.3.2 ICWC experiments in tokamak TEXTOR

ICWC (Ion Cyclotron Wall Conditioning) is a technique usually applied in superconducting fusion devices for wall conditioning purposes and also planned for application in future devices (Wauters 2011). The basic mechanisms of plasma heating are similar to ECR discharges, since the plasma confinement is also based on magnetic fields and usually most of the input power (>80%) is also coupled to the electrons, with a minor part coupled into the ions. The difference is that a lower frequency, close to the hydrogen or deuterium ion cyclotron frequency, usually at the vessel centre, is applied. The main physical differences between TEXTOR and TOMAS, leading to different plasma and removal parameters, are the better confinement, through size and magnetic field strength, and the higher input power density of TEXTOR. The large differences in these values provide a valuable test bed for the modelling analysis. Furthermore TEXTOR utilizes carbon plasma facing components, providing higher impurity influx to the plasma. With the TEXTOR parameters being significantly closer to future tokamaks, extrapolation of the results becomes credible.

Based on the results of section 5.3.1 and the considerations on the plasma removal rate R_P discussed in section 4.2, three gases are chosen for removal experiments in the tokamak TEXTOR. The gases are chosen to offer removal rates large enough to yield detectable results with the lower exposure times obtainable in TEXTOR, but also provide significant differences in their plasma relevant properties. The experiments employed H_2, D_2 and $^{18}O_2$ gas and are conducted in a duty cycle discharge scenario. This technique intends to limit the accumulation and re-deposition of removed material in the plasma to keep $R_P \approx R_{eff}$ (Wauters 2011). Plasma exposure times of several hundred seconds are necessary to achieve significant removal, which is only possible with a low magnetic field strength of 0.23T, due to the heating of TEXTOR´s copper coils. Some of the results are also included in cooperative publications (Carrasco et al. 2014), (Wauters et al. 2013).

The experiments are conducted using the staircase holder in TEXTORs limiter lock 1 (section 3.2.2). Samples coated with 400nm a-C:D are placed at the different radial positions of the stairs. The coatings are produced in PADOS with 100V bias at 6Pa pressure. Uncoated silicon samples of the same type used for the coated samples are installed at neighbouring positions to monitor re-deposition. Sample surfaces are installed parallel and perpendicular to the magnetic field vector. The holder is heated and outgassed at 320°C over-night prior to the experiments, to obtain clean surfaces and vacuum. During the exposure the holder is kept at 320°C. The plasmas are investigated using the surface Langmuir probe with sweeping voltage of -200V to +30V (section 3.2.1). In a dedicated D_2-ICWC experiment the rotatable Langmuir probe is implemented to investigate spatial differences and also the influence of the magnetic field on the ion flux density. The experiments are intended to study, beside the plasma-surface interaction, also other physics aspects of ICWC, which is documented in

other publications. Varying plasma conditions are applied, but the sample exposure is limited to discharges with constant plasma conditions. In standby phases the holder front surface is kept at r=0.67m, way behind the liner where no ion flux is present. For exposure the holder is moved to r=0.44m so that the first two stairs are inside the plasma, while the other stairs stay behind the main limiter shadow. The vacuum vessel of TEXTOR is kept at 150°C.

In the H_2-ICWC experiment the samples are exposed to 242s of plasma at 100kW generator power and 0.23T toroidal field, with a power coupling efficiency of about 90% (Lissoyvan 2013). In this experiment no gas pressure feedback is installed and as a result the gas pressure during the discharges varies, due to strong gas consumption of the walls. The initial, targeted pressure of $6*10^{-4}$mbar is reduced below the pressure gauge sensitivity (10^{-6}mbar) in the first 100ms (the plasma breakdown). The pressure recovers over time but, as the discharges last only 0.5s, could not reach the initial value. After each discharge 19.5s of pumping are employed. The sample exposure in the D_2-ICWC experiment consists of 163s of 100kW generator power plasma and 137s of 200kW generator power plasma, both with $5*10^{-4}$mbar feedback controlled total pressure. 2s of plasma are followed by 18s of pumping. The ion saturation current is determined in the 100kW phase for better comparison to the other experiments. When applying the linear scaling of removal with generator power (section 4.2.1) the scaled 100kW plasma exposure time is 437s. Since the a-C:D layers are completely removed in this experiment, the removal rate and yield are only lower limits. In the O_2 experiment $4*10^{-4}$mbar of feedback controlled total pressure are blended with about $1*10^{-4}$mbar of He for technical reasons of antenna operation. The discharges are conducted at 1.9T with 100kW for 4s followed by about 5min of pumping. The optical light emission from the plasmas exhibits inhomogeneity in all experiments, see Figure 43.

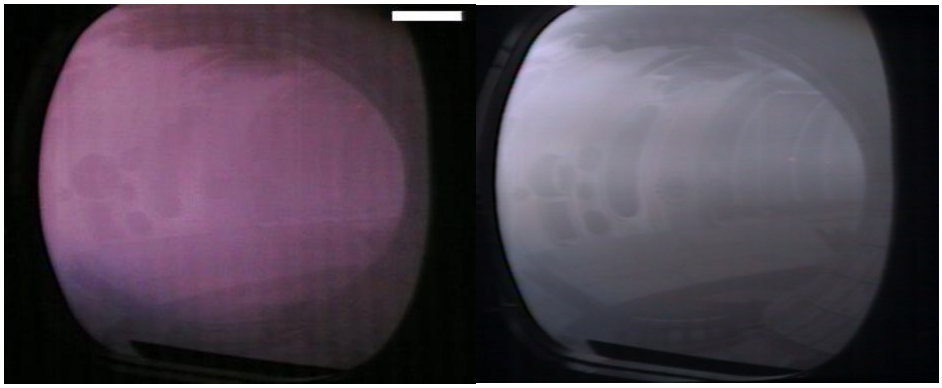

Figure 43: Toroidal view on the optical light emission of an ICWC discharge in H_2 at 0.23T (left) and O_2 at 1.9T (right). The plasma light emission seems to mainly originate from the antenna region (upper left), giving a hint for a spatially non-uniform plasma distribution, especially in the O_2 plasma.

Langmuir probe characteristics are fitted with the equations presented in section 3.2.1. Time frames related to the plasma breakdown (<100ms) are not considered for the evaluation.

The remaining part of the discharges is averaged to improve the signal to noise ratio. Despite the probe guard ring, a linear sheath expansion coefficient >0 is found in all measurements. It is not possible to collect the full probe characteristics, due to the high current in the electron saturation region. Significant noise is present in the transition region, leading to an inconclusive result for the electron temperature. The modelled plasma temperatures in the region of 2.7eV are compatible with the Langmuir probe data and can be used as a substitute. By multiplication of the average ion saturation currents with the discharge time the ion fluence is derived. The removal rate is determined by pre-/post comparison of the shadowed and exposed surface parts of the samples located at radial positions behind the limiters (r>47.5cm), where no re-deposition of carbon is observed. The removal rates of D and C agree with the D/C ratio of the layers. Since D/C≈1 the rates are similar for both constituents. The sputtering yield is calculated by the ratio of removed material and incident ion fluence. The results are presented in Figure 44.

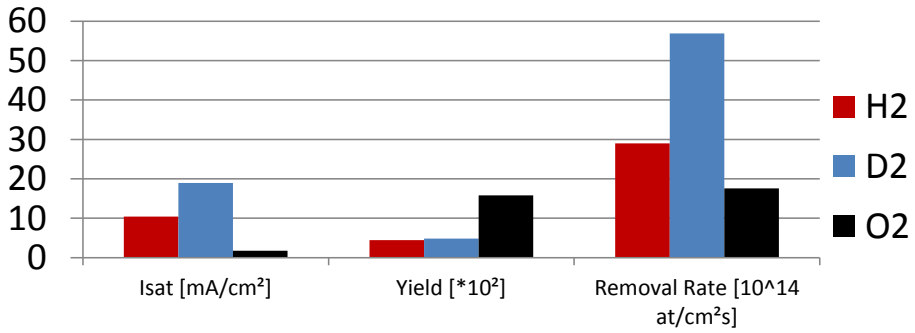

Figure 44: Comparison of the ion flux densities, sputtering yields and net removal rates of the three gases tested in TEXTOR.

The determined yield of D_2-ICWC of 4.8% is in agreement with several sources for sputtering at about 10eV, see e.g. (Dadras and Krstic 2011), (Reinhold et al. 2010) and also with the value of 3.3% measured in TOMAS (section 5.3.1). O_2 exhibits a yield of 16%, in TEXTOR and TOMAS. The literature states a higher value of about 75% at an impact energy of 50eV. For TEXTOR and TOMAS only 8eV impact energy are predicted by modelling. The observed sputtering yield of hydrogen is 4.4% which is about a factor of 3 above the literature and TOMAS values. Deviations of the plasma parameters due to the initial pressure drop and resulting higher impact energies, sputtering yields or wrong I_{sat} measurements are possible explanations. A contribution of the neutral and impurity fluxes or of molecular ions and with that an underestimation of the incident particle fluxes is also possible.

Beside the net removal observed on surfaces behind the limiters (r>47.5cm), deposition is observed on uncoated silicon samples and the holder itself and suppressed removal on a-C:D inside the plasma (r<47.5cm). This hints on significant re-deposition of material originating from the carbon limiters, for surfaces inside the plasma, probably enhanced by the funnelling effect (Stangeby 2000) of parallel transport. Pumping speeds given in section 3.2 can be used to estimate the actual removal of material from the surfaces in the TEXTOR

vessel. The partial pressures are provided by calibrated quadrupole mass spectrometry in similar H_2-ICWC plasma discharge in earlier investigations (Wauters 2011). By comparing with the removal rates behind the limiters, where no re-deposition is observed, the re-deposition fraction can be estimated by the ratio of surface release to pumping. The pumping speed can be used with equation (62) to estimate the maximum removal rate of ICWC, assuming removal only by pumping of released volatile species. For H_2 and D_2-ICWC methane (CH_4) and ethyne (C_2H_2) are the main volatile products, with H representing the mixture of H and D. For O_2-ICWC CO, CO_2 and H_2O are the dominating exhaust products, but no data on partial pressures are available for these plasmas.

In H_2-ICWC a partial methane pressure of $8*10^{-6}$mbar (2%) at a vessel temperature of 420K was observed. The according areal removal rate by pumping from the 14.4m² of PFCs is $R_{eff}(CH_4)=9.2*10^{11}$ C/cm²s. According to modelling ethyne will add a similar contribution (Dadras and Krstic 2011), leading to $R_{eff}=2.6*10^{12}$C/cm²s. The contribution of other hydrocarbons is neglected. This value is about 3 orders of magnitude lower than the measured surface release rate of H_2-ICWC of $2.9*10^{15}$C/cm²s. With the applied 10% duty cycle the effective removal by pumping increases to $R_{eff}= 2.6*10^{13}$C/cm²s in the plasma phase, which is still two orders of magnitude below the measured surface release rate.

For the removal of hydrogen isotopes by hydrogen plasmas more volatile channels exist (hydrogen molecule, etc.) than for carbon, so that the pumping will be more effective. Furthermore with respect to the removal plasmas, arbitrary hydrogen isotopic ratios are possible, since hydrogen does not introduce increased power loss to the plasma. The part of the removed material and hydrogen which is not pumped will be migrated by the removal plasma. To return to the surfaces the material released from a surface has to be ionized in the plasma. Ions follow the magnetic field lines and, as a result, their transport in parallel direction to the magnetic field lines is faster than the perpendicular transport. By this the re-deposition will preferentially occur on surfaces close to the plasma. After several deposition and removal steps, the material will finally end on remote areas, from where the plasma cannot remove it anymore. Due to the small pumping removal rate, about 99% of the released carbon is migrated in the TEXTOR vessel.

The impact of $^{18}O_2$-ICWC on the vessel inventory of oxygen is assessed directly after the corresponding removal experiment, as already presented in section 5.2.3. Fusion plasma start-up is not possible due to the high plasma-facing surface loading with oxygen. Subsequent D_2- and He-ICWC is able to recover the surface status and even improve it in comparison to the glow-discharge conditioning applied before pre-characterisation of TEXTOR (Wauters et al. 2013). Oxygen co-deposits are removed from the plasma-facing surfaces as indicated by surface analysis. The effect on oxygen content on remote surfaces is comparably small, in agreement with the understanding of ion transport. A possible explanation for the improved conditioning effect of ICWC is the similarity of plasma wall contact between the magnetized plasmas (fusion plasma and ICWC) in contrast to glow-discharges.

5.3.3 Plasma characterization and radial profiles

The rotatable multi-langmuir probe (section 3.2.1) is used in TEXTOR for the determination of the radial distribution of ion saturation current density during several dedicated D_2-ICWC discharges. All discharges ran with 200kW of input power coupled with 2 antennas at a feedback controlled pressure of $4*10^{-4}$mbar. Toroidal fields of B_T=0.23T, 1.1T, 2.25T and with inverted direction B_T=-0.23T are investigated. By this, the direction of the charge separating vertical drifts is inverted and its effect on inhomogeneity can be studied. With positive B_T the electrons drift upward and the ions downward, with negative B_T the drift directions are exchanged. Since positive (ions) and negative (mainly electrons) charges are separated by toroidal magnetic fields and the power is mainly coupled to the electrons, a shifted asymmetry can be expected. In order to obtain a larger span than possible with the probe length of 54mm in the radial tokamak coordinate *r* the rotatable probe is positioned at different radial coordinates in consecutive D_2 plasma discharges with constant parameters. The currents on the probe heads are recorded while the probe head is rotated by 360° in each individual discharge, resulting in directional ion saturation current values as shown in the example in Figure 45. Data points for 0° and 180° show the current collected on the probe head facing upwards and downwards, respectively. The data points at 90° represent the probe surface being perpendicular to the toroidal magnetic field vector. No significant difference is found between 270° and 90°. The data are fitted with a sinus function with offset, see section 2.5.3

$$I_{sat} = P_1 * sin(\Pi(x - P_2)/P_3) + P_4 \quad (64)$$

With the fitting coefficients $P_{1\text{-}4}$, the collected current I_{sat} and the angle of rotation *x*. Information is extracted from the fitted function, as it also filters out measurement noise.

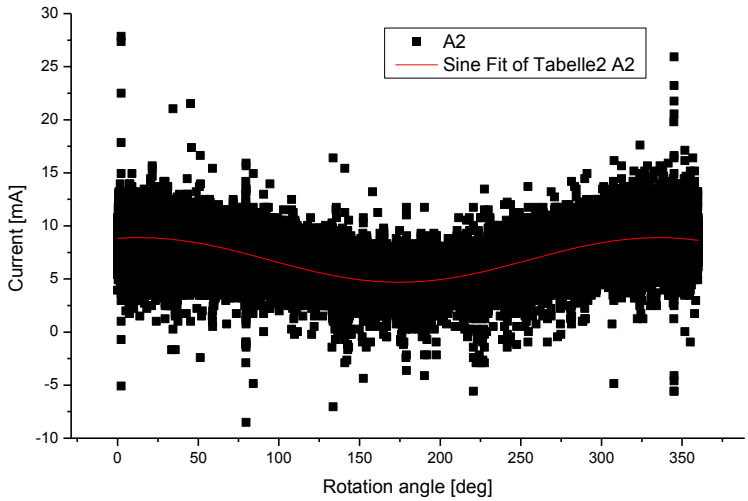

Figure 45: Current collected by 2nd probe head on side A at a position of r=44.9cm with a toroidal magnetic field of 0.23T and fit. 0° corresponds to the probe facing upwards, at 90° the probe surface is perpendicular to the toroidal magnetic field. Background currents are subtracted.

The result is in contrast to the theoretical expectation of minimum, or even zero, current density on surfaces parallel to the magnetic field (0° and 180°) and maximum at perpendicular orientation (90° and 270°) (Stangeby 2000). Only a difference between upward (0°) to downward (180°) facing probe orientation is observed. By applying equation (15) the contribution of charge separating drifts to this difference can be calculated using a temperature of 2.7eV (modelling result) and a density in accordance to equation (17) to

$$I_V(B_T = 0.23T) = 4.1 \pm 1.2\ A/m^2 \tag{65}$$

In case of positive B_T this will add to the 0° value and subtract from the 180° value, but the total impact is much smaller than the observed difference in the order of 190A/m². At larger fields the vertical current density of the drifts will further decrease below the value of (65), down to a value of 0.1A/m² calculated for the O_2-ICWC at 1.9T. The observed differences between B_T=0.23T and -0.23T are also more than a factor 10 larger than the drift contribution. The existence of an additional contribution to flux inhomogeneity, e.g. by plasma density inhomogeneity due to the antenna positions, has to be concluded.

The data show a clear effect of the toroidal field strength on the collected ion current. The reduced ion current can be attributed to a lower plasma ion density. Lower currents are observed at higher field strength, in contrast to the modelling in Figure 32. The current reduced by a factor of 2 for an increase in the field strength by an order of magnitude. Similar results are found in a study investigating the influence of the toroidal field strength in more detail (Lyssoivan et al. 2009). A reduced ion density was attributed to a reduced power coupling efficiency to the plasmas at higher field strength and also the development of spatial variations of the plasma parameters.

In radial direction two zones can be distinguished. Inside the plasma (r<47.5cm) a constant ion flux is received. This constant flux even extends behind the limiter position up to about 51cm. The staircase holder samples are exposed in the region of r=44 to 50cm. The data show that all samples received the same ion flux density and the definition of the net removal rate to be observed on surface outside the re-deposition zone is validated. Behind the radial position of 51cm an exponential decay of the ion flux is observed with a decay constant of about 1cm for all magnetic field values. The liner, as the largest remote area of TEXTOR, with a position r=55cm receives nearly no ion flux from the D_2-ICWC plasma.

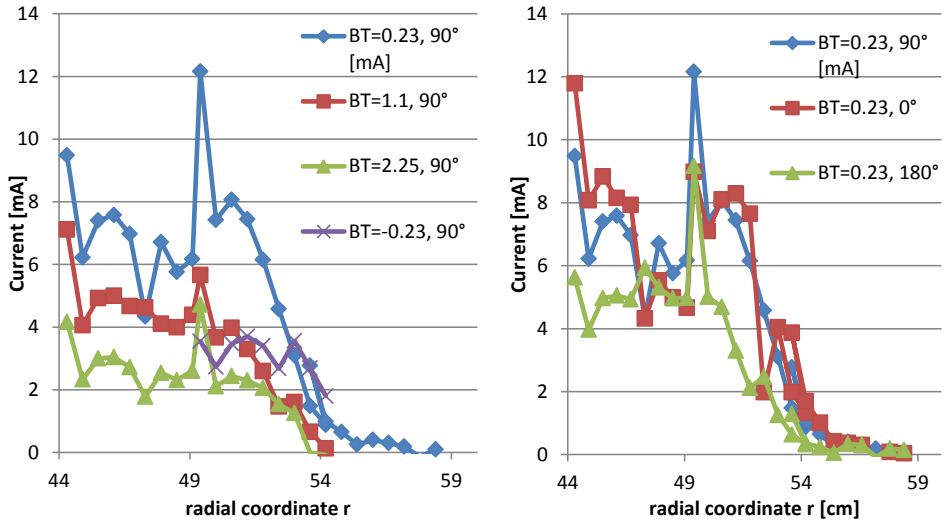

Figure 46: Radial profiles of the ion saturation current observed for different magnetic fields and angles between probe surface and magnetic field lines. The plasma ion flux was in all situations constant up to a radial position of about r=51cm and exhibited an exponential decay on higher radial coordinates. The limiter is at r=47.5cm, the liner at r=55cm.

5.3.4 Conclusions for plasma impact removal

The existing model for removal plasma parameters is investigated with respect to several input parameters and extended by plasma sheath and ion surface interaction models. In this understanding the setup of experimental parameters defines the removal plasma. The plasma parameters translate to ion fluxes and impact energies via the plasma sheath. At the surfaces the yield of the sputter process is given by the ion impact energy. The product of ion flux and the sputtering yields is the surface removal rate. The removal rate can be limited by this surface release rate or the removal of released species by pumping.

In the laboratory device TOMAS eight base gases for the removal plasma are compared. Only chemically reactive species are found to be effective at the typically low plasma temperatures of the discharges in the range of 2-10eV, which is in agreement with the understanding of ion impact energies and sputtering yields. Ion impact energies of 10-50eV are resulting from the plasma parameters. Physical sputtering of carbon, which is the only mechanism for chemically inactive ions (noble gases), has negligible yields at these energies and thus also negligible removal rates. The sputtering yield for deuterium removal is higher. Modelling reveals that due to deuterium depletion in the interaction zone by preferential sputtering only the carbon sputtering yield is relevant and also deuterium removal became impossible with chemically inert gases. Chemical sputtering, in contrast, has higher carbon yields at the given ion impact energies, explaining the removal by reactive species.

In line with the preferential sputtering model is that deuterium removal rates are found to correlate with the original D/C ratio of the co-deposits and the removal rates in terms of thickness and content are found to correlate. This identifies plasma impact removal as a

method removing material only from the outer surface. A surface layer of <5nm thickness is affected by the removal, according to ion-surface calculations (SDTRIM.SP). Deeper parts of the co-deposits cannot be accessed, so the removal by plasmas has to be able to remove all constituting elements of the co-deposit in parallel. Each species will be sputtered with its own yield. Plasma impact removal rates of mixed co-deposits will be limited by the lowest yield of all co-deposit constituents, since only this component will remain in the ion interaction zone.

The mixing of argon and deuterium (1:1) is not seen to increase the removal rate. The ion flux will be dominated by the light deuterium ions (equation (17)) and the ion impact energy will thus also be dominated by the deuterium ion mass (equation (56)). In conclusion the argon part of the plasma only contributes to the plasma losses, without increasing the removal rate, due to its low sputtering yields at the calculated ion impact energy of 38eV. Mixing several gases will in general not provide benefits in terms of removal rate. The ion impact energy will be defined by the lightest ions and thus be low. The plasma losses on the other hand will probably be dominated by the heaviest ions (with most electrons), resulting in a low ion flux.

In TEXTOR H_2, D_2 and O_2-ICWC are investigated with respect to their removal rates and ion wall fluxes. The removal rates are found to be significantly higher than in TOMAS. O_2 offers the highest removal rate in TOMAS but the lowest in TEXTOR. Underlying systematic differences of the devices are revealed by the modelling of plasma parameters (Table 5) using the plasma model (section 4.2.1). The electron temperatures in TEXTOR ICWC is defined by the onset of collisional processes at about T_e=2.7eV, while in TOMAS the low confinement leads to a reduced collisional transfer of energy from the electrons, which received most of the input power, to other particles. As a consequence of the distribution of energy to more particles, the electron temperatures in TEXTOR are lower and the plasma densities increases to balance the input power. Since the wall flux scales linear with the plasma density and sputtering yields of chemically reactive species are mostly independent of the ion impact energy, above a certain threshold, much higher removal rates are observed in TEXTOR than in TOMAS.

	H_2 (TEXTOR)	H_2 (TOMAS)	He (TEXTOR)	He (TOMAS)	O_2 (TEXTOR)	O_2 (TOMAS)
T_e [eV]	2.76	6.38	5.08	13.79	1.9	3.73
n_e [10^{16}/m³]	46.6	2.27	76.9	1.17	16.1	1.5
E_i [eV]	7.4	17.6	17.5	48.2	7.6	15.3
I_{sat} [A/m²]	739.3	54.8	827.6	20.7	53.0	6.9

Table 5: Modelling results for the plasma and plasma wall interaction parameters achieved in TOMAS and TEXTOR.

A ratio of the plasma densities of 3.1 between D_2 and O_2 is modelled for TEXTOR. The main effect is the significantly more effective plasma cooling of oxygen than of deuterium (at T_e=3eV about 8-fold). The ion flux density of D_2 plasmas becomes a factor 10.4 (14 for H_2) higher than of O_2 plasmas, due to this higher density and the higher ion mass of O^+. This

value is in agreement with the observed suppression, determined by Langmuir probes, by a factor of $I_{sat}(D_2)/I_{sat}(O_2)=11\pm4$. Since hydrogen and helium offer the lowest plasma cooling rates in the relevant plasma temperature range, they offer an intrinsic advantage in flux density compared to other plasma base gases which can only be compensated by significantly higher sputtering yields.

The observed sputtering yield of oxygen is only 0.16 C/O^+ in comparison with yields observed in the literature of 0.75 at 50eV impact energy. The same yield of 0.16 is observed in TOMAS, where a similar plasma temperature of about 2-3eV is achieved. Ion impact energies of about 8eV are calculated by the fluid model (equation (56)) for the experimentally observed electron temperature in TOMAS. This low ion impact energy can be hold responsible for the yield being significantly smaller than the literature value. As for hydrogen a threshold in the range of 5-15eV (Reinhold et al. 2010) is expected to exist for chemical sputtering of carbon by oxygen. The hydrogen and deuterium sputtering yields are slightly larger than the literature data. In addition to the ions in hydrogen plasmas large amounts of neutrals (>10 times the ion flux), produced by molecular dissociation and charge exchange, are predicted by the modelling. These neutrals possess energies of ≤3eV, which is found to be below the threshold for chemical sputtering on carbon (Reinhold et al. 2010), but due to their number they might yield a contribution to the ion removal rate. The experimental and modelled yields for NH_3 are compatible, within their error-bars. Since nitrogen chemical effects are not taken into account in this modelling, the removal by NH_3 at the given plasma temperature seems to be dominated by the hydrogen sputtering. In other publications relevant nitrogen chemistry was observed in N_2/H_2 mixed plasmas. A possible explanation is the lower ion energy in the experiments presented here in the order of 38eV for the NH_3 molecule.

The comparison of modelling and experimental results (Figure 47) exhibits an overestimation of the plasma wall fluxes by modelling. Impurities and spatial inhomogeneity are observed, but not included in the model. To match the modelled with the observed wall flux, a plasma carbon content of 1% has to be included. This value seems realistic in a carbon PFC tokamak as TEXTOR bombarded with chemically active species, as reported in (Wauters 2011). It has to be noted that the model treats the C impurity only as a global average and in a simplified way according to Figure 9. Different charge states and molecular contributions are not considered. Figure 47 compares the three cases for the three tested gases. The modelling results on the ion surface flux density (I_{sat}) without impurities are found to be about a factor 3 above the experimental results. Including 1% carbon affects practically only the plasma density and ion flux. The agreement can be considered as good, taking into account the 0D nature of the model.

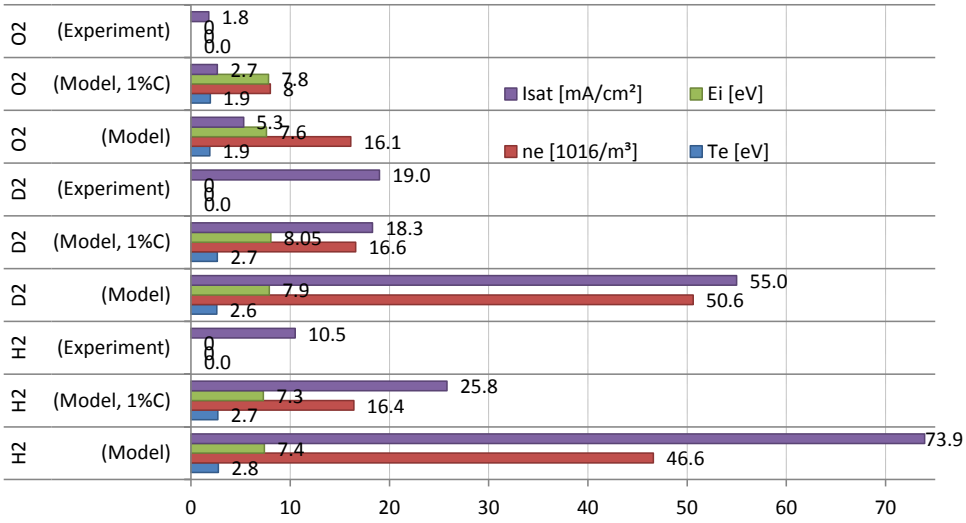

Figure 47: Comparison of two modelling scenarios and the experiments for the three gases in TEXTOR. With 1% carbon impurity the modelling results agree to the measured ion flux densities (Isat).

The understanding of the physics of removal plasmas leads to several conclusions for the removal rate maximization. For the choice of the plasma gas species not only the sputtering yield, but the product of attainable wall flux density times yield has to be considered. In the special case of carbon co-deposit (a-C:H) removal D_2 provides the highest product. For removing other co-deposits other base gases can be better, since the total yield is limited by smallest individual yield of the constituents. The wall flux is mainly determined by the plasma density, which is, for the applied ICWC and ECR plasmas, determined by the balance of input power and plasma cooling. Collisional and transport losses contribute to the cooling, but collisional processes dominate at the larger plasma volumes relevant for fusion devices. Hydrogen species are seen to be more effective than oxygen in TEXTOR, which can be attributed to an about 10-fold higher ion wall flux in the hydrogen plasmas. The effect of higher electron cooling efficiency and mass of oxygen compared to hydrogen and deuterium shows good agreement between modelling and observations, confirming the understanding. In TOMAS on the other hand oxygen is more effective. The higher surface to volume ratio and lower magnetic field lead to a transport loss dominated plasma cooling. Particle heat transport losses are lower for heavier particles, so plasma density and removal rate in TOMAS of O_2 are higher than of D_2. The modelling is successful in explaining the observed behaviour. With respect to removal rates the case of TOMAS can be considered as irrelevant for fusion devices, due to the different power loss mechanism in the small device with low magnetic field strength.

Plasma inhomogeneity is observed by cameras and Langmuir probes located at two different positions. A higher ion flux is observed closer to the power coupling antennas of TEXTOR. The contribution of vertical drifts to the observed current density difference is negligible, as calculated from tokamak drift theory. The effect can more likely be related to the power

coupling and antenna positions resulting in a non-uniform plasma density distribution. The TEXTOR ion cyclotron frequency range antennas are located at the top low field side of the vessel. The antenna wave electric field decays with distance from the antenna so that the plasma power input and with that its density is larger close to the antenna.

The radial investigation of plasma ion fluxes at several toroidal magnetic field values shows a rather homogenous distribution of the flux density around the radial position of the limiting surfaces of the tokamak in D_2-ICWC. About 3cm behind the radial position of the limiters the plasma flux decays. The independence of this behaviour from the toroidal magnetic field strength indicates that Bohm diffusion and ion larmor radii are not responsible for this effect. Diffusion by $E \times B$ drifts, where the magnetic field strength cancels out due to the impact on the vertical *E*-field, can explain the behaviour. The radial decay allows applying the removal only to the surfaces in contact with the plasmas, remote areas will not be affected by the energetic ions.

The actual mechanism for hydrogen isotope removal from the device is pumping. Only volatiles can be pumped, so the removal has to produce them. Calculations of the volatile pumping indicated that >99% of the particles released from the surfaces are not pumped in TEXTOR and $R_{eff} << R_P$, due to the low pumping speed in comparison to the surface release rates. The presence of re-deposition of carbon, originating from the carbon based limiters in TEXTOR, also indicates that D_2-ICWC in TEXTOR is in this pumping speed limited regime. The samples outside the plasma receive little carbon deposition, since the perpendicular transport in magnetized plasmas is smaller than the parallel transport. The particles not pumped will eventually be re-ionized by the plasma interaction and then re-deposited. The particles can undergo this process several times, but eventually they have to be pumped or remain in an area inaccessible to the plasma (remote areas). Lower surface release rates, different chemistry (and pumping channels) and higher pumping speed are ways to reach the surface release rate limited regime. This limits the application of a pumping speed limited removal discharge for hydrogen isotope recovery, since most of the released hydrogen will be trapped on remote surfaces. By adding pumping time (duty cycling) to the procedure, effective pumping speed can be increased, since the gas inventory has to build up in the initial phase (as in Figure 12). The capacity for exhaust gas of the plasma acts as an "inertial pump" until it is filled. The lower average partial pressure reduces the re-deposition. The length of the plasma discharge has to be larger than the plasma breakdown of typically 1-100ms. Together with the outgassing time constant after the discharge a lower limit for the duty cycle is defined. For wall conditioning a 100% duty cycle can be advantageous to push the impurities to the remote areas as fast as possible, from where they cannot be released as impurities to fusion plasmas. For hydrogen isotope recovery a small duty cycle with short pulses offers more efficient removal by pumping.

The results of removal rates presented in section 5.3.2 show higher removal rates compared to literature results on glow discharge cleaning (Hopf et al. 2007). Within the presented models this can be understood as a more efficient energy use by magnetized discharges

(ICWC) by improved confinement and lower ion impact energies (in the range of 10eV instead of >100eV), compared to glow discharges. This efficiency yields higher plasma densities and proportionally higher wall fluxes per input power. For the formation of volatiles by chemical interaction of the removal plasma with the co-deposits the yields are independent of the ion impact energy in a wide range (about 7-200eV for carbon). For the physical sputtering by chemically inactive species the ion impact energies of magnetized discharge can be too low. As the removal rate is given by the product of yield and flux, the magnetized removal plasmas are faster, at least for removal by chemical sputtering. The wall conditioning effectivity of ICWC was demonstrated in the tokamak TEXTOR (Wauters et al. 2013). As a conclusion ICWC should be favoured over glow discharge conditioning for tokamak and probably also stellarator application.

6 Conclusions for nuclear fusion application

Co-deposit removal for hydrogen isotope recovery in a fusion device, both experimental and commercial, should cost as little time as possible. This is the general application goal. New ways to achieve this and the various limitations preventing higher removal rates are revealed by the physical understanding gained in this work. In this section this understanding is transferred to the application.

6.1 Influence parameters of thermo-chemical removal

To increase the speed of TCR, the outer parameters gas species, wall temperature, gas pressure and size of co-deposit inventory/thickness are identified as parameters to optimize. By extrapolation, using the new understanding with fitted coefficients of NO_2-TCR, the effect on the removal times can be extrapolated.

Since the amount of co-deposit inventory has a linear connection with the removal rate, TCR should be applied after accumulating as much inventory as possible (or allowed). This way the integral time spent for removal of a total amount of inventory can be minimized.

The wall temperature is found to have an Arrhenius like effect in the investigated range. It should be chosen as high as technically feasible. Significant rates can only be expected above the lower application limit of 200°C. The gas pressure probably has little impact (<20%) on the removal rate in a range of 5mbar to 200mbar. From 5mbar to 1mbar a 3-fold decrease of the rate is extrapolated. In order to keep the gas input into the device and the amount of adsorbed oxygen small the gas pressure should be minimized. The pressure has a lower limit defined by the dilution of the reactive gas by the exhaust gas. Either a sufficient amount of reactive gas has to be supplied, leading to a minimum pressure (with fixed volume), or continuous pumping and resupply is necessary.

The reactive gas is the most important choice, as it defines the volatile release channels. The atoms donated to the exhaust species, in case of NO_2 the single bond O, has to be as weakly bound as possible. Oxygen gas species seem to be very efficient for carbon and hydrogen isotope removal. Other species, e.g. H_2 or NH_3, are possible as well, but lower removal rates can be expected. To deplete metallic co-deposits other species are probably necessary, e.g. F to produce WF_6 and HF. The removal rate of F can be expected to be even higher than that of NO_2, due to the reactive nature of F. The production of HF and other potentially dangerous and etching components may limit its applicability in nuclear fusion context.

A rather difficult (in the sense of optimisation) impact factor on the removal rate of thermo chemical removal is the structural property of the co-deposit. The a-priori assessment of diffusion and adsorption properties, material mixture and chemical bindings is, so far, a very difficult task. The amount of influential parameters during deposition from the plasma is large and fusion plasmas are very dynamic. According to the literature, a-C:H layers have a

limited parameter space, which allows to categorize them to hard and soft types. The removal of mixed tungsten carbon layers with non-carbon and hydrogen contents is seen to be ineffective, probably due to small diffusion coefficients. Layers deposited at higher ion impact energies (hard a-C:H) in PECVD are found to be significantly more resistant to TCR than low energy deposited soft layers. The trend seems to be in general that lower impact energies and surface temperatures lead to less dense layers with larger inner surfaces (Thornton 1977), which will be beneficial for removal. The study on the influence of the gas pressure on the refractive index gave further indication for the growth of fast diffusion layers (low refractive index) at higher deposition gas pressures. The low ion impact energies and higher neutral gas pressures expected for the plasma boundary in future devices (Kukushkin et al. 2011) give confidence that the layers will be soft and possible to remove by TCR. A dedicated optimization of the fusion boundary to obtain fast removing co-deposits seems to be unnecessary, since the usual aims of low sputtering of plasma-facing components coincide with this aim.

6.2 Removal discharge tailoring

The optimisation of removal plasmas requires knowledge about the co-deposits elemental composition. Plasma removal attacks co-deposits only in a thin ion interaction layer (<5nm). Preferential sputtering reduces, after depleting this layer of all other components, the total sputtering yield to the lowest individual value of the co-deposit constituents. The removal of this remaining component, sputtering with the lowest yield, is determining the removal rate.

The new understanding of removal plasmas allows tailoring the removal plasma according to this composition. The base gas is the most important choice for the removal discharge. Together with the co-deposit constituents it determines the sputtering yields (physical or chemical) and the release path (volatile pumping or re-deposition). Deuterium is found to provide the highest product of ion flux and sputtering yield for a-C:D, offering the highest surface release rate.

Physical sputtering cannot form volatile compounds, thus the material will only be migrated within the device, without being removed from the vessel, and finally end on remote areas. Hydrogen isotopes can be released and pumped, since with the hydrogen molecule they can form volatiles with themselves. Their release may be suppressed by re-deposition, since deeper parts of the co-deposits can remain inaccessible. Chemical sputtering, in contrast, can form volatiles which can be removed by pumping. The accumulation and consequent effective re-deposition of the produced volatiles has to be considered, if pumping removes the volatiles slower than they are released from the surfaces by the plasma (pumping limited removal). Equation (62) shows, that the choice of the reactive gas has also impact on the pumping rate, by providing a certain set of volatile molecules. An approach to increase the effective pumping and decrease the surface release rates is the cycling of plasma and pumping phases. A lower surface release rate is not relevant for the removal rate, if the process is pumping speed limited. The minimum duration of the plasma phase is given by

the discharge breakdown time. The maximum length of the pumping phase is defined by the volatile release behaviour and the pumping speed. By decreasing the input power to the plasma, the density and with that the ion flux and surface removal rate can also be reduced to prevent pumping speed limitation. For hydrogen isotope removal the surface removal rate limited regime offers the possibility to remove most of the hydrogen isotopes from the vessel before they are re-deposited on inaccessible remote areas.

With a given base gas, the plasma density (defines ion flux) and temperature (defines ion impact energy) can be adjusted by the gas pressure. As studied by modelling in a range of 10^{-6} to 10^{-4}mbar (Figure 33) the density of H_2-ICWC reaches a maximum at $5*10^{-5}$mbar, while the plasma temperature increases towards lower pressures at the expense of density. If a fast gas pressure feedback injection is available the plasma temperature and thus ion impact energy can be adjusted according to the value necessary for sputtering. In the limit of $T_e >> T_i$ equation (55) can be solved for the plasma temperature necessary for a specific ion impact energy

$$T_e = \frac{2 * E_i * e}{k_B * ln(2\pi * \frac{m_e}{m_i})} \tag{66}$$

As an example the removal of W-D-T co-deposits can be calculated. For the effective sputtering of tungsten by oxygen (or nitrogen) an impact energy of about 100eV is necessary (Behrisch 2007). According to equation (66) this corresponds to about 37eV in a H_2 plasma and 24eV in an O_2 plasma. In H_2-ICWC this impact energy can be reached with a pressure of $2*10^{-6}$mbar. For sputtering O or N can be introduced as traces. It is not possible to obtain a stable solution with the plasma model to reach 24eV in O_2, but pressures $<10^{-6}$mbar and significantly increased input power would be necessary. Sputtering of tungsten by deuterium requires about 300eV ion impact energy and thus $T_e \approx 100$eV. To reach this temperature region pressures below 10^{-6}mbar are required, which seems unfeasible for an ICWC application scenario due to fusion vessel base pressures usually in the order of 10^{-7}mbar.

6.3 Integral approach for co-deposit removal

Experiments and theoretical models presented in this section show a systematic difference between plasma impact removal (PIR) and TCR: Plasma impact removes material from the surface (affected layer <5nm) at a constant rate, while TCR removes material from the volume with a rate proportional to the current material content. TCR is seen to provide higher removal rates than plasma removal, but needs to introduce amounts of oxygen into the vessel, which can have a detrimental effect on fusion plasma operation. Plasma removal in contrast offers very good wall conditions, as is seen in the D_2-ICWC studies.

These fundamental differences yield different optimal scenarios for a maximum removal rate or a minimum time to remove a defined amount of co-deposit, respectively. A turning point D_t has to exist in co-deposit content/thickness where, at higher content, TCR is faster

and at lower content PIR is faster. The turning point thickness depends on the co-deposit properties and the possible removal parameters, e.g. surface temperature and removal plasma density, through their impact on the removal rates of the methods. The compatibility with fusion plasma operation requires the use of PIR after TCR for wall conditioning purposes (see section 5.2.3), in agreement to the maximum removal rate consideration. Applying TCR, followed by PIR thus offers advantages with respect to removal rates and wall conditions. By combining the advantages of both methods the integral scenario is defined.

The turning point can be calculated, based on the obtained data for NO_2-TCR and D_2-ICWC on a-C:D layers, which were identified as the best choices of the investigated options. As depicted in section 4.1 the removal rate of TCR is proportional to the content, so the rate drops exponentially with time during the removal. The content *D* of a co-deposit will drop accordingly with time *t* from its initial value D_0 with a fall-off time τ

$$D(t) = D_0 * e^{-\frac{t}{\tau}} \tag{67}$$

The effect of reactive gas depletion in the diffusion limited regime (thick layers, low diffusion coefficient) is neglected here, since it was not observed even for thick tokamak co-deposits (Davis and Haasz 2009). Solving this equation for the time necessary to reach a targeted remaining content D_t gives

$$t(D_t) = -\tau * ln\left(\frac{D_t}{D_0}\right) \tag{68}$$

The fall-off time is experimentally determined in section 5.2.2. To calculate it from the observations of 95% inventory removal, the following transformation is applied

$$\tau = t(95\%\, removal)/3 \tag{69}$$

Plasma impact removal rates R_P are understood as time and content independent (section 4.2.3) and thus give a linear relation for the removal time *t*

$$t(D) = D_0/R_p \tag{70}$$

The turning point can be calculated by finding the minimum of the sum of equation (68) and (70) with respect to D_t, switching to PIR when D_t is reached

$$t(D_t) = \frac{D_t}{R_P} - \tau * \ln\left(\frac{D_t}{D_0}\right) \tag{71}$$

$$t'(D_t) = \frac{1}{R_P} - \frac{\tau}{D_t} = 0$$

$$D_t = R_P \tau \tag{72}$$

The predicted evolution of removal time with co-deposit thickness is calculated for a fast and

a technically realistic scenario. The fast scenario features a wall temperature of 350°C during TCR and a 100% plasma removal duty cycle. A sufficiently high pumping speed is assumed. The removal time is depicted by the red curve in Figure 48. A turning point of D_t=3.4*10^{17} C/cm² is derived, corresponding to a thickness of 60nm at a typical a-C:H density of 1.4 g/cm³ observed for the layers used in this work. In a fusion device with a deposition dominated area of 100m², 50µm of a-C:D:T (D/T=1, D+T/C=1) with 1.4g/cm³ correspond to a tritium inventory of 700g (ITER limit). The integral procedure takes *t*=8min for removing a 50µm layer including 1min used for PIR. Taking into account a duty cycle of 10% for the plasma discharge and 200°C (technically realistic scenario) the time significantly increases, as depicted by the blue curve. The turnover shifts to D_t=4.2*10^{18} C/cm² (700nm), removing 50µm co-deposits takes *t*=10.7h (2h PIR) in this scenario.

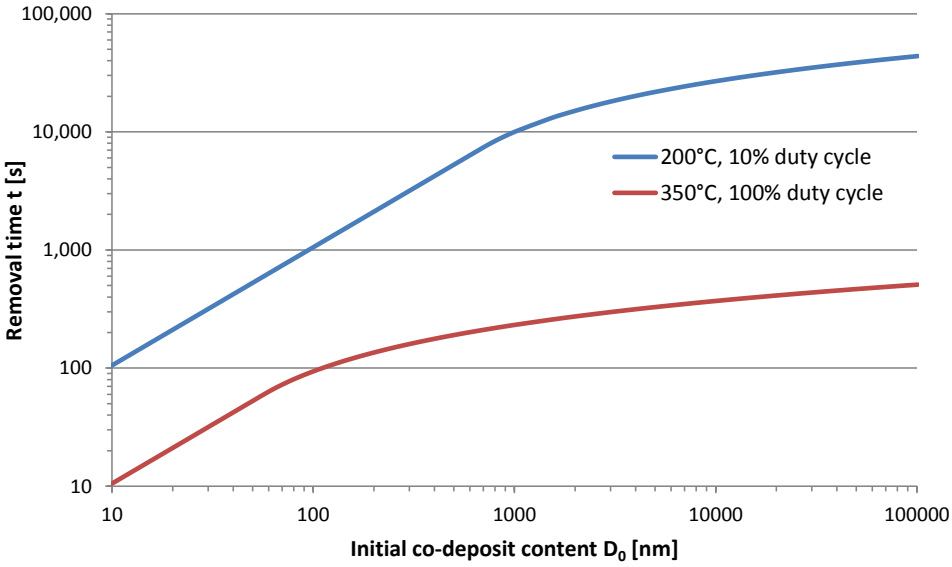

Figure 48: The evolution of removal time in an integral approach with a-C:H co-deposit initial content for a combination of NO_2-TCR at 10mbar and D_2-ICWC. By applying TCR above the turning point thickness a logarithmic scaling is obtained in the range of thicker layers. Below the turning point thickness PIR is applied, resulting in a linear scaling.

After co-deposit removal a helium plasma may be necessary to de-saturate the plasma-facing surfaces from D implanted by the D_2-ICWC into the wall material by preferential sputtering of D in the ion interaction zone. Depending on the vessel size, the wall material, the wall temperature and targeted fusion plasma density the deuterium outgassing may have a strong impact on the gas influx during subsequent fusion plasma discharges, with relatively higher impact for devices with lower fuelling rates. 23min of He-ICWC with 10% duty cycle were found to be sufficient even on the low density device TEXTOR (Wauters et al. 2013). The necessary desaturation time will probably be zero for future high power devices, since high fuelling rates will be needed anyway.

The integral approach presented in this section is only one of several options for the control of the hydrogen inventory in a future device. The scenarios are aimed at a complete clean-up/removal of the co-deposits. A different option would be just to remove a part, e.g. 95%, of the inventory by TCR and apply a removal plasma for device conditioning afterwards. A part of the inventory will remain, but the required removal time will be significantly shorter. In general it is always a trade-off between percentage of removal and time spent on the removal, if TCR is used (due to the log-scaling). For an experimental device, reproducible conditions and thus 100% removal are advisable, while for a power reactor it is probably only necessary to stay within the technical and safety limits of the in-vessel content between subsequent removal actions, without spending too much time on efforts not related to generating power. Applying TCR in between subsequent plasma pulses may be enough for a power reactor to limit the tritium inventory to an acceptable size, without significantly affecting its duty cycle.

6.4 Extrapolations to future devices

With the help of the model presented in section 4.2 and the confidence gained in the results, plasma removal for a device of the planned size of ITER can be modelled. At a coupled input power of 2MW, a feedback controlled D_2 pressure of 10^{-4}mbar and 5.4T toroidal field a plasma density of $4.2*10^{17}/m^3$ with T_e=2.4eV and 16% ionisation is modelled. The plasma parameters of this setup are similar to the TEXTOR reference case and thus the calculated removal rate R_P is similar as well. The electron temperatures in a larger device with higher magnetic field strength are modelled to be slightly lower than in TEXTOR, due to the improved confinement and with that energy transfer from electrons to ions. The plasma temperature has to be kept at a value guaranteeing an ion impact energy which is above the threshold for effective sputtering at 5-10eV. As stated in section 4.2, the input power is linearly connected to the removal rate and can be changed according to technical, pumping speed and time restrictions. The coupling efficiency, and with that the actual generator power needed, achieved in ITER is so far not known, but the combination of magnetic field strength, the large device, special antennas and frequencies could be optimized for high coupling efficiency.

For extrapolating the results obtained for TCR rates, the co-deposit properties are the most influential unknown. Carbon co-deposits can be expected to retain most hydrogen isotopes on remote areas in the divertor region, if carbon PFCs are used. The pressures in the ITER divertor are expected to be in the range of 5-15Pa and the plasma temperatures are intended to be low by applying a detached divertor regime to reduce target sputtering (Kukushkin et al. 2011). This would favour a reactive and hydrogen rich, yet easy to remove co-deposits (Robertson 2002). The maximum surfaces temperatures, especially in the deposition dominated divertor region (PFCs and remote areas), are in a TCR compatible range of 240-350°C, with >240°C only accessible by complete exchange of the coolant (Pitts et al. 2009). Fortunately the lower application limit of NO_2-TCR of 200°C is well inside this window. The use of tungsten and beryllium, which are easily oxidized, for plasma facing

components may limit the applicability of oxygen compounds, but no studies are conducted on the dangers of NO_2-TCR with these materials, so far. Self-passivating materials offer a solution currently under development.

The decisive parameters R_P and τ for the turnover thickness D_t and removal time, as defined in section 6.3, are not known for ITER and other future devices. R_P is estimated with the model, but also depends on the unknown co-deposit composition. τ on the other hand needs detailed information on the co-deposits reactive gas diffusion, adsorption and reaction properties essential for TCR. These properties are so far not accessible by a-priori calculations. For a final statement on the application and the removal time in a future device further research is necessary. The numbers given in section 6.3 might still be in the correct order of magnitude, since several deposition parameters of the produced a-C:D layers were already similar to the expected ones (e.g. deposition gas pressure, surface temperature, ion impact energy). The formation of mixed and hydrogen rich beryllium based co-deposits might also contribute a significant proportion to hydrogen isotope retention, which has to be resolved by further studies.

According to Figure 2 with an all carbon ITER the hydrogen isotope retention limit (700g T) could be reached within about 50 discharges. Assuming a homogenous deposition dominated area (including plasma wetted and remote) of 100m², the typical D/C of 1 and density (1.4g/cm³) as observed with the co-deposits in this work, this would correspond to a layer thickness of about 50µm. 50 discharges may correspond to a full week of operation, making a removal necessary every weekend. With the number of 10.7h for complete removal using the integral approach, a weekend or overnight applications seems feasible.

The turning point is found in the last chapter at a wall temperature of 200°C to be at an inventory of $4.2*10^{18}$C/cm², which leaves a total of $4.2*10^{24}$C (of initially $2.8*10^{26}$C) in the device to be removed by PIR and pumped over 2h at 10^{-4}mbar pressure. The necessary pumping speed for volatile removal under these conditions, assuming mostly methane CD_2T_2 and ethyne C_2DT with both contributing 2% to the total pressure, is 5550m³/s. This value is technically unfeasible high, even the pumping speed of the extremely effective cryopumps of the ITER system only provide a total of 300m³/s with 4 cryopumps. So TCR should be continued beyond the turning point inventory to avoid the pumping speed limit of plasma removal. Further reduction of the plasma removal duty cycle to 0.5% could increase the effective pumping speed to the necessary value, but the plasma breakdown time may prevent such short discharges.

With the 5 to 6 orders of magnitude higher pressure of TCR, pumping speed is not an issue and mechanical pumps will be sufficient. TCR can also accept arbitrary partial pressure of exhaust gas, since re-deposition is very improbable and the effect on removal rates can be calculated by the model. A high exhaust gas share will also reduce the total amount of gas to reprocess for tritium recovery and with that the cost for this final step of removal. A continuous gas exchange during TCR is not necessary, since the amount of exhaust gas of

700g tritium stored in a-C:DT corresponds to 8.6m³ at SATP (300K and 1bar pressure, SATP). Here CO_2 and CO are taken as the main products of carbon and DTO as the main product of hydrogen removal in a D-T fusion reactor. One exhaust gas particle will be generated for each C and T included in the co-deposits. 700g tritium corresponds to $1.4*10^{26}$ T-atoms. Co-deposits with D+T/C=1 and D=T produce $1.4*10^{26}$ DTO and $0.7*10^{26}$ CO + CO_2 totalling to $2.1*10^{26}$ particles (8.6m³ at SATP). Minor amounts of other products, e.g. TCN, can also contribute. Depending on the acceptable pressures and corresponding ratio of exhaust to reactive gas, unreacted NO_2 will add to this volume. With an ITER torus volume of 1400m³ the exhaust gas would correspond to 6.2mbar partial pressure, so operating at e.g. 20mbar initial pressure would provide sufficient reactive gas to remove all co-deposits. This amount of gas has to be stored and/or reprocessed during or after the removal process (≈11h) with a respective storage volume and isotope separation throughput.

It can be concluded, that the pumping speed will be a critical limitation for most hydrogen isotope removal methods in ITER, if low working pressures are envisaged and the removal is to be done in the gas phase (e.g. plasma removal). In comparison to this class of methods TCR has the two advantages that it can operate at arbitrary total and partial pressures. With an exhaust gas share of about 4%, as observed in TEXTOR, and a pressure of 10^{-4}mbar the surface release rates of PIR will be about two orders of magnitude faster than the subsequent removal by pumping. The removal rate becomes pumping speed limited. An operation pressure of 10^{-3}mbar and 10% exhaust gas share is roughly necessary for any removal method to overcome the pumping speed limit of the cryopumps of the ITER design. With the lower pumping speed of mechanical pumps $>10^{-2}$mbar will be necessary. The existence of this limitation is an important result for the general assessment of hydrogen isotope removal in D-T fusion reactors. Methods removing the inventory in solid form, e.g. by mechanical abrasion or transferring the co-deposit to a surface which can be removed from the device, are not affected by this limit.

A workaround for the pumping speed issue is the use of materials with lower retention rates, e.g. W or Be. As indicated in Figure 2 a factor of 10 to 100 can be gained in terms of the removal frequency necessary to limit the hydrogen isotope retention to acceptable levels. On the other hand it may be more difficult to remove the inventory stored in materials not forming volatiles as easily as carbon, e.g. metals.

Fuel removal from co-deposition remains a complex task with many influence parameters involved. A possible solution is presented and limits are described, but the issue still seems to need further research to give an elaborate solution for nuclear fusion`s future.

7 Summary

Magnetic confinement nuclear fusion research is currently facing major challenges in the field of plasma-wall interaction. One of these, the retention of hydrogen isotopes (especially tritium) by co-deposition, is assessed in this work. Their retention by co-deposition can reach values up to about 10% of the injected amount, dominating the in-vessel retention (Roth et al. 2008). Especially carbon based co-deposits, so called a-C:H, exhibit high retention values. As the tritium does not occur in nature, it needs to be obtained by breeding, using the neutrons released in the fusion reactions in a D-T reactor. In the current technical layouts of tokamaks, a breeding ratio of 1 to 1.2 is assumed to be realistic. The observed ratios of tritium retention can thus endanger the tritium self-sufficiency of a reactor, if the retained tritium cannot be recovered. In addition safety issues arise from large tritium inventories.

This work is intended to understand possible solutions for the problem of retention by co-deposition by means of plasma and thermo-chemical removal of carbon co-deposits. Both methods are chosen in accordance to the restrictions of nuclear fusion application and bear distinct advantages, as discovered in this work. Extensive studies on individual aspects of both methods are found in the literature, but a complete understanding of the involved physics was, so far, lacking. New models are developed within this work, combining the status of knowledge with new ideas to a coherent physical description of the involved processes. Experiments, designed according to this understanding, are conducted to support the models. The new understanding of the physics is used for optimisation and extrapolation to future devices.

Detailed studies of thermo-chemical removal (TCR) are found in the literature, investigating individual effects of several parameters with tokamak and laboratory co-deposits, mainly using O_2 as reactive gas. Higher gas pressures were found to cause higher removal rates. The removal rates exhibited an Arrhenius relation to the surface temperature, typical for thermally activated processes. The removal rates of not well defined tokamak co-deposits were seen to show a linear connection to the initial co-deposit content, indicating that the removal took place in the advantageous reaction limited regime. The new model successfully connects the different literature observations. A simplified model is derived from the reaction-diffusion model of TCR to describe the reaction limited regime with a lower number of parameters, preferable for experimental verification. Physical considerations also yield an equation for the time evolution of the removal rates, which is in line with literature observations. The time evolution is understood as a combination of an increase in reactive gas capacity of the co-deposit in the beginning of the removal process, with an exponential decrease of reaction partner density and thus lower removal rates dominating the final stage of removal.

An analytical model based on reaction-diffusion processes is formulated to describe the process of TCR on the basis of physical chemistry. The model assumes diffusion of the reactive gas into the co-deposits bulk. Thermally activated chemical reactions remove

material, including hydrogen isotopes, from the co-deposits. The reactions occur inside the co-deposit bulk. Volatile species, e.g. H_2O and CO, are formed in the chemical reactions between co-deposit constituents and reactive gas. These volatiles are removed from the vessel by pumps and can be reprocessed to recover the hydrogen isotopes. Diffusion acts as a source for reactive gas in the co-deposit bulk, while the chemical reactions act as a sink for the reactive gas present in the bulk. In quasi-steady state the reactive gas density distribution in the bulk is determined by the balance of these processes. Two distinct regimes are identified, the reaction and the diffusion limited regime. If the diffusive reactive gas influx rate is limiting the process, material is only removed from a zone close to the surface, due to the reactive gas depletion in deeper parts of the material. In this case the removal rate is not proportional to the co-deposit inventory. In reaction rate limitation on the other hand the reactive gas can reach the whole bulk due to the absence of effective sinks. The removal rate becomes proportional to the co-deposit inventory.

The model of thermo-chemical removal is tested with O_2 and NO_2 as reactive gases. Well defined a-C:D layers are produced in a laboratory device, as modelling reveals the layer properties as a significant influence factor for the removal rates. A removal with five a-C:D layer thicknesses in the range of 140 to 700nm but otherwise constant properties is conducted using O_2-TCR. The results approve the linear relation between removal rate and co-deposit thickness typical for the reaction limited regime and the related volume removal of the co-deposits. Oxygen is stored in remaining co-deposits, further indicating chemical volume reactions. To investigate the effects of chemistry on removal rate, the reactive gases O_2 and NO_2 are compared. The study consists of several exposures, comparing the two gases and testing the model assumptions for the influence of gas pressure (20 and 200mbar), surface temperature (200°C, 275°C and 350°C), co-deposit thickness (140nm and 550nm) and structure (soft and hard a-C:D) with the alternative gas NO_2. 95% of the deuterium and carbon inventory of 550nm thick soft a-C:D layers is removed by NO_2 at 350°C within 3 minutes. NO_2 is found to be more effective than O_2 and also exhibits a lower limit for the surface temperature of 200°C, in agreement with the weaker oxygen binding in the NO_2 molecule. The fundamental behaviour of NO_2-TCR is in agreement to the literature observations for O_2. In comparison to O_2, NO_2 demonstrates in the experiments about the same removal rates for the deuterium and carbon components of the layers, depicting the high importance of chemistry for TCR. The co-deposit properties and growth conditions are seen to have a strong impact on the removal rates, as layers deposited at 300eV ion impact energy are not removed under the same conditions where 100eV layers are nearly completely removed. In the literature the ion impact energy was seen to strongly affect the a-C:H layer nano-structure. The interaction of a-C:H structure with parameters as chemistry, reactive gas transport and inventory explains this observation.

Studies on plasma removal were, so far, conducted by analysis of global particle exhaust by mass spectrometry. These global analysis yielded removal rates of different co-deposit species, but the origin of the released particles and corresponding processes are impossible to investigate by global analyses. In this work the removal by plasmas is understood in the

frame of a three step model. The removal plasma properties are modelled in a 0D approach using an existing computer program. In this model the plasma parameters are determined by the balance of input power to power losses of the plasma. Plasma temperature and density arrange accordingly, with coefficients depending on the radiative, collisional and transport losses of the species contributing to the plasma. The ratios of these loss channels are determined by the plasma volume to surface ratio, the strength of the confining magnetic field, the interaction with the neutral background and the fundamental properties of the involved plasma species. Several parameter studies are conducted with the model to assess the impact of toroidal magnetic field, input power, neutral gas pressure and elemental composition on the plasma parameters.

The plasma parameters cause a certain ion flux density and ion impact energy to the wall surfaces, which are defined by the plasma sheath. The sheath arises by the ambipolar flux of electrons and ions at plasma-wall interaction surfaces and connects the plasma to its surroundings. A negative voltage establishes over the sheath, accelerating the ions to a narrow energy distribution centred at the sheath potential. With the help of a plasma fluid model this potential is calculated. The electron temperature of the removal plasma is found to be the dominating factor for the sheath potential and thus the ion impact energy. The sheath transmission coefficient for ions is calculated using the Bohm-criterion. The plasma ion density is the determining factor for the ion flux reaching the surfaces. The final step of the model is the process of surface sputtering by ion impact. Physical sputtering yields are derived using a binary collision approximation (SDTrim.SP) with the ion impact energies of the sheath model. Chemical sputtering yields are found in the literature. Sputtering simulations with dynamic surface composition reveal, that for a-C:D removal by plasmas the deuterium content is quickly depleted in the ion interaction layer (<5nm) by preferential sputtering. After deuterium depletion the total sputtering yield is dominated by the carbon sputtering yield. For a maximum surface release rate ion wall flux density and sputtering yield are equally important, since it results from their product.

For the removal process the re-deposition by subsequent ionisation of the surface released particles is considered. Two limits are identified, depending on the ratio of surface release rate to pumping speed. The pumping speed limited regime is found to be more relevant in application, resulting in significant re-deposition of the released material, ultimately in areas inaccessible by the removal plasma (remote areas). The effective hydrogen isotope recovery rate by plasma removal in this regime is limited by the pumping speed and partial pressures of the released volatile products.

Plasma impact removal experiments are conducted in the laboratory-scale toroidal magnetic plasma device TOMAS and the tokamak TEXTOR with in total nine different base gases to inspect the models prediction for plasma density and temperature. To assess the model predictions on surface release rates, well defined laboratory a-C:D layers are prepared. The plasmas are powered by electron cyclotron and ion cyclotron frequency range generators, respectively. The sputtering yields are determined by surface analysis and Langmuir probe

ion flux measurements. The obtained values are in agreement with the model predictions on sputtering yields. Noble gases show small removal rates in grounded sample conditions which rise significantly when applying a bias to increase the ion impact energy E_i on the samples and with that the physical sputtering yield. The chemically active species exhibit higher sputtering yields with values from 0.013 C/H^+ (H_2) to 0.16 C/O^+ (O_2). O_2 exhibited the highest removal rate in TOMAS. The removal rate of NH_3 is similar to that of D_2, both 2.4 fold slower than O_2. No significant synergistic effect of the nitrogen chemistry is observed at the ion impact energies accessible by the removal plasmas. Plasmas produced in H_2, D_2 and $^{18}O_2$ are tested in the tokamak TEXTOR to investigate the changeover from particle transport (in TOMAS) to collision dominated (in TEXTOR) plasma power losses, induced by the one order of magnitude larger plasma volume and magnetic field strength in TEXTOR. In TEXTOR plasmas in D_2 exhibit the highest removal rate ($5.7\pm0.9*10^{15}$ C/cm²s), which is accounted to its highest ion wall flux density and moderate sputtering yield (0.048 C/D^+). In D_2 an ion flux density of 19±0.5mA/cm² is found, in comparison to 1.8±0.5mA/cm² in O_2. The ratio of 11±4 is found to be in good agreement with the value of 10.4 provided by modelling. In TEXTOR the higher sputtering yield of O_2 is counteracted by its effective radiative cooling resulting in an about 3-fold lower plasma density than in D_2. The O ion flux is further reduced due to the higher ion mass. Spatial ion flux inhomogeneity is observed in the TEXTOR removal plasmas. Vertical tokamak drifts are ruled out as origin, but rather the spatial inhomogeneity of the antenna electric fields resulting in inhomogeneous power coupling dominates the effect.

The removal by pumping in TEXTOR is determined from the partial pressure decays of exhaust species. The removal rate of the pumps is calculated to $2.6*10^{12}$C/cm²s which is only 0.05% of the surface release rates observed on local, re-deposition free samples, when assuming a homogenous release from all carbon surfaces inside TEXTOR. This and the observed carbon deposition on the samples deeper inside the plasma than the main limiter of TEXTOR indicate that most of the released material is re-deposited and the removal in TEXTOR is thus pumping speed limited. Applying a duty cycle, where plasma and pumping phases are alternated, provides a possibility to decrease the ratio of surface release rate to pumping speed to reach the surface release rate limited regime. The duty cycle approach is limited due to characteristic times of plasma breakdown and gas release.

The start-up behaviour of fusion plasma discharges and wall conditioning is studied in TEXTOR to assess the issue of oxygen wall loading by TCR. Oxygen is loaded into the walls by $^{18}O_2$-ICWC. The effective plasma cooling of oxygen prohibits subsequent fusion plasma start-ups, indicated by oxygen line radiation. By applying 1.75h of D_2-ICWC followed by 0.5h of He-ICWC the oxygen inventory on plasma-wetted surfaces is largely removed, as measured by surface analysis of local samples and global gas balance. Plasma start-up is possible and the oxygen radiation levels are significantly reduced. The recovery from oxygen loading, e.g. from NO_2-TCR, using D_2-ICWC offers a possible solution to guarantee fusion plasma operation after oxygen based removal. ICWC is seen to offer advantages over glow discharge conditioning with respect to magnetic field compatibility (important for superconducting devices), conditioning time and final wall conditions.

A fundamental result for the application of the removal methods is, that the time required for plasma removal of co-deposits is in linear relation to their material content, while thermo-chemical removal (bulk removal methods in general) only scales with a logarithmic relation. Plasma removal in D_2 on the other hand induces good wall conditions for fusion plasmas, while TCR introduces detrimental oxygen to the device. A turning point in co-deposit inventory, above which removal by TCR becomes faster than plasma removal, exists. Turning points of 60nm and 700nm a-C:H thickness are calculated with the obtained removal rates of D_2-ICWC and NO_2-TCR at 350°C and 200°C surface temperature, respectively. Based on the different inventory scaling of TCR (logarithmic) and plasma removal (linear), an integral scenario is developed using TCR for removal of co-deposits and plasmas for removal of remaining layers and oxygen (introduced by TCR) from the plasma-facing surfaces. This scenario uses the advantage of the high removal rate of TCR without suffering from its detrimental effects on fusion plasma operation by oxygen wall loading.

The models are used for extrapolations to future devices, based on the experimentally determined removal rates, the specifications of ITER and the assumption of carbon dominated hydrogen isotope retention. With 2MW of input power, 10^{-4}mbar D_2 pressure and a magnetic field of 5.4T similar plasma removal rates as in TEXTOR can be projected. The wall temperatures in the ITER divertor, as the main deposition zone, are planned to be above the lower application limit of NO_2-TCR of 200°C. By accumulating co-deposits up to the safety limit of 700g the operational time spent for removal can be limited. Similar a-C:H co-deposit properties as used in this work are assumed for the ITER divertor conditions. The assumption is supported by similar ion impact energies, gas pressures and surface temperatures, however the presence of other elemental contributions than D and C is not taken into account. At 200°C wall temperature the extrapolations yield a time of 8.7h of NO_2-TCR and 2h of D_2-ICWC necessary to remove the co-deposits and recover fusion plasma compatible wall conditions. This would allow an overnight or weekend application of the removal scenario. An amount of 8.6m³ (SATP) of partly tritiated exhaust gas (DTO, CO) is calculated to be produced during the removal of the 700g tritium inventory.

In conclusion this work presented a physical understanding of the fundamental processes of hydrogen removal methods and their limits in support of future nuclear fusion science and application, as the author believes in its utmost importance for the society.

8 References

Acsente, T., E.R. I. D. Colceag, A. Moldovan, C. Luculescu, R. Birjega, and G. Dinescu. 2011. "Properties of composite a-C:H/metal layers deposited by combined RF PECVD/magnetron sputtering techniques." *Thin solid films 519*, pp. 4054-4058.

Alegre, D., T.J. Finlay, J.W. Davis, A.A. Haasz, and F.L. Tabarés. 2013. "Oxidative removal of tokamak codeposits using NO2 and O2." *Journal of Nuclear Materials 438*, pp. 1104-1108. http://dx.doi.org/10.1016/j.jnucmat.2013.01.243.

Ashby, D.E.T.F. and M.H. Hughes. 1981. "A study of the effect of impurity radiation from the peripheral plasma of a tokamak reactor." *Nuclear Fusion 21*.

Balden, M., W. U. Klages, W. Jacob, and J. Roth. 2005. "Oxidative erosion of graphite in air between 600 and 1000 K." *Journal of Nuclear Materials 341*, pp. 31-44.

Behrisch, R. 2007. *Sputtering by particle bombardment : experiments and computer calculations from threshold to MeV energies*. Berlin: Springer.

Berberich, B. 2012. *Entwicklung und Anwendung eines Tree-Codes in Simulationsszenarios der Plasma-Wand-Wechselwirkung*. Düsseldorf: Universität Düsseldorf.

Carrasco, A. G., S. Möller, P. Petersson, D. Ivanova, A. Kreter, and T. W. M. Rubel. 2014. "Impact of Ion Cyclotron Wall Conditioning on Fuel Removal from Plasma-Facing Components." *Physica Scripta T159*, pp. 014017.

Coad, J.P., M. Rubel, N. Bekris, D. Brennan, D. Hole, J. Likonen, and E. Vainonen-Ahlgren. 2005. "Distribution of hydrogen isotopes, carbon and beryllium on in-vessel surfaces in the various JET divertors." *Fusion science and technology 48*.

Czeslik, Claus, Heiko Semann, and Roland Winter. 2007. *Basiswissen physikalische Chemie*. Stuttgart: Teubner.

Dadras, J. and P. Krstic. 2011. "Chemical sputtering of deuterated carbon surfaces at various surface temperatures." *Nuclear Instruments and Methods in Physics Research B 269*.

Davis, J. W. and A. A. Haasz. 1999. "Oxygen Removal of Codeposited a-C:D layers from Tokamak Tiles." *Journal of Nuclear Materials*, pp. 478-484.

Davis, J. W. and A. A. Haasz. 2001. "Overview of Thermo-oxidation of Tokamak Codeposits." *Physica Scripta T91*.

Davis, J. W. and A. A. Haasz. 2009. "Oxidation of carbon deposits as a fuel removal technique for application in fusion devices." *Journal of Nuclear Materials 390-391*, pp. 532-537.

Dejarnac, R., M. Komm, J. Stöckel, and R. Panek. 2008. "Measurement of plasma flows into tile gaps." *Journal of Nuclear Materials 382*, pp. 31-34.

Douai, D., A. Lyssoivan, V. Philipps, V. Rohde, T. Wauters, T. Blackman, V. Bobkov, S. Brémond, S. Brezinsek, F. Clairet, E. d. l. Cal, T. Coyne, E. Gauthier, T. Gerbaud, M. Graham, S. Jachmich, E. Joffrin, R. Koch, A. Kreter, and R. Laengner. 2011. "Recent results on Ion Cyclotron Wall Conditioning in mid and large size tokamaks." *Journal of Nuclear Materials 415*.

Emmert, G., R. Wieland, T. Mense, and J. Davidson. 1980. "Electric sheath and presheath in a collisionless, finite ion temperature plasma." *Phys. Fluids 23*, pp. 803.

Giesen, B., F.H. Bohn, T. Denner, 0. Neubauer, M. Poier, W. Schalt, and P.W. Huttemann. 1997. "The Engineering Design of the Dynamic Ergodic Divertor (DED) for TEXTOR-94." *Fusion Engineering*, pp. 705-708.

Haasz, A. A. and J. W. Davis. 1998. "The removal of codeposited layers from TFTR tiles by O2 gas." *Journal of Nuclear Materials 256*, pp. 65-68.

Hopf, C., V. Rohde, W. Jacob, A. Herrmann, R. Neu, and J. Roth. 2007. "Oxygen glow discharge cleaning in ASDEX Upgrade." *Journal of Nuclear Materials 363-365*, pp. 882-887.

IAEA Nuclear Data Services. n.d. "IBANDL." http://www-nds.iaea.org/exfor/ibandl.htm.

Jacob, W. and W. Möller. 1993. "On the structure of thin hydrocarbon films." *Applied Physics Letters 63*.

Jacobsohn, L.G., G. Capote, M.E.H. Maia da Costa, D.F. Franceschini, and F.L. F. Jr. 2002. "Nanoporosity in plasma deposited amorphous carbon films investigated by small-angle X-ray scattering." *Diamond and Related Materials 11*, pp. 1946–1951.

Kögel, G., D. Schödelbauer, W. Triftshäuser, and J. Winter. 1988. "Investigation of micropores in amorphous hydrogenated carbon by a pulsed positron beam." *Physical Review Letter 60*.

Kukushkin, A.S., H. D. Pacher, V. Kotov, G. W. Pacherd, and D. Reiter. 2011. "Finalizing the ITER divertor design: The keyrole of SOLPS modeling." *Fusion Engineering and Design 86*, pp. 2865–2873.

Lissoyvan, A. 2013. " P1.27." *20th Topical Conference on Radio Frequency Power in Plasmas*.

Lyssoivan, A., G. Sergienko, V. Rohde, V. Philipps, G. v. Wassenhove, M. Vervier, and V. Bobkov. 2009. "Influence of toroidal and vertical magnetic fields on Ion Cyclotron wall conditioning in tokamaks." *Journal of Nuclear Materials*, pp. 907-910.

Marchand, R., C. Illescas, X. Botero, and J. Bonnin. 1995. "Radiative Losses and Electron Cooling Rates of Hydrogen, Helium, Carbon and Oxygen." *IAEA Nuclear Data Section*.

Martin, C., M. Richou, C. Brosset, W. Sakaily, B. Pegourie, and P. Roubin. 2007. “Porous carbon deposits in controlled fusion reactor: adsorption properties and structural characterization.” *Studies in Surface Science and Catalysis 160*, pp. 249-256.

Matveeva, Maria 2008. “Masterarbeit.” in *Investigation of the capability of ECRH discharge to clean the mirrors of ITER diagnostics*. Forschungszentrum Jülich GmbH.

Maximov, Andrey. 2011. *Development of probe diagnostics for studies of plasma-surface interactions*. Universiteit Gent.

Mayer, M. 1997. *SimNRA User´s Guide IPP Report Number: IPP 9/113*. Garching: Max-Planck-Institut für Plasmaphysik, www.simnra.com.

Möller, Sören 2010. “Diplomarbeit.” in *Zersetzung von Kohlenstoffschichten in reaktiven Gasen zur Reduktion der Wasserstoffrückhaltung in Fusionsanlage*. Forschungszentrum Jülich.

Möller, S., D. Alegre, A. Kreter, P. Petersson, H. G. Esser, and U. Samm. 2014. “Thermo-chemical fuel removal from porous materials by oxygen and nitrogen dioxide.” *Physica Scripta T159*, pp. 014065.

Mutzke, Andreas, Ralf Schneider, Wolfgang Eckstein, and Renate Dohmen. 2011. “SDTrimSP Version 5.00.” http://edoc.mpg.de/552734.

Neubauer, O., G. Czymek, B. Giesen, P. W. Hüttemann, M. Sauer, W. Schalt, and J. Schruff. 2005. “Design features of the tokamak TEXTOR.” *Fusion Science and Technology 47*.

Ochoukov, R., A. A. Haasz, and J. W. Davis. 2006. “Pressure dependence of oxidative removal of tokamak codeposits.” *Physica Scripta T124*, pp. 27-31.

Piel, A. 2010. *Plasma Physics*. Heidelberg: Springer.

Pitts, R. A., A. Kukushkin, A. Loarte, A. Martin, M. Merola, C. E. Kessel, V. Komarov, and M. Shimada. 2009. “Status and physics basis of the ITER divertor.” *Physica Scripta T138*.

Rack, M., Y. Liang, H. Jaegers, J. Aßmann, and G. Satheeswaran. 2013. “A rotating directional probe for the measurements of fast ion losses and plasma rotation at Tokamak Experiment for Technology Oriented Research.” *Review of Scientific Instruments 84*.

Randers, Jorgen. 2012. *2052: A Global Forecast for the Next Forty Years*. Chelsea Green Publishing.

Reinhold, C.O., P.S. Krstic, S.J. Stuart, H. Zhang, P.R. Harris, and F.W. Meyer. 2010. “Isotope dependence of chemical erosion of carbon.” *Journal of Nuclear Materials 401*.

Richou, M., C. Martin, R. Denoyel, P. Llewellyn, and P. Roubin. 2009. “Microporosity of carbon deposits collected in the Tore Supra tokamak probed by nitrogen and carbon dioxide adsorption.” *Carbon 47*, pp. 109-116.

Robertson, J. 2002. “Diamond-like amorphous carbon.” *Materials Science and Engineering R37*.

Roque-Malherbe, Rolando M. A. 2007. *Adsorption and diffusion in nanoporous materials*. CRC Press.

Roth, Joachim, Emmanuelle Tsitrone, Thierry Loarer, Volker Philipps, Sebastijan Brezinsek, and Alberto Loarte. 2008. “Tritium inventory in ITER plasma-facing materials and tritium removal procedures.” *Plasma Phys. Control. Fusion 50*, pp. 103001.

Schulz, C., A. Kreter, V. Philipps, A. Litnovsky, and U. Samm. 2011. “Fuel removal from castellated structures by plasma discharges in hydrogen and oxygen.” *Journal of Nuclear Materials*, pp. 781-784.

Schwarz-Selinger, T., A. v. Keudell, and W. Jacob. 1999. “Plasma chemical vapor deposition of hydrocarbon films: The influence of hydrocarbon source gas on the film properties.” *Journal of Applied Physics 86*, pp. 3988-3996.

Sergienko, G., A. Lyssoivan, V. Philipps, A. Kreter, C. Schulz, A. Huber, H.G. Esser, J.S. Hu, M. Freisinger, H. Reimer, and U. Samm. 2009. “Ion cyclotron wall conditioning in reactive gases on TEXTOR.” *Journal of nuclear materials 390-391*.

Stangeby, P. 2000. *The Plasma Boundary of Magnetic Fusion Devices*. Bristol and Philadelphia: Institute of Physics Publishing.

Temmerman, G. D., M.J. Baldwin, R.P. Doerner, D. Nishijima, R. Seraydarian, and K. Schmid. 2009. “Insight into the co-deposition of deuterium with beryllium: Influence of the deposition conditions on the deuterium retention and release.” *Journal of Nuclear Materials 390-391*.

Thornton, J. A. 1977. “High rate thick film growth.” *Ann. Rev. Mater. Sci. 7*, pp. 239.

Vasquez-Borucki, S., W. Jacob, and C. A. Achete. 2000. “Amorphous hydrogenated carbon films as barrier for gas permeation through polymer films.” *Diamond and Related Materials 9*.

Wang, Yongqiang. 2009. *Handbook of modern ion beam materials analysis*. Pittsburgh: Materials Research Society.

Wang, P., W. Jacob, M. Balden, T. Höschen, and A. Manhard. 2012. “Erosion of tungsten-doped amorphous carbon films exposed to deuterium plasmas.” *Journal of Nuclear Materials 426*, pp. 277-286.

Wang, W., W. Jacob, and J. Roth. 1997. “Oxidation and hydrogen isotope exchange in amorphous, deuterated carbon films.” *Journal of nuclear materials 245*.

Wauters, Tom 2011. “Dissertation.” in *Study and Optimization of Magnetized ICRF Discharges for Tokamak Wall Conditioning and Assessment of the Applicability to ITER*. Brüssel.

Wauters, T., A. Lyssoivan, D. Douai, O. Marchuk, D. Wünderlich, R. Koch, G. Sergienko, M. V. Schoor, and G. V. Oost. 2011. “0D model of magnetized hydrogen–helium wall conditioning plasmas.” *Plasma Phys. Control. Fusion*, pp. 125003.

Wauters, T., S. Möller, A. Kreter, M. Rubel, A. Garcia-Carrasco, K. Crombé, D. Douai, M. Freisinger, D. Ivanova, D. Kogut, R. Koslowski, A. Lyssoivan, D. Nicolai, P. Petersson, V. Philipps, M. Rack, H. Reimer, G. Sergienko, and M. Vervier. 2013. “Self-consistent application of ion-cyclotron wall conditioning for co-deposited layer removal and recovery of tokamak operation on TEXTOR.” *Nuclear Fusion 53*, pp. 123001.

Wesson, J. 2004. *Tokamaks*. Oxford: Clarendon Press.

Ziegler, J. F., J. P. Biersack, and U. Littmark. 2013. “SRIM - The Stopping and Range of Ions in Matter.” www.srim.org. New York: Pergamon.

Acknowledgment

An einem Projekt wie dieser Dissertation sind viele Menschen beteiligt. Manche mit einer Leistung die direkt sichtbar ist, manche mit Hilfestellungen die eher im Hintergrund stattfinden. Es gibt fachliche und private Unterstützung welche im Endeffekt gleichermaßen wertvoll sind. Einige Personen waren dabei besonders hilfreich.

Mal geht es nur um eine warme Mahlzeit nach stundenlangen Experimenten, mal hilft es mit einem Nicht-Physiker über die Dinge zu sprechen die mich beschäftigen. Kathrin Pytel danke ich für die bedingungslose Unterstützung zuhause und die Bereitstellung des sicheren Hafens. Mir ist im Laufe der Dissertationszeit klar geworden wie wichtig das ist.

Meinen Freunden aus der alter Zeit danke ich für die unveränderliche Freundschaft. Exemplarisch möchte ich Giovanni Nocera, Florian Schmitz und Miguel Martinez-Fernandez erwähnen. Ausgezeichneterweise haben wir uns eine wöchentliche Fußballrunde während meiner Dissertationszeit aufbauen und erhalten können die mir neben Entspannung auch die körperlichen Voraussetzungen für diese Promotion geliefert hat.

Fachlich bin ich insbesondere meinem Betreuer im Forschungszentrum Jülich, Arkadi Kreter zu großem Dank verpflichtet. Ich habe während der Dissertationszeit viel von ihm gelernt und er hat stets Zeit für meine Fragen gehabt. Außerdem ist es, nach meiner Erfahrung, alles andere als selbstverständlich die neuen und zum Teil kontrovers diskutierten Theorien zu akzeptieren und zu unterstützen die am Ende tatsächlich die physikalische Essenz dieser Arbeit ausmachten. Tom Wauters danke ich, dass er wertvoller und angenehmer Kollege war ohne den ein Großteil meiner plasmabezogenen Erkenntnisse nicht gewonnen worden wäre. Per Petersson danke ich für die fachliche Unterstützung im Bereich der Oberflächenanalytik und die Begeisterung für Ideen, die er auch ausstrahlt. Beide haben mir durch ihre wissenschaftliche Qualität deutlich gemacht, wie wichtig internationale Kooperation zur Lösung komplexer Aufgaben ist. Christian Scholtysik danke ich für den Betrieb des Tandembeschleunigers, an dem er bewiesen hat, dass ein Einzelner den Unterschied machen kann. Christian Linsmeier danke ich für die Unterstützung der Ausarbeitung der Dissertation.

Ich möchte allen weiteren Kollegen aus dem Forschungszentrum Jülich, der Uppsala Universität und der Helsinki Universität danken das sie mir gezeigt haben wie angenehm die Verknüpfung von Freundschaft und Beruf ist. Ohne Beschränkung der Allgemeinheit möchte ich ein paar Kollegen erwähnen mit denen ich am meisten Zeit verbracht habe. Carolina Björkas und Simon Freutel danke ich, dass sie mir eine neue Seite an mir offenbart haben. Adalbert Kubina, Tobias Wegener, Felix Hasenbeck und Maren Hellwig danke ich für die zahllosen Gespräche und entspannten Abende die mir nicht nur Spaß gemacht haben sondern auch für meine persönliche Weiterentwicklung entscheidend waren.

Meinen Eltern danke ich für ihre Unterstützung in psychologischer und auch materieller Weise. Beide haben mir mit ihren unterschiedlichen Stärken stets zur Seite gestanden.

Band / Volume 209
Kühlkonzepte für Hochtemperatur-Polymerelektrolyt-Brennstoffzellen-Stacks
J. Supra (2014), III, 191 pp
ISBN: 978-3-89336-946-1

Band / Volume 210
Eigenschaften des Phosphorsäure-Polybenzimidazol-Systems in Hochtemperatur-Polymerelektrolyt-Brennstoffzellen
A. Majerus (2014), viii, 141 pp
ISBN: 978-3-89336-947-8

Band / Volume 211
Study on the Complex Li-N-H Hydrogen Storage System
L. Du (2014), I, 132 pp
ISBN: 978-3-89336-952-2

Band / Volume 212
Transport and Retention of Stabilized Silver Nanoparticles in Porous Media
Y. Liang (2014), IV, 109 pp
ISBN: 978-3-89336-957-7

Band / Volume 213
Effizienzoptimierte CO_2-Abtrennung in IGCC-Kraftwerken mittels Wassergas-Shift-Membranreaktoren
S. T. Schiebahn (2014), XXII, 203 pp
ISBN: 978-3-89336-958-4

Band / Volume 214
Lebensdauer und Schädigungsentwicklung martensitischer Stähle für Niederdruck-Dampfturbinenschaufeln bei Ermüdungsbeanspruchung im VHCF-Bereich
S. Kovacs (2014), IV, 140 pp
ISBN: 978-3-89336-959-1

Band / Volume 215
Micro- and Macro- Mechanical Testing of Transparent $MgAl_2O_4$ Spinel
O. Tokariev (2014), X, 99 pp
ISBN: 978-3-89336-960-7

Band / Volume 216
Potentiale des Strommanagements zur Reduzierung des spezifischen Energiebedarfs von Pkw
T. Grube (2014), IX, 255 pp
ISBN: 978-3-89336-961-4

Schriften des Forschungszentrums Jülich
Reihe Energie & Umwelt / Energy & Environment

Band / Volume 217
Transmutation von Transuranen in einem gasgekühlten beschleunigergetriebenen System
K. H. Biß (2014), IV, 157 pp
ISBN: 978-3-89336-964-5

Band / Volume 218
Untersuchung des photochemischen Terpenoidabbaus in der Atmosphärensimulationskammer SAPHIR
M. Kaminski (2014), 148, VI pp
ISBN: 978-3-89336-967-6

Band / Volume 219
Interaction of Phosphoric Acid with Cell Components in High Temperature Polymer Electrolyte Fuel Cells
F. Liu (2014), i, 147 pp
ISBN: 978-3-89336-972-0

Band / Volume 220
Machbarkeitsstudie zum Aufbau und Betrieb eines Prüfstandes für Antriebsstränge von Windenergieanlagen mit Getriebe im Leistungsbereich bis 15 MW am Standort Forschungszentrum Jülich
(2014), 72 pp
ISBN: 978-3-89336-973-7

Band / Volume 221
Phenotyping Nannochloropsis gaditana under different conditions in controlled photobioreactors in laboratory and upscaled photobioreactors in greenhouse
R. Braun (2014), III, 177 pp
ISBN: 978-3-89336-975-1

Band / Volume 222
Fundamental processes of plasma and reactive gas surface treatment for the recovery of hydrogen isotopes from carbon co-deposits in fusion devices
S. Möller (2014), 99 pp
ISBN: 978-3-89336-977-5

Weitere ***Schriften des Verlags im Forschungszentrum Jülich*** unter
http://wwwzb1.fz-juelich.de/verlagextern1/index.asp

Energie & Umwelt / Energy & Environment
Band / Volume 222
ISBN 978-3-89336-977-5